



Michigan Technological University
Create the Future Digital Commons @ Michigan Tech

Dissertations, Master's Theses and Master's
Reports - Open

Dissertations, Master's Theses and Master's
Reports

2012

Effect of external electric field on hydrogen adsorption over activated carbon separated by dielectric materials

Zheng Zhang
Michigan Technological University

Follow this and additional works at: <https://digitalcommons.mtu.edu/etds>


 Part of the [Engineering Science and Materials Commons](#)

Copyright 2012 Zheng Zhang

Recommended Citation

Zhang, Zheng, "Effect of external electric field on hydrogen adsorption over activated carbon separated by dielectric materials", Dissertation, Michigan Technological University, 2012.
<https://doi.org/10.37099/mtu.dc.etds/16>

Follow this and additional works at: <https://digitalcommons.mtu.edu/etds>

 Part of the [Engineering Science and Materials Commons](#)

EFFECT OF EXTERNAL ELECTRIC FIELD ON HYDROGEN ADSORPTION OVER
ACTIVATED CARBON SEPARATED BY DIELECTRIC MATERIALS

By
Zheng Zhang

A DISSERTATION

Submitted in partial fulfillment of the requirements for the degree of

DOCTOR OF PHILOSOPHY

(Environmental Engineering)

MICHIGAN TECHNOLOGICAL UNIVERSITY

2012

© 2012 Zheng Zhang

This dissertation, “Effect of External Electric Field on Hydrogen Adsorption over Activated Carbon Separated by Dielectric Materials,” is hereby approved in partial fulfillment of the requirements for the Degree of DOCTOR OF PHILOSOPHY IN ENVIRONMENTAL ENGINEERING.

Department of Materials Science and Engineering

Signatures:

Dissertation Advisor

Jiann-Yang Hwang

Department Chair

Mark R. Plichta

Date

Contents

List of Figures	vii
List of Tables	ix
Acknowledgements	x
Abstract	xii
CHAPTER 1 INTRODUCTION	1
1.1 Hydrogen energy	2
1.1.1 Hydrogen production	3
1.1.2 Hydrogen fuel cell	4
1.1.3 Hydrogen storage	7
1.2 Hydrogen storage materials	9
1.2.1 Metal hydrides	9
1.2.2 Complex hydrides	11
1.2.3 Nanostructured carbon	12
1.2.4 Metal organic frameworks (MOFs)	14
1.2.5 Metal oxides	15
1.3 New approaches to hydrogen storage	16
1.3.1 Hydrogen spillover	16
1.3.2 Combination of light metal hydrides and carbon materials for hydrogen storage	17
1.3.3 Electric field assisted hydrogen adsorption	17
CHAPTER 2 BACKGROUND AND LITERATURE REVIEW	19
2.1 Hydrogen adsorption mechanism	19
2.2 Hydrogen cluster	22
2.2.1 Hydrogen ion cluster	22
2.2.2 Metal hydrogen cluster	23
2.3 Influential factors of hydrogen storage on carbon materials	23
2.3.1 Porous structure	24
2.3.2 Temperature	26

2.3.3 Pressure.....	27
2.4 Hydrogen adsorption measurement methods	27
2.4.1 Gravimetric method.....	27
2.4.2 Volumetric method	27
2.5 Scope of this study	28
CHAPTER 3 MATERIALS AND METHODS	30
3.1 Materials.....	30
3.1.1 Carbon sources	30
3.1.2 TiO ₂ sources	30
3.1.3 Other sources	30
3.2 Samples preparation	31
3.2.1 Carbon mixture	31
3.2.2 TiO ₂ /Carbon species	31
3.2.3 MgO/Carbon species	32
3.2.4 ZnO/Carbon species	32
3.2.5 BaTiO ₃ /Carbon species.....	33
3.3 Hydrogen adsorption measurements	33
3.3.1 Measurements with electric field generated by piezoelectric element	35
3.3.2 Measurements with electric field generated by applied electric potential.....	38
3.4 Characterization methods	38
CHAPTER 4 CHARACTERIZATIONS.....	40
4.1 Characterizations of TiO ₂ /Carbon species	40
4.1.1 Mechanically mixed TiO ₂ /Carbon mixture	40
4.1.2 TiO ₂ /Carbon synthetics prepared from Premix of TiO ₂ powder	40
4.1.3 TiO ₂ /Carbon synthetics prepared through chemical deposition	44
4.2 Characterizations of MgO/Carbon species.....	47
CHAPTER 5 EXAMINATION OF HYDROGEN ADSORPTION ON ACTIVATED CARBON UNDER ELECTRIC FIELD.....	49
5.1 Hydrogen adsorption on pristine activated carbon.....	50

5.1.1 Positive electric potential.....	50
5.1.2 Negative electric potential.....	52
5.2 Hydrogen adsorption on Pt-doped activated carbon	53
CHAPTER 6 EXAMINATION OF HYDROGEN ADSORPTION ON ACTIVATED CARBON SEPARATED BY TITANIUM DIOXIDE UNDER ELECTRIC FIELD	55
6.1 Hydrogen adsorption on mechanically mixed TiO ₂ /Carbon mixture.....	55
6.2 Hydrogen adsorption on TiO ₂ /Carbon synthetics prepared from TiO ₂ premix	56
6.2.1 Hydrogen adsorption with applied electric field	56
6.2.2 Hydrogen adsorption with the presence of piezoelectric element.....	62
6.3 Hydrogen adsorption on chemically deposited TiO ₂ /Carbon synthetics	66
6.4 Hydrogen adsorption on TiO ₂ -coated Pt/AC	74
CHAPTER 7 EXAMINATION OF HYDROGEN ADSORPTION ON ACTIVATED CARBON SEPARATED BY OTHER DIELECTRIC MATERIALS UNDER ELECTRIC FIELD	76
7.1 Hydrogen adsorption on MgO/Carbon species	76
7.2 Hydrogen adsorption on ZnO/Carbon species	77
7.3 Hydrogen adsorption on BaTiO ₃ /Carbon species	78
CHAPTER 8 COMPUTATIONAL CALCULATIONS	80
8.1 Introduction	80
8.2 Computational methods.....	83
8.3 Results and discussion.....	85
8.3.1 Hydrogen adsorption on charged TiO ₂ molecule	85
8.3.2 Hydrogen adsorption on TiO ₂ molecule under electric field.....	86
8.3.3 Hydrogen adsorption on coronene under electric field	87
8.3.4 Hydrogen adsorption on TiO ₂ -doped coronene under electric field.....	89
CHAPTER 9 SUMMARY AND CONCLUSIONS	92
REFERENCES	94
APPENDIX A.....	110
APPENDIX B	111
APPENDIX C	112

APPENDIX D	113
APPENDIX E	114
APPENDIX F	116
APPENDIX G	118
APPENDIX H	119

List of Figures

Figure 1.1	World consumption of primary energy of 2007	1
Figure 1.2	Illustration of PEM fuel cell	6
Figure 1.3	Estimates of gravimetric and volumetric capacities projected for on-board systems from year 2005 to 2010	9
Figure 2.1	Hydrogen adsorption capacity at 77 K and 1 bar for different carbon samples versus total pore volume and micropore volume	25
Figure 2.2	Isobars for hydrogen desorption from a certain activated carbon at 1 bar and isotherm data from adsorption at 1 bar	26
Figure 2.3	Approach for charged zone enlargement	29
Figure 3.1	Outlook of the PCT-Pro 2000 instrument	33
Figure 3.2	Master control panel of PCT-Pro 2000	34
Figure 3.3	Experimental setup for hydrogen adsorption measurement in the presence of PMN-PT	36
Figure 3.4	Configuration of PMN-PT	37
Figure 3.5	Cross-section view of modified sample holder	37
Figure 3.6	Cross-section view of sample holder used for resistivity test	39
Figure 4.1	XRD patterns of TiO ₂ /Carbon synthetics P1H1, P2H1, P3H1 and P4H1	41
Figure 4.2	FE-SEM images of P4 and P4H1	42
Figure 4.3	Relationship between BET surface area and micropore volume of TiO ₂ /Carbon synthetics	43
Figure 4.4	XRD patterns of chemical deposited TiO ₂ /Carbon synthetics TC1 and TC2	44
Figure 4.5	FE-SEM images of chemically deposited TiO ₂ /Carbon synthetics	45
Figure 4.6	TGA analyses of TiO ₂ /Carbon synthetics TC1 and TC2	46
Figure 4.7	XRD pattern of MgO/Carbon synthetic MC	48
Figure 4.8	FE-SEM images of MgO/Carbon synthetic MC	48
Figure 5.1	Hydrogen adsorption on blank sample holder with and without 1000 V electric potentials	49
Figure 5.2	Hydrogen adsorption on NAC under various electric potentials	51
Figure 5.3	Hydrogen adsorption on NAC with and without -1000 V electric potential	53
Figure 5.4	Hydrogen adsorption on PAC with and without 2000 V electric potential ..	54
Figure 6.1	Hydrogen adsorption on sample MM with and without 2000 V electric potential	56
Figure 6.2	Hydrogen adsorption on TiO ₂ /Carbon synthetics P1H1, P2H1, P3H1, P4H1 and NAC	57
Figure 6.3	Hydrogen adsorption isotherms of PTPD and blank test	57

Figure 6.4	Hydrogen adsorption on TiO_2 /Carbon synthetics P1H1, P2H1, P3H1 and P4H1 with and without 1000 V electric potential	59
Figure 6.5	Hydrogen adsorption normalized by BET surface area	60
Figure 6.6	Hydrogen adsorption on P4 with the presence of a PMN-PT	63
Figure 6.7	Change rate of hydrogen adsorption with the presence of a PMN-PT	63
Figure 6.8	Schematic of charge distribution with the presence of PMN-PT(+)	65
Figure 6.9	Relationship between hydrogen pressure and charges generated.....	66
Figure 6.10	Hydrogen adsorption on TC1, TC2 and NAC.....	67
Figure 6.11	Hydrogen adsorption on TC1 and TC2 with and without 1000 V electric potential	68
Figure 6.12	Hydrogen adsorption on HCl/NAC with and without 1000 V electric potential	69
Figure 6.13	Hydrogen adsorption on TiO_2 /Carbon synthetics TC2 under various electric potentials.....	70
Figure 6.14	Electricity detected by ammeter under various electric potentials.....	71
Figure 6.15	Adsorption change rate of TC2 at 20, 50 and 80 bar under various electric potentials.....	72
Figure 6.16	Illustration of hydrogen adsorption mechnisam under electric field.....	72
Figure 6.17	Hydrogen adsorption on TiO_2 -coated Pt/AC synthetic TPC under electric potential	75
Figure 7.1	Hydrogen adsorption on MgO/Carbon synthesis MC with and without electric potential	77
Figure 7.2	Hydrogen adsorption on ZnO/Carbon mixture ZC with and without electric potential	78
Figure 7.3	Hydrogen adsorption on BaTiO_3 /Carbon mixture BC with and without electric potential	79
Figure 8.1	Structure of coronene	84
Figure 8.2	Initial state of H_2 - TiO_2 system.....	85
Figure 8.3	Initial state of H_2 -coronene system.....	88
Figure 8.4	Initial state of H_2 - TiO_2 -coronene system.....	90

List of Tables

Table 1.1	Techniques for producing hydrogen.....	3
Table 1.2	Comparison of current fuel cell technologies	5
Table 2.1	Comparison of physisorption and chemisorption	20
Table 4.1	BET analyses of TiO ₂ /Carbon synthetics prepared from premix of TiO ₂ powder	43
Table 4.2	Electrical resistivity of TiO ₂ /Carbon synthetics prepared from premix of TiO ₂ powder	44
Table 4.3	BET analyses of chemically deposited TiO ₂ /Carbon synthetics TC1 and TC2	47
Table 4.4	Electrical resistivity of chemically deposited TiO ₂ /Carbon synthetics TC1 and TC2	47
Table 8.1	Geometric parameters and binding energies of H ₂ and charged TiO ₂	86
Table 8.2	Geometric parameters and binding energies of H ₂ and TiO ₂ under electric field	87
Table 8.3	Geometric parameters and binding energies of H ₂ and coronene under electric field	89
Table 8.4	Geometric parameters and binding energies of hydrogen and TiO ₂ -doped coronene under electric field	91

Acknowledgements

This dissertation would never have been finished without the guidance of my committee members, help of my friends and support from my family. It is a pleasure to convey my gratitude to them all in this acknowledgement.

In the first place, I would like to express my deepest gratitude to my advisor, Dr Jiann-Yang Hwang, for his excellent guidance, encouragement, and financial support. He guided me to the real research and taught me the way to think logically. His optimistic attitude to the life encouraged me to step out one difficulty and another.

I would like to thank my committee members Dr. Yun Hang Hu, Dr. David W. Hand, Dr. Paul V. Doskey and Dr. Xinli Wang for their precious advices.

I also would like to thank my current and previous group members, Shangzhao Shi, Xiang Sun, Zhiwei Peng, Chienyu Wen, Xiaodi Huang, Bowen Li, Matthew Andriese, Wayne Bell and Allison Hein for their collaborations.

I am very grateful to Ming Ning for his time and the patient guidance in computational calculations.

I would also like to thank Stephen F. Forsell, Owen P. Mills, Edward A. Latitila, Patrick D. Quimby and Ruth I. Kramer for their technical assistances in instrument operations and material preparations.

Special thanks go to my friends Shuhan Ding and Shuqian Xie, who have accompanied

my through the most difficult periods in Houghton. Chatting and laughing with them was the happiest thing of those days. Many thanks go to my other lovely friends, Xinxin Jin, Ming Xie, Wei Wang, Yunhua Li, Zhiyao An, Hui Wang, Yao Li, Liu Chen, Ding Chu. They have made my life more colorful.

Finally, I would like to thank my mother Xinmin Zeng, my father Wu Zhang and my husband Xuan Li. They were always supporting me and encouraging me with their best wishes.

This dissertation is dedicated to Xinmin, Wu and Xuan.

Abstract

Energy crisis and worldwide environmental problem make hydrogen a prospective energy carrier. However, storage and transportation of hydrogen in large quantities at small volume is currently not practical. Lots of materials and devices have been developed for storage hydrogen, but to today none is able to meet the DOE targets.

Activated carbon has been found to be a good hydrogen adsorbent due to its high surface area. However, the weak van der Waals force between hydrogen and the adsorbent has limited the adsorption capacity. Previous studies have found that enhanced adsorption can be obtained with applied electric field. Stronger interaction between the polarized hydrogen and the charged sorbents under high voltage is considered as the reason.

This study was initiated to investigate if the adsorption can be further enhanced when the activated carbon particles are separated with a dielectric coating. Dielectric TiO_2 nanoparticles were first utilized. Hydrogen adsorption measurements on the TiO_2 -coated carbon materials, with or without an external electric field, were made. The results showed that the adsorption capacity enhancement increased with the increasing amount of TiO_2 nanoparticles with an applied electric field. Since the hydrogen adsorption capacity on TiO_2 particles is very low and there is no hydrogen adsorption enhancement on TiO_2 particles alone when electric field is applied, the effect of dielectric coating is demonstrated.

Another set of experiments investigated the behavior of hydrogen adsorption over TiO_2 -coated activated carbon under various electric potentials. The results revealed that the hydrogen adsorption first increased and then decreased with the increase of electric

field. The improved storage was due to a stronger interaction between charged carbon surface and polarized hydrogen molecule caused by field induced polarization of TiO_2 coating. When the electric field was sufficient to cause considerable ionization of hydrogen, the decrease of hydrogen adsorption occurred. The current leak detected at 3000 V was a sign of ionization of hydrogen.

Experiments were also carried out to examine the hydrogen adsorption performances over activated carbon separated by other dielectric materials, MgO, ZnO and BaTiO_3 , respectively. For the samples partitioned with MgO and ZnO, the measurements with and without an electric field indicated negligible differences. Electric field enhanced adsorption has been observed on the activated carbon separated with BaTiO_3 , a material with unusually high dielectric constant.

Corresponding computational calculations using Density Functional Theory have been performed on hydrogen interaction with charged TiO_2 molecule as well as TiO_2 molecule, coronene and TiO_2 -doped coronene in the presence of an electric field. The simulated results were consistent with the observations from experiments, further confirming the proposed hypotheses.

CHAPTER 1 INTRODUCTION

Over the next decades, decreasing world supply of fossil fuels, and increasing global warming and climate change will be two major concerns. United States' development highly relies on petroleum, as shown in Figure 1.1. Among them, 2/3 of the petroleum is consumed in transportation ¹. US imports half of its petroleum and the dependence on foreign oil is expected to grow in the future. However, petroleum is a kind of non-renewable energy, which will probably run out in next 50 years if people keep the steps. Thus, an alternative energy source is highly demanded.

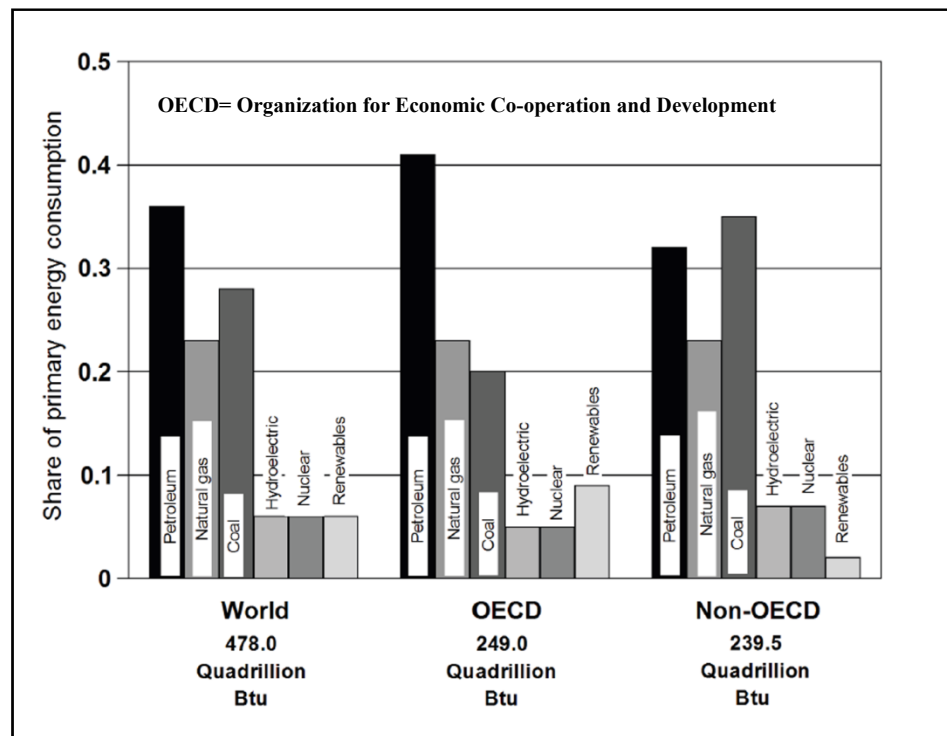


Figure 1.1 World consumption of primary energy of 2007 ¹ (graph courtesy of DOE, see Appendix A)

These years, environmental problem and global warming have attracted more and more attention. Scientific research is focused on clean and renewable energy source. According to US Department of Energy (DOE) database, transportation is responsible for 73% of

CO, 58% of NO_x and 33% of CO₂ in air pollution ¹. The pollutants come from the combustion of gasoline or diesel and need to be reduced by adopting clean energy. Hydrogen, which does not generate pollutants and greenhouse gas, is considered an ideal energy source to compensate or even take the place of fossil fuels. Application of vehicle powered by hydrogen will not only reverse today's situation, but also benefit long-term development.

Due to great advantages of hydrogen energy, President Bush launched the Hydrogen Fuel Initiative in 2003, which commits \$1.2 billion over five years to fund hydrogen fuel cell research. The fund would be used in the research of powering automobiles by hydrogen fuel cells, and also the studies of producing, storing and transporting hydrogen. The goal is to put hydrogen fuel cell vehicles in the showroom and hydrogen at fueling station by 2020 ².

1.1 Hydrogen energy

Hydrogen is qualified as ideal energy carrier largely due to its unique characteristics. Hydrogen is very abundant in the universe, which constitutes normal matters 75% by mass and >90% by number of atoms. Hydrogen is also the lightest element. Only a single proton is included in the protium (H), the most common isotope of hydrogen. Hydrogen possesses the highest gravimetric energy content (142 kJ/g) of all fuels, whereas liquid hydrogen's volumetric energy density (8 MJ/L) is only one quarter of that of gasoline ³. Water is the only product when hydrogen reacts with oxygen, so no pollutant is produced. Moreover, efficiency can be significantly increased if fuel cells with hydrogen are applied.

1.1.1 Hydrogen production

Although hydrogen is abundant, naturally occurring elemental hydrogen is relatively rare on Earth. In order to take use of hydrogen as energy carrier, molecular hydrogen is required to be produced. Generally, technologies for producing hydrogen can be classified into seven areas, as listed in Table 1.1. The first three ones have been commercialized and the others are still being studied in the lab.

Table 1.1
Techniques for producing hydrogen ⁴

	Technologies	Raw materials
Commercialized	Steam reforming	Light hydrocarbon gases (mainly CH ₄) and H ₂ O
	Gasification	Coal and H ₂ O
	Water electrolysis	H ₂ O
R&D	Gasification	Biomass and H ₂ O
	Thermo-chemical	Sulfur-iodine water-splitting cycle
	Bioprocess	Biomass or H ₂ O
	Photolysis	H ₂ O

Currently the dominant technology for direct production is steam reformation from natural gas, methanol, coal or even gasoline ⁵. In US, around 95% of the hydrogen is produced through this way ⁶. Gasification is also a process usually used to obtain hydrogen. It first converts fossil based carbonaceous materials into hydrogen, carbon monoxide and carbon dioxide and then separates the hydrogen from the resultant gas products. Another major source is collecting hydrogen as the product of water electrolysis. At present, the electric energy used to split water molecule is mainly from coal. All the three methods are largely depends on limited fossil fuel source, so it is highly demanded

to find out sustainable techniques for hydrogen production.

The latter four techniques under development are very promising due to the utilization of renewable energy sources. The novel gasification is producing hydrogen from gasification of biomass resources such as agricultural residue, including waste grease, peanut shells or crops ⁷. The thermo-chemical way only uses solar and nuclear energy in waste splitting cycle. Bioprocess system use natural photosynthetic microbes such as green algae and bacteria to produce hydrogen by splitting water. Photolysis is a process that splits water to obtain hydrogen using sunlight as the only energy source.

1.1.2 Hydrogen fuel cell

To make best use of hydrogen energy, fuel cell is introduced. A fuel cell is an electrochemical cell to convert fuel to electricity and chemical products. A single fuel cell is composed of an electrolyte sandwiched between two catalyst-coated electrodes, a porous anode and a porous cathode. Depending on the difference of electrolytes, fuel cells can be sorted as alkaline fuel cell (AFC), polymer electrolyte membrane or proton exchange membrane fuel cell (PEM), phosphoric acid fuel cell (PAFC), molten carbonate fuel cell (MCFC) and solid oxide fuel cell (SOFC). Operating temperature, efficiency of each type of fuel cell is given in table 1.2. Efficiency of fuel cell lies between 45%-60%, which is much higher than that of internal combustion engines using fossil fuels (< 20%)

^{8,9}.

Table 1.2
Comparison of current fuel cell technologies ⁸

Fuel Cell Type	Operating Temperature	Typical Stack Size	Efficiency	Advantages	Disadvantages
Polymer Electrolyte Membrane (PEM)	50-100 °C	<1kW-100kW	60% transportation 35% stationary	<ul style="list-style-type: none"> • Solid electrolyte reduces corrosion • Low temperature • Quick start-up 	<ul style="list-style-type: none"> • Expensive catalysts • Sensitive to fuel impurities • Low temperature waste heat
Alkaline (AFC)	90-100 °C	10-100kW	60%	<ul style="list-style-type: none"> • Cathode reaction faster in alkaline electrolyte • Low cost components 	<ul style="list-style-type: none"> • Sensitive to CO₂ in fuel and air • Electrolyte management
Phosphoric Acid (PAFC)	150-200 °C	400kW 100kW module	40%	<ul style="list-style-type: none"> • Higher temperature enables CHP • Increased tolerance to fuel impurities 	<ul style="list-style-type: none"> • Pt catalyst • Long start up time • Low current and power
Molten Carbonate (MCFC)	600-700 °C	300kW-3MW 300kW module	45-50%	<ul style="list-style-type: none"> • High efficiency • Fuel flexibility • Can use a variety of catalysts • Suitable for CHP 	<ul style="list-style-type: none"> • High temperature corrosion and breakdown of cell components • Long start up time • Low power density
Solid Oxide (SOFC)	700-1000 °C	1kW-2MW	60%	<ul style="list-style-type: none"> • High efficiency • Fuel flexibility • Can use a variety of catalysts • Solid electrolyte • Suitable for CHP&CHHP • Hybrid/GT cycle 	<ul style="list-style-type: none"> • High temperature corrosion and breakdown of cell components • High temperature operation requires long start up time and limits

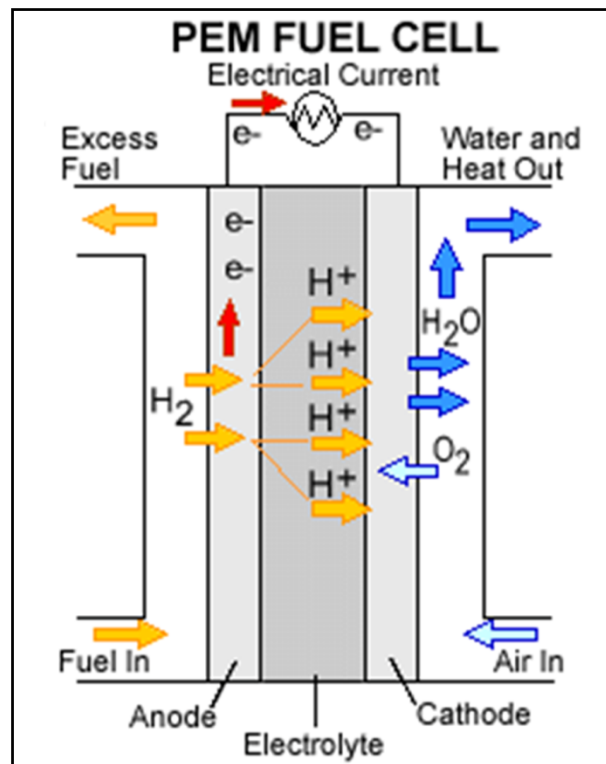


Figure 1.2 Illustration of PEM fuel cell ⁹ (graph courtesy of DOE, see Appendix B)

PEM is widely considered as the most suitable fuel cell for light duty transportation. Configuration of PEM is shown in Figure 1.2. Hydrogen and oxygen gases are fed through each bipolar plate to anode and cathode, respectively. At the anode Hydrogen molecules are dissociated to protons and electrons and then protons move through the membrane to the other side of the cell while the electrons flow along the external circuit to the cathode. At the cathode, oxygen molecules arrest the electrons from the anode and form water with protons by exothermic reaction. Current operation cost of PEM is too high to afford, which indicates existing technologies need further improvement.

Although hydrogen owns attractive bright sides for being the new generation of energy, there is still a long way to go to put it into commercial use due to critical barriers, among which, hydrogen storage is the most crucial one.

1.1.3 Hydrogen storage

The application of hydrogen energy may proceed probably via portable storage of hydrogen first. A medium with high-capacity hydrogen storage is hunted to better promote the use of hydrogen as an energy source, particularly applications in transportation. Conventional methods to store hydrogen include compression and liquefaction of hydrogen. However, these methods are unlikely able to satisfy practical application in the future due to safety and economic issues¹⁰⁻¹². The storage approach most researchers interested in is to make hydrogen interact with a host material, like metal hydrides, complex hydrides, nanostructured carbon and metal organic frameworks (MOFs)^{10,11}.

Table 1.3 illustrate the requirements renewed by DOE in 2011 on a storage system for fuel cell electric vehicles running on hydrogen. It is noted that the targets shown in the table (5.5 wt.% and 40 g hydrogen/L by 2017) are capacities for the whole storage system, including adsorbent materials, container, and all the other related components. Previous targets by 2010 have not been really fulfilled. Research on hydrogen storage has been pursued for decades and improvement in storage system capacity obtained in recent years can be seen in Figure 1.3. The data points are obtained by averaging all the analyzed values during each year. The bars indicate the range of values acquired in each year. Although recent achievements indicate materials-based capacities exceeding 5 wt.%, capacities will fall far below the targets if system is counted. None of the current systems meets the combination target of gravimetric, volumetric and system cost for 2017¹³.

Table 1.3
DOE's hydrogen storage target ¹³ (table courtesy of DOE, see Appendix C)

Storage Parameter	Units	2017	Ultimate
System Gravimetric Capacity:			
Usable, specific-energy from H ₂ (net useful energy/max system mass) ^a	kWh/kg (kg H ₂ /kg system)	1.8 (0.055)	2.5 (0.075)
System Volumetric Capacity:			
Usable energy density from H ₂ (net useful energy/max system volume)	kWh/L (kg H ₂ /L system)	1.3 (0.040)	2.3 (0.070)
Storage System Cost ^b:			
Fuel cost ^c	\$/kWh net (\$/kg H ₂) \$/gge at pump	TBD (TBD) 2-4	TBD (TBD) 2-4
Durability/Operability:			
Operating ambient temperature ^d	°C	-40/60 (sun)	-40/60 (sun)
Min/max delivery temperature	°C	-40/85	-40/85
Operational cycle life (1/4 tank to full) ^e	Cycles	1500	1500
Min delivery pressure from storage system; FC= fuel cell, ICE= internal combustion engine	bar (abs)	5FC/35 ICE	3 FC/35 ICE
Max delivery pressure from storage system ^f	bar (abs)	12 FC/100 ICE	12 FC/100 ICE
Onboard Efficiency	%	-	90
"Well" to Powerplant Efficiency	%	-	60
Charging / Discharging Rates:			
System fill time (5 kg)	min	3.3	2.5
Minimum full flow rate	(kg H ₂ /min)	(1.5)	(2.0)
Start time to full flow (20 °C) ^g	(g/s)/kW	0.02	0.02
Start time to full flow (-20 °C) ^g	s	5	5
Transient response 10%-90% and 90% - 0% ^h	s s	15 0.75	15 0.75
Fuel Purity (H₂ from storage) ⁱ	% H ₂	SAE J2719 and ISO/PDTS 14687-2 (99.97% dry basis)	
Environmental Health & Safety:			
Permeation & leakage ^j	Scch/h	Meets or exceeds applicable standards	
Toxicity	-		
Safety	-		
Loss of useable H ₂ ^k	(g/h)kg H ₂ stored	0.05	0.05

* Useful constants: 0.2778kWh/MJ; 33.3kWh/kg H₂; 1 kg H₂ ≈ 1 gal gasoline equivalent.

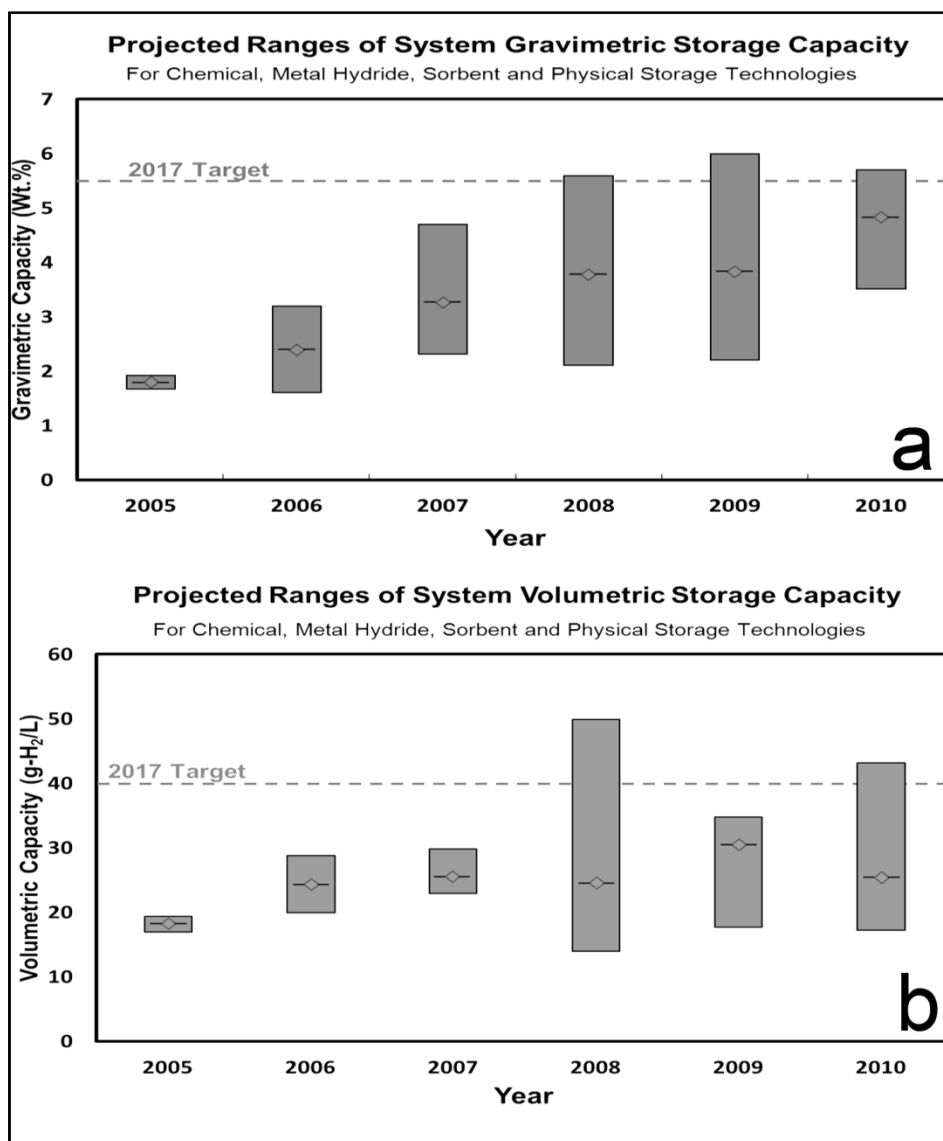


Figure 1.3 Estimates of (a) gravimetric and (b) volumetric capacities projected for on-board systems from year 2005 to 2010 ¹³ (graph courtesy of DOE, see Appendix D)

1.2 Hydrogen storage materials

1.2.1 Metal hydrides

Hydrogen can react with metals and alloys at elevated temperature to form metal hydrides. Hydrides are considered to exist in ionic, covalent, and metallic forms, but the boundary between them is not that sharp ¹⁴. Metal hydrides are very promising as they

allow the storage of large amounts of hydrogen in a small volume at room temperature. MgH_2 is considered as the most possible hydride for on-board hydrogen storage, since it is a costless and reversible medium with storage capacity as high as 7.7 wt.%. However, the temperature required to release hydrogen is around 300 °C^{15,16}, which is much higher than the operation temperature of PEM fuel cell. The binary hydrides of the transition metals predominantly show metallic characteristics, like conductive and metallic-like appearance. In such compounds (MH_n), the hydrogen usually takes up interstitial sites, resulting in large scales of non-stoichiometry. Many transition metals have stable hydrides except for the part from group 6 (Cr) to group 11 (Cu), resulting in the demand of very high temperature to harvest hydrogen from the hydrides¹⁴. This drawback makes the binary hydrides unable to be applied in a vehicle driven by hydrogen.

Typical alloys for hydrogen storage can be divided into three categories: AB, AB₂ and AB₅, in which A is a rare earth or alkaline earth metal tending to form stable hydrides and B is a transition metal forming only unstable hydrides¹⁷⁻¹⁹. A typical AB₅ alloys LaNi_5 can adsorb ~1.4 wt.% hydrogen at 0.2 MPa room temperature²⁰. Not to mention the low storage capacity, the high price of lanthanum largely prevents the further development of this material. For some AB₂ compounds (A=Ti, Zr, Mg; B=V, Cr, Fe, Mn) with cheaper elements, up to 2 wt.% hydrogen uptakes can be obtained¹⁵. However, at room temperature, the hydrogen pressures at equilibrium are relatively low and not suitable for practical uses.

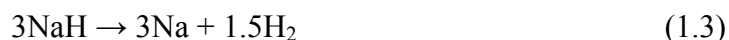
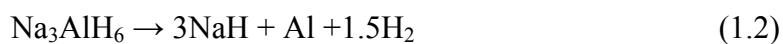
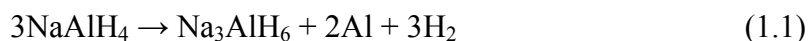
As most metal hydrides are in solid phase, the volumetric target of DOE (> 0.040 kg H₂/L) is not a big issue for such materials. Classical metal hydrides usually contain transition metals, so the gravimetric capacity for hydrogen is limited to roughly 2 wt.%, much lower than the DOE target (>5.5 wt.% H₂). To realize on-board automotive applications,

most current research on metal hydrides for hydrogen storage is focused on using light weight metals, such as Al, Mg and Na, to develop new materials that have high gravimetric hydrogen density and also satisfy the kinetic and thermodynamic requirements for hydrogen uptake and release.

1.2.2 Complex hydrides

As conventional metal hydrides only have hydrogen storage capacities no greater than 2 wt.% at room temperature, much attention has been paid to the complex hydrides which are composed primarily of light elements ($Z \leq 13$) with the interest of high gravimetric capacities. In a complex hydride, hydrogen is covalently bonded to a central atom to form a complex anion and stabilized by a cation, typically an alkali or alkaline earth metal.

Complex hydrides have shown surprising gravimetric capacities. One of the best performing and well studied reversible complex hydrides is sodium alanate (NaAlH_4), which has a theoretical storage capacity of 6.7 wt.% in total that can be described in a three-step reaction ²¹

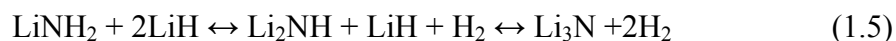


The first and second decomposition steps can release 3.7 wt.% and 1.9 wt.% hydrogen at 0.1 MPa and reasonable temperature. The decomposition temperature required for the third step is very high for on-board applications and thus most of the time it is not regarded as a hydrogen source. Another very popular complex hydride LiBH_4 is able to

discharge 13.5 wt.% hydrogen at temperature $> 380\text{ }^{\circ}\text{C}$ according to the following reaction²²



Hydrogen uptake by Li_3N was first discovered by Dafert and Miklauz²³ a hundred years ago. Significant attention has not been paid to it until Chen and co-workers recently proposed it as a promising candidate for hydrogen storage with overall 10.4 wt.% adsorption capacity. The hydrogen storage and generation process is composed of following two steps²³



At temperature of up to $200\text{ }^{\circ}\text{C}$, 6 wt.% hydrogen can be desorbed, while a complete desorption requires temperature as high as $420\text{ }^{\circ}\text{C}$.

As a result of high thermodynamic stability of complex hydrides, high temperature is usually needed to release hydrogen. Current research efforts are devoted to reducing the decomposition enthalpy by introducing a second species that can stabilize the reaction product. In addition, creating nanoscale powders and incorporating the hydride into nanoporous scaffolds or frameworks have also been tested to improve the reaction kinetics²⁴.

1.2.3 Nanostructured carbon

The carbon materials with porous structure have attracted considerable attentions as potential hydrogen storage media mainly due to their low cost, low density and good

chemical stability.²⁵ A series of carbon materials have been intensively studied, like carbon nanofibers (CNFs), carbon nanotubes (CNTs), activated carbons (ACs), and ordered porous carbons²⁶⁻³¹. As most porous materials, the hydrogen adsorption mechanism on nanostructured carbon is primarily based on physisorption.

As ACs have the characteristics of enormous chemical and structural complexity and heterogeneity, the hydrogen uptakes on ACs differed with a marked dependency on the materials employed^{25,27,32,33}. Yang and colleagues obtained an exceptionally high hydrogen storage capacity of around 7 wt.% at 77 K and 20 bar over a microporous carbon synthesized by templating using zeolite beta³². However, at room temperature and high pressure (100 bar) the highest storage value is still below 1 wt.%, even via highly developed porous carbon specific with surface area of greater than 3700 m²/g³⁴.

Dillon et al.³⁵ reported for the first time on hydrogen storage in CNTs in 1997. Since then, single-wall carbon nanotubes (SWCNTs) and multi-wall carbon nanotubes (MWCNTs) have attracted considerable attention for hydrogen storage. The known carbon structure is considered as the major advantage of CNTs, which can correlate experimental results with theoretical predictions and better illuminate the adsorption mechanism. However, the presence of metal impurities in CNTs from production process may cause unpredictable influence on the storage behaviors, because the distribution and chemisorption effects of those metals are very various³⁶. Some exciting results have been reported in early time, even with hydrogen storage value up to 14 wt.%^{35,37,38}. Nevertheless, these extremely high results were finally proven to be caused by errors in the experiments^{39,40}. The hydrogen adsorption capacities of SWCNTs and MWCNTs have been demonstrated by abundant studies to be no greater than 1 wt.% at ambient temperature and around 100 bar⁴¹⁻⁴⁵, but can be enhanced to between 5 to 8 wt.% when

conducting tests at 77 K ^{42,44,46,47}.

Countless reports have demonstrated that the hydrogen storage capacities in pure carbon materials achieved by physisorption are impossible to meet targets of DOE.

1.2.4 Metal organic frameworks (MOFs)

Metal organic frameworks are porous crystalline compounds constructed by metal ions or small metal cluster joint together by organic ligand linkers. Recently, MOFs has been developed to store hydrogen due to their extremely large surface area and potential applications as sorbents ⁴⁸⁻⁵². Typical MOFs have inorganic groups $[\text{OZnO}_4]^{6+}$ at the corner of the structure and are connected with carboxylate organic links ⁴⁸. The linkers are isolated from each other but can be accessed from all sides, leading to extremely high surface areas up to 5000 m²/g of such materials. According to theoretical calculations, hydrogen preferred to be adsorbed to the sites of metal oxide clusters in MOFs, but increasing the pressure would cause the effect of organic linker more evident ⁵³. Also, the character of the organic bridges affected the interaction of hydrogen with the inorganic cluster sites ⁵⁴. To achieve relatively high adsorption capacity, MOFs are required to possess high surface area structure with interconnected small pores for a strong interaction with hydrogen ⁵².

In 2003, Yaghi et al. first reported a high hydrogen adsorption of 4.5 wt.% on MOF-5 ($\text{Zn}_4\text{O}(\text{bdc})_3$) at 77 K and less than 1 bar ⁴⁸. The results were lower in their latter work ^{55,56}. Other publications revealed MOF-177 ($\text{Zn}_4\text{O}(\text{BTB})_2$) had a super large BET surface area up to 4700 m²/g and the highest hydrogen storage of 7.5wt.% at 77 K and 70 bar ^{57,58}. Although some kinds of MOFs have remarkable hydrogen capacities at 77 K, no significant hydrogen storage capacity was observed on MOFs at room temperature. The

temperature is apparently a crucial factor to assess hydrogen storage behavior in MOFs, just like the ACs. No finding has been addressed that the increase of pressure alone is likely to improve hydrogen adsorption at room temperature to a comparable level at 77 K⁴⁶. Extensive work will be directed toward the synthesis of effective MOFs with larger heat of hydrogen adsorption.

1.2.5 Metal oxides

Metal oxides attract attention for hydrogen adsorption due to their wide application in catalysis⁵⁹⁻⁶¹, gas storage⁶²⁻⁶⁴, and sensors⁶⁵. Most metal oxides possess unsaturated metal centers, which accounts for strong interaction with hydrogen^{66,67}. Synthesizing highly porous metal oxides for hydrogen storage remains a tough task.

Titanium oxide (TiO₂) is the most studied metal oxide for hydrogen storage^{62, 68-71}. Lim et al.⁷⁰ reported hydrogen storage capacities up to ~2 wt.% at room temperature and 6 MPa over synthesized TiO₂ nanotube. Around 75% stored hydrogen was releasable under ambient pressure and others could be desorbed at 120 °C. Experimental results from Bavykin et al.⁷¹ showed that around 1.5 mol H₂ could be adsorbed to 1mol TiO₂ at 77 k and 2 bar, corresponding to 3.75 wt.% storage capacity. Complete desorption needed to heat the sample in a vacuum to 200 °C. For a commercial pure ZnO (nanopowder, 30 nm in diameter), hydrogen uptake at room temperature and 860 psi was 1.05 wt.% , 65.2% of which could be released⁷². The incomplete desorption indicated that both physisorption and chemisorption are responsible for the hydrogen uptake on metal oxides^{72,73}. Hydrogen uptakes on porous NiO (382.56 m²/g) and MgO (363.59 m²/g) at room temperature were 0.08 wt.% at 135 bar and 0.2 wt.% at 90 bar, respectively⁶⁴. Although the reported hydrogen storage capacities of the metal oxides are not that impressive, efforts may be devoted to combine the oxides with other materials for better results.

1.3 New approaches to hydrogen storage

1.3.1 Hydrogen spillover

The introduction of spillover techniques to hydrogen adsorption process encourages scientists who are working on hydrogen storage. Hydrogen spillover may be broadly defined as the transportation of dissociated hydrogen adsorbed or formed on a first surface onto another surface. The first surface is typically a metal and the second surface is usually the support on which the metal is doped³⁴. It was theoretically predicted that isolated transition metal atoms (Sc, Ti, V, Pt, Pd, etc) stabilized on sp^2 -hybridized carbons (nanotubes, fullerenes, graphenes etc) induce multiple bonding of molecular H_2 with adsorption energies intermediate between physisorption and chemisorption⁷⁴. By applying the spillover approach, considerable enhancement can be obtained at 298 K on a lot of sorbents, which includes both SWCNTs and MWCNTs⁷⁵⁻⁷⁸, CNFs⁷⁶, ACs^{78,79}, MOFs^{80,81}, and so on.

Lueking and Yang⁷⁵ studied hydrogen storage on MWCNTs with various degrees of catalyst (Ni, Mg) removal and observed that removal of the catalyst decreased the uptake from 0.6 wt.% to below detection limits. Yang and Li⁷⁹ doped Pt nanoparticles on a superactivated carbon (AX-21). The hydrogen storage capacity of carbon sample without doping was just 0.6 wt.% at 298 K and 100 bar, while that of doped carbon achieved 1.2 wt.% under the same condition. Furthermore, MOF-177 got an enhancement factor of ~ 2.5 at 298 K and 100 bar by doping with Pt, from 0.62 wt.% to 1.5 wt.%⁸¹. A large number of computational results have also demonstrated the dissociative chemisorption of hydrogen on different solid state materials⁸².

1.3.2 Combination of light metal hydrides and carbon materials for hydrogen storage

In recent years, carbon materials have been reported to lead to improvement in kinetics and thermodynamics of hydrogen adsorption for different metal hydride systems. Carbon materials have been chosen as additive or support because of their light weight, relative inertness, porosity and abundance. Carbon is also able to bond with itself (and other atoms) with different hybridizations, giving rise to allotropes of completely different properties. In addition, the ability of carbon to efficiently conduct heat and the fast hydrogen diffusion along the carbon phase can improve the hydrogen adsorption properties⁸³.

A lot of research has been devoted to ball-milling of MgH_2 or NaAlH_4 with different carbon materials⁸⁴⁻⁸⁶, among which CNTs and CNFs show the best performance. Imamura et al.⁸⁷ reported enhanced hydrogen adsorption properties for supported Mg nanoparticles that were synthesized by solution impregnation of activated carbon with magnesium dissolved in ammonia. Liang and Kung⁸⁸ calculated a decrease in enthalpy of formation by 50% for the confinement of MgH_2 clusters in (10, 10) CNTs of 1.2 nm in diameter. Another example for the kinetics improvement of hydrogen discharge is NaAlH_4 particles of 2-10 nm deposited on CNFs. Activation energy of the first decomposition step decreased from 116 kJ/mol to 58 kJ/mol⁸⁹.

1.3.3 Electric field assisted hydrogen adsorption

Over decades, hydrogen storage development is focused on searching novel materials and improving fabrication techniques. Recently a novel method has been proposed by Hwang's group⁹⁰⁻⁹³ to increase hydrogen storage capacity by applying an external electric field. Polarization of hydrogen molecule may occur under electric field and thus

leads to a stronger interaction between hydrogen and adsorbents ⁹³. The approach is expected to make materials synthesis less complicated while improving the thermodynamics and reversibility of hydrogen storage.

It was observed by Li et al. ⁹⁰ that electric field could lead to enhanced hydrogen adsorption over activated carbon and the adsorption increased with the increase in applied voltage. At 83 bar, the adsorption capacity increased from 0.45 wt.% at 0V to 0.46, 0.49, 0.53 and 0.55 wt.% at 500, 1000, 2000 and 3000 V, respectively. Sun et al. ⁶⁴ introduced an external electric field to metal oxide sorbents and found that it could increase hydrogen uptake by 37.5% for NiO and 25% for MgO in range of 0 to 60 bar. A computational work conducted by Liu and co-workers ⁹⁴ also reported that hydrogen storage over graphenes can be enhanced by introducing an electric field. Additionally, calculations by Zhou et al. ⁹⁵ showed an applied electric field can substantially improve the hydrogen capacity of polarizable boron nitride (BN) substrates. These findings may stimulate further research in this direction.

CHAPTER 2 BACKGROUND AND LITERATURE REVIEW

2.1 Hydrogen adsorption mechanism

No matter how developed the materials or methods for hydrogen storage are, adsorption properties are ultimately determined by the nature and strength of the fundamental binding between hydrogen and the storage material. A weak binding would lead to very low hydrogen storage capacity at ambient temperature, while a strong interaction might result in irreversible adsorption or need extreme conditions to discharge hydrogen. Therefore, it is essential to understand the hydrogen adsorption mechanism for better developing adsorbents that possess desired interactions with hydrogen.

The process of trapping or binding hydrogen to surface of adsorbent is known as adsorption. There are two types of adsorption: physisorption and chemisorptions. All the hydrogen adsorption processes can be attributed to either or both of them. The major properties of physisorption and chemisorption are given in Table 2.1. Physisorption theoretically can take place between any gas molecule and any solid surface if the temperature is low enough, and multilayer adsorbate molecules can be attached during this exothermic process. Interactions based on physisorption are usually very weak and will decrease with increasing temperature. Chemisorption takes place only at specific sites and only a monolayer of adsorbates can be attached to adsorbent surface. Chemisorption can be either exothermic or endothermic, so its behaviors in different cases highly depend on surrounding temperature.

It was estimated that ideal hydrogen binding affinity should be in the range of 20-40 kJ/mol⁹⁶. Binding energy lower than 20 kJ/mol correspond to complexes that can hardly exist at ambient condition, while binding energy higher than 40 kJ/mol would cause

trouble in hydrogen desorption. As shown in the Table 2.1, adsorption heat of physisorption is only ~ 10 kJ/mol, while that of chemisorptions is much higher than desired binding energy. Thus, reversible hydrogen storage cannot depend on either physisorption or chemisorption alone.

Table 2.1
Comparison of physisorption and chemisorption ⁴

	Physisorption	Chemisorption
Cause	Van der Waals forces	Chemical bonding
Adsorbents	All solids	Some solids
Adsorbates	All gases	Some chemical reactive gases
Temperature	Low temperature	Higher temperatures
Heat of adsorption	Low (~ 10 kJ/mol)	High (80-200 kJ/mol)
Rate	Very fast	Temperature-dependent
Surface coverage	Multilayer	Monolayer
Reversibility	High reversible	Temperature-dependent
Application	Determination of surface area and pore size	Determination of active site of catalysts

Hydrogen can either interact with the adsorbent as a molecular or dissociate to bond with the material. The former interaction can be achieved via either physisorption or chemisorption, which is the way nanostructured carbon and MOFs interact with hydrogen. The latter is chemisorption involving breakdown and formation of chemical bonds. Hydrogen storage using metal hydrides and complex hydrides is classified to this category. Some light metal hydrides like MgH_2 possesses very attractive storage capacity, but strong hydride bond of around 75 kJ/mol requires temperature up to 300 °C to completely release hydrogen. In most cases, such processes are irreversible or partially

irreversible¹¹.

Adsorption of molecular hydrogen over sorbent materials depends on three types of interactions: van der Waals force, electrostatic interactions and orbital interaction⁹⁶. Van der Waal attraction is the weakest and always exists between electron clouds that do not overlap. The interaction between hydrogen and neutral carbon is considered primarily van der Waals force, which is typically in the order of a few kJ/mol. Theoretical investigations suggest that hydrogen adsorption materials rely only on this interaction is impossible to fulfill DOE target at ambient temperature.

When hydrogen gets close to the charged sites, an interaction known as electrostatic interaction which is stronger than van der Waals can be formed. In the presence of other charges, hydrogen would be moderately polarized, which induces a dipole moment in the molecule by distorting the bonding σ orbital. Overlap of the electron clouds may occur and makes the binding stronger. The strength of the binding mainly depends on the nature of the charged site⁹⁷. Adsorption energy is expected to be enhanced by introducing alkali metal ions to matrix materials such as carbon through doping treatment. Interaction of hydrogen and alkali-doped graphene was simulated to be around 10 kJ/mol^{98,99}.

Orbital interaction is a strong existing binding between hydrogen molecule and transition metal (TM). TM-H₂ bond is stabilized by the “forward donation of the H-H electron density into low-lying vacant metal d-orbital and back-donation from the metal to the anti-bonding σ^* H₂ orbital”. Transition metal-hydrogen complexes can capture and release H₂ reversibly and the range of the TM-H₂ binding energy varies between 20 and 160 kJ/mol⁹⁷. Although the very high atomic weights of the transition metals are not beneficial for obtaining high gravimetric density, the idea of strong σ -bonded H₂

complexes is still possible to be exploited for further development of novel hydrogen storage materials.

2.2 Hydrogen cluster

2.2.1 Hydrogen ion cluster

Unlike van der Waals bonded neutral cluster, hydrogen ion cluster is at transition from a chemical bound molecular to a van der Waals bound cluster¹⁰⁰. Since Thomson first discovered H_3^+ in 1912¹⁰¹, a lot of experimental and theoretical work has been thrown into the investigation of H_n^+ ($n = 3, 5, 7, 9, 11, 13$) clusters. H_3^+ has been proven to be a very stable ion with a structure of equilateral triangular¹⁰². The reaction of $H_3^+ \rightarrow H_2 + H^+$ is endothermic and its required energy was calculated as 106 kcal/mol¹⁰³. The geometrical structures of H_n^+ clusters have been simulated to be composed of a H_3^+ in the core, which is surrounded by weakly bound H_2 molecules¹⁰¹. As the cluster size n increases, the distance between the core triangle and external molecules increases, and the dissociation energies decreases. In addition, the interaction between the electron-hole delocalization and ion-molecules polarization also becomes significantly reduced, resulting in lower bonding energies. Hiraoka and Kebarle¹⁰⁴ plot Van't Hoff curves for equilibrium $H_n^+ + H_2 = H_{n+2}^+$ and showed the dissociation enthalpies were 9.6, 4.1, 3.8, and 2.4 kcal/mole for $n = 3, 5, 7, 9$, respectively.

Negative hydrogen ion clusters H_n^- ($n = 3, 5, 7, 9, 11, 13$) have also been reported^{105,106}. The existence of negative ion clusters is critical, as their stabilization energy is very small (< 1 kcal). Hirao and Yamabe¹⁰⁶ examined the structure and stability of H_n^+ and H_n^- , revealing that H_n^+ is a “charge-transfer complex”, while the stability of H_n^- comes primarily from the “ion-induced-dipole attractions”.

2.2.2 Metal hydrogen cluster

Besides hydrogen ion cluster, hydrogen is capable of forming clusters with metals. The experimental work by Kubas et al.¹⁰⁷ first showed that H₂ could be attached as an uninserted species to an oxidized transition metal center. Since then, lots of experiments and simulations have been conducted on metal hydrogen clusters. The results showed that monovalent alkali metal cations (Na⁺ and K⁺) have much lower gas phase H₂ binding energies than the transition metal cations. H₂ molecules and the first row transition metals typically form clusters with the general formula of [M(H₂)_n]⁺ (M = Sc, Ti, V, Cr, Mn, Fe, Co, Ni, Cu, Zn; n = 1-6)¹⁰⁸. Unexpectedly, the gas phase measurements revealed that the bond dissociation energy (BDE) typically increases from n = 1 to n = 2 for the transition metal ions. For example, a experiment was conducted to generate [Ti(H₂)_n]⁺ clusters using TiCl₄ as ion source and the BDEs were 7.5, 9.7, 9.3, 8.5, 8.2, 8.7 kcal/mol for n=1-6, respectively¹⁰⁹. This initial increase has been attributed to the mixing between the 3dσ orbital and the empty 4s orbital, which is already present in the [M(H₂)⁺] cluster. The linear geometry of the [M(H₂)₂]⁺ cluster allows both H₂ ligands to share the cost of the hybridization, resulting in a larger BDE to the second H₂ molecule¹¹⁰. Further increase of n for all transition metal ions just leads to a mild decrease in BDE.

The binding of H₂ to transition metal dimer cations ([M₂(H₂)_n]⁺) has been rarely examined. Manard and co-workers⁶⁷ used equilibrium methods to measure binding energies and entropies for the attachment of up to six H₂ ligands to ground-state Cu₂⁺. BDEs of the six H₂ ligands added are 12.4, 10.1, 4.9, 3.8, 2.1 and probable 1.7 kcal/mol for dissociated H₂ number of 1, 2, 3, 4, 5 and 6, respectively.

2.3 Influential factors of hydrogen storage on carbon materials

Although pristine carbon adsorbents primarily capture hydrogen molecules by weak

attractions, their fast adsorption and desorption kinetics is still attractive for fast charging and discharging of hydrogen. Several factors are responsible for hydrogen adsorption characteristics on carbon materials such as the accessible surface area, the pore sized and the applied temperature and pressure.

2.3.1 Porous structure

Porous structure of carbon materials is the key factor in determining hydrogen storage capacity. As a portion of the pores in the carbon is small enough to capture the H₂ molecule, the narrowest porosity in the carbon sample play a decisive role in hydrogen adsorption characteristics. Micropores with pore size smaller than 0.6 nm have been reported to be the effective sites for hydrogen adsorption in porous materials ²⁵. Mesopores contribute to the total pore volume but relatively very little to adsorption capacity. Thomas ⁴⁶ collected hydrogen adsorption data obtained at 77 K and 1 bar on a bunch of nanostructured carbon materials with wide ranges of total pore volume and micropore volume, as shown in Figure 2.1. The correlation between hydrogen uptake and total pore volume showed greater scatter in the data. Some of the carbon materials only adsorbed a small amount of hydrogen, even though they possessed very high total pore volume. However, an approximately linear relation was found between hydrogen captured and micropore volume, which indicated larger micropore volume could lead to more captured hydrogen molecules.

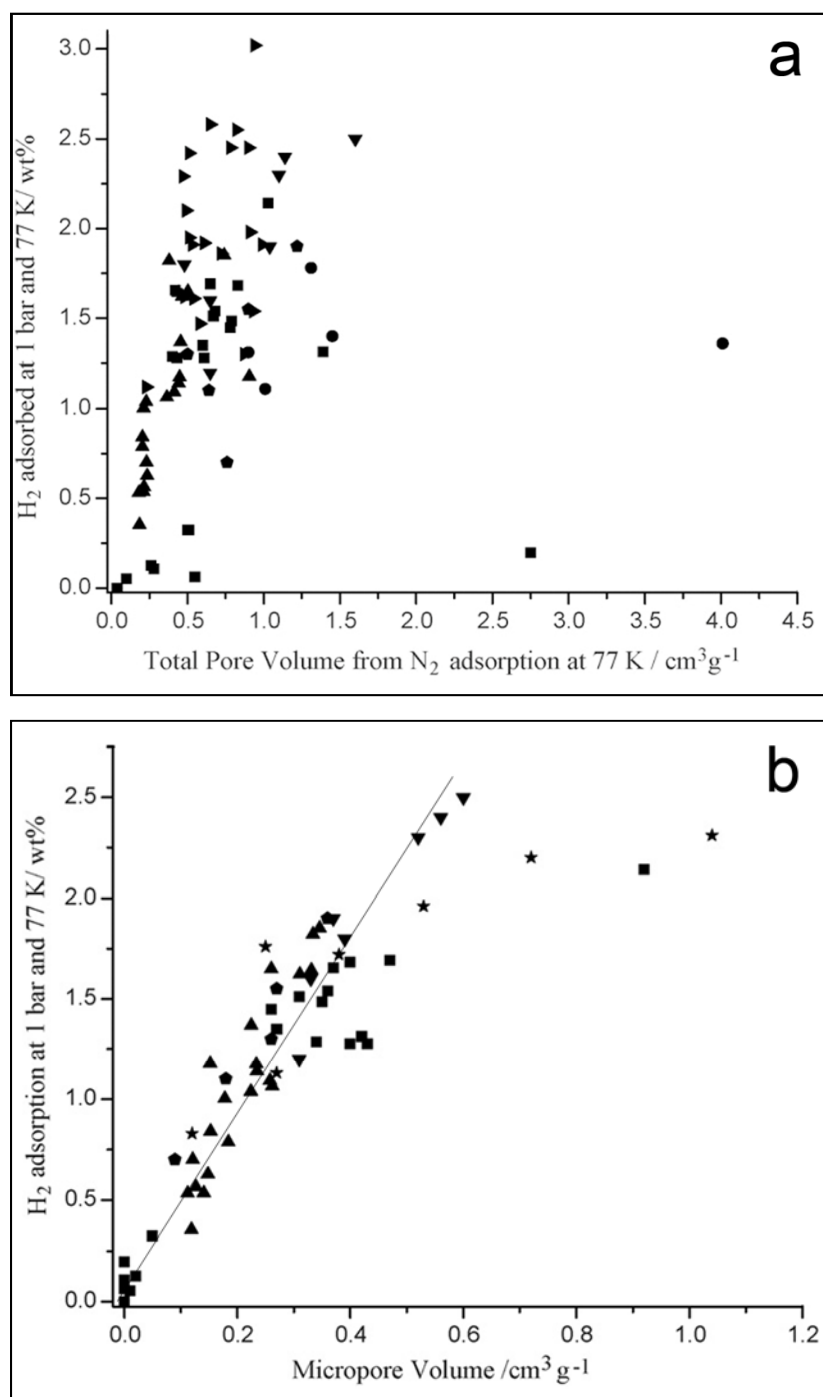


Figure 2.1 Hydrogen adsorption capacity at 77 K and 1 bar for different carbon samples versus (a) total pore volume and (b) micropore volume ⁴⁶ (reprinted with permission from Elsevier, see Appendix E)

2.3.2 Temperature

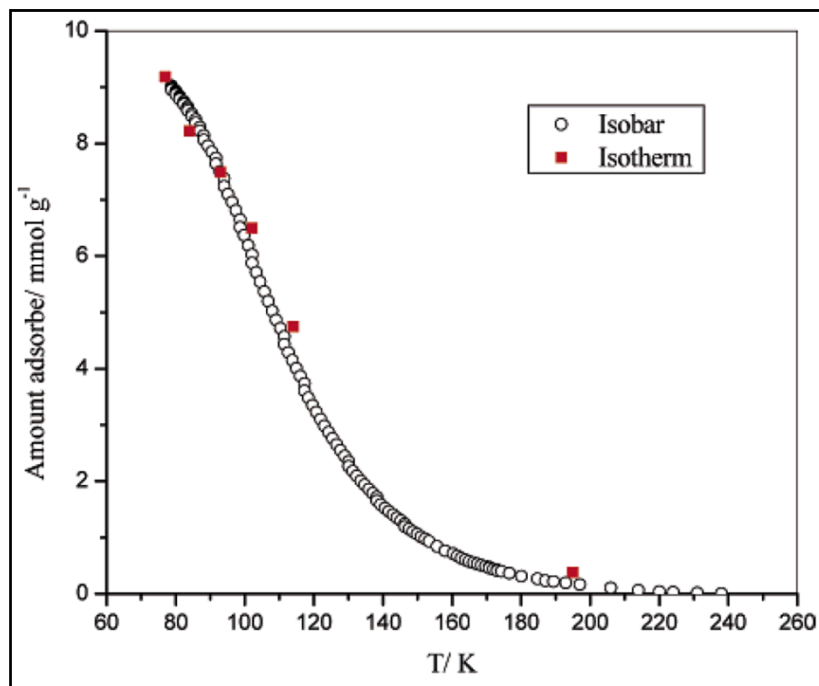


Figure 2.2 Isobars for hydrogen desorption from a certain activated carbon at 1 bar (heating rate 0.3 K/min) and isotherm data from adsorption at 1 bar ¹¹¹ (reprinted with permission from American Chemical Society, see Appendix F)

Remarkable temperature dependence of hydrogen adsorption over carbon materials has been demonstrated by a large number of experimental results. Usually storage capacities up to 8 wt.% H₂ could be obtained at 77 K while reliable results only showed <1 wt.% adsorbed H₂ at ambient temperature ⁴¹⁻⁴⁷. Temperature dependence of hydrogen adsorption has been experimentally studied by Zhao et al. ¹¹¹. They tested hydrogen desorption isobars at pressure of 1 bar on a certain activated carbon and compared the results with the adsorption isotherm data in the same temperature range, as shown in Figure 2.2. The image shows very low amount adsorption when the temperature was higher than 200 K. To store significant hydrogen at ambient temperature, applying high pressure is the method generally used. However, it is unlikely to realize an extent

comparable at 77 K by increasing pressure alone.

2.3.3 Pressure

A high pressure ensures a higher hydrogen adsorption capability, but the measurements at high pressure and ambient temperature usually lead to greater errors. This is because corrections for buoyancy and dead volumes in gravimetric system and volumetric system will become much larger at high pressure. Moreover, more available impurities from hydrogen under high pressure and they are adsorbed to adsorbent materials and thus lead to greater influence on measured results ⁴⁶.

2.4 Hydrogen adsorption measurement methods

It is a tough task to accurately measure the hydrogen adsorption over porous material. Many errors have been created due to invalid measurements ^{35,38}. Two conventional methods used for determining hydrogen capacities during adsorption and desorption are gravimetric and volumetric method.

2.4.1 Gravimetric method

Gravimetric method provides a direct measurement of adsorption. The major problem of this method is that any impurity, either from hydrogen used or within the vacuum system, can end with a considerable error. The reason is that the weight of an impurity molecule like H₂O is equal to that of nine H₂ molecules. 0.6 wt.% of H₂O adsorbed is referred to 5.4 wt.% of H₂ capacity. As a result, an ultra-clean high vacuum system and ultra-pure hydrogen are needed for valid measurements ⁵².

2.4.2 Volumetric method

Volumetric method indirectly determines hydrogen uptake through the pressure change in

a closed chamber filled with hydrogen. Compared to gravimetric method, hydrogen adsorption data obtained through this way lead to a much lower error. Currently most measurements of hydrogen adsorption were taken out by using this method. One big concern of this method is that extremely small leaks in the instrument may lead to inaccurate data at high pressure⁴⁶.

2.5 Scope of this study

The toughness of conventional approaches is the weak interactions between hydrogen and adsorbent materials. The effect of an external electric field on hydrogen adsorption over carbon materials has been experimentally and theoretically demonstrated⁹⁰⁻⁹⁵. The applied electric field is able to introduce charges to the adsorbent. Meanwhile, hydrogen may be polarized or dissociated under the field and form interaction stronger than van der Waals with charged adsorbents. However, carbon is electrically conductive and the induced charges would distribute onto the layer of sample surface, resulting in a limited region named charged zone where strong interactions take place.

This study was initiated to investigate if the adsorption can be further increased by enlarging the size of the charged zone. One approach for the charged zone enlargement is illustrated conceptually in Figure 2.3, which is using a dielectric phase to separate the carbon particles to hold the charges generated by electric field at the interface of carbon and dielectric material. TiO_2 is primarily examined as candidate of dielectric phase mainly due to its good dielectric properties. Besides, the inclusion of transition metal Ti provides possibility of forming metal hydrogen clusters during hydrogen adsorption process under electric field. Furthermore, other dielectric materials like magnesium oxide (MgO), zinc oxide (ZnO) and barium titanate (BaTiO_3) were introduced to the activated carbon respectively and hydrogen adsorption behaviors of the synthetics under electric

field were tested.

Another primary goal of this study is to examine the influence of parameters of the applied electric field on the hydrogen adsorption performance over prepared samples. Electric fields with different strengths and different directions were applied during the adsorption process. Computational calculations were also carried out corresponding to the experiments for understanding the underlying principles and verify our observations.

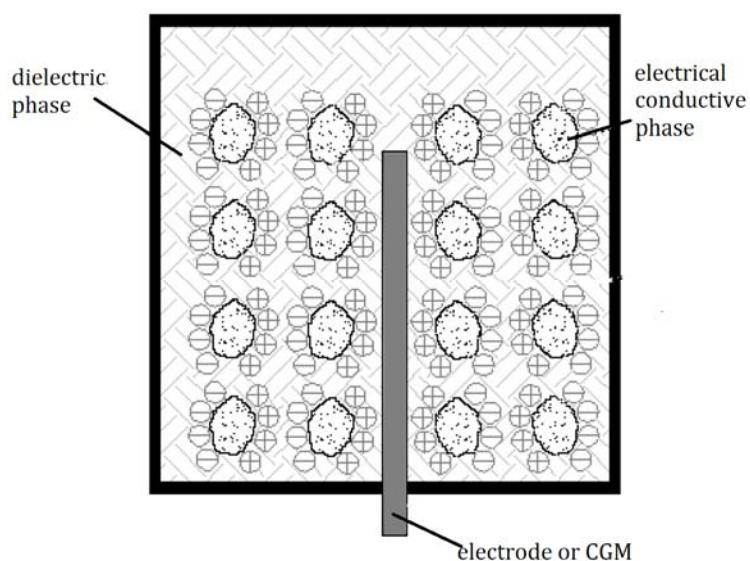


Figure 2.3 Approach for charged zone enlargement (CGM = charge generating material)

CHAPTER 3 MATERIALS AND METHODS

3.1 Materials

3.1.1 Carbon sources

The pristine activated carbon used in this study was a commercial product of Norit (denoted as NAC), with a Brunauer-Emmett-Teller (BET) surface area of 1836.2 m²/g and an average particle size of 20 μ m. Another carbon source, Pt-doped activated carbon (contains 5 wt.% platinum, denoted as Pt/AC) was purchased from Aldrich.

3.1.2 TiO₂ sources

TiO₂ powder in anatase phase with an average particle diameter of 30 nm (NanoTek Ltd., USA) was used as a starting material. Another TiO₂ source was a commercial premix of TiO₂ powder (200 nm average diameter) dispersed in an aqueous polyacrylic solution with propylene glycol, ester-alcohol, and ethylene glycol as stabilizer (Colorplace, Walmart). This premix is denoted as PTP (Premix TiO₂ powder). PTP contains around 10% TiO₂, 33% organics and 57% water. TiCl₄ ($\geq 99.0\%$) purchased from Aldrich was also used to prepare TiO₂ nanoparticles through hydrolysis.

3.1.3 Other sources

The MgO powder (> 98%) used in this study was from Aldrich. ZnO nanopowder with particle size < 10 nm was purchased from Aldrich. BaTiO₃ powder (> 99%) with particle size < 3 μ m was from Aldrich. Aluminum oxide (Al₂O₃) aerosol was from ZYP Coatings, Inc.

3.2 Samples preparation

3.2.1 Carbon mixture

A mixture of carbon (denoted as PAC) was prepared by mixing NAC and Pt/AC in a ball mill at a ratio of 4:1.

3.2.2 TiO₂/Carbon species

Three techniques were used to prepare various TiO₂/Carbon synthetics.

3.2.2.1 Mechanical mixing

The TiO₂/Carbon mixture (denoted as TCM) was prepared by ball milling TiO₂ nanopowder and NAC at a ratio of 1:1 by weight for 30 min.

3.2.2.2 Preparation with premix

A standard solution was first prepared by adding 5.0 g PTP into 500 ml pure ethanol and magnetically stirring for 20 min. Then 10ml, 50 ml, 100 ml and 150 ml standard solutions, which contained 0.01 g, 0.05 g, 0.1 g and 0.15 g TiO₂ respectively, were taken out to mix with 1.0 g NAC. Ultrasonication was used to ensure the distribution of TiO₂ particles on NAC. Next, the obtained cloudy liquids were heated, accompanied by stirring, to promote volatilization until thick slurries formed. The obtained slurries were dried at 105 °C overnight to remove the solvents (water and ethanol) and other volatiles. The dried samples were denoted as P1, P2, P3 and P4. The residual organics were removed by heating P1, P2, P3 and P4 at 300 °C for 2 h (referred to as P1H1, P2H1, P3H1, and P4H1) in a high temperature tube furnace (59300, Thermolyne) in air. For contrast, dehydrated PTP (denoted as PTPD) was prepared by dried PTP at 105 °C overnight.

A species named TPC was prepared following the same procedure as P4 except using Pt/AC to replace NAC.

3.2.2.3 Chemical deposition

The synthesis procedure is similar to the method developed by Lin et al.¹¹². In brief, 0.5g NAC was first separately added into 100ml solution containing 5M HCl, 0.25 M TiCl_4 and 100ml solution containing 5M HCl, 0.5 M TiCl_4 . Then the mixtures were kept in an oven at 100 °C for 4h for hydrolysis. The final products (referred to as TC1 for the product from 0.25 M TiCl_4 and TC2 for the 0.5 M one) were obtained by filtering and drying the slurry at 120 °C for 0.5 h. For contrast, sample HCl/NAC was prepared as follows: 0.5 g NAC and 100 ml 5 M HCl solution were mixed and magnetically stirred at room temperature for 24 h. The obtained slurry was then filtered and dried in an oven at 105 °C overnight to obtain the final product.

3.2.3 MgO/Carbon species

The method of preparing MgO/Carbon species (denoted as MC) followed a previous technique conducted by Yacob et al.¹¹³ to prepare MgO nanoparticles. Around 6.0 g of MgO powder was dispersed in 150 ml distilled water and stirred at about 100 °C for 24 h to obtain magnesium hydroxide, $\text{Mg}(\text{OH})_2$. 3.0 g NAC was added to the hydroxide solution and stirred for another 4 h under the same conditions. The $\text{Mg}(\text{OH})_2$ /NAC precipitate was then yielded by filtration and dried in oven at 105 °C overnight to remove excess water. The obtained solid was grinded using mortar and pestel and afterward activated by heating in an oven in air at 400 °C for 1 h to obtain the final product.

3.2.4 ZnO/Carbon species

A ZnO/Carbon mixture (denoted as ZC) was prepared by ball milling ZnO nanopowder

and NAC at a ratio of 1:1 by weight for 30 min.

3.2.5 BaTiO₃/Carbon species

A BaTiO₃/Carbon mixture (denoted as BC) was prepared by ball milling BaTiO₃ powder and NAC at a ratio of 1:1 by weight for 30 min.

3.3 Hydrogen adsorption measurements

Hydrogen adsorption measurements were carried out with an automatic Sieverts' instrument (PCT-Pro 2000, Hy-Energy LLC) at pressure range of 0-80 bar. Figure 3.1 and Figure 3.2 show the outlook and master control panel of the instrument.



Figure 3.1 Outlook of the PCT-Pro 2000 instrument

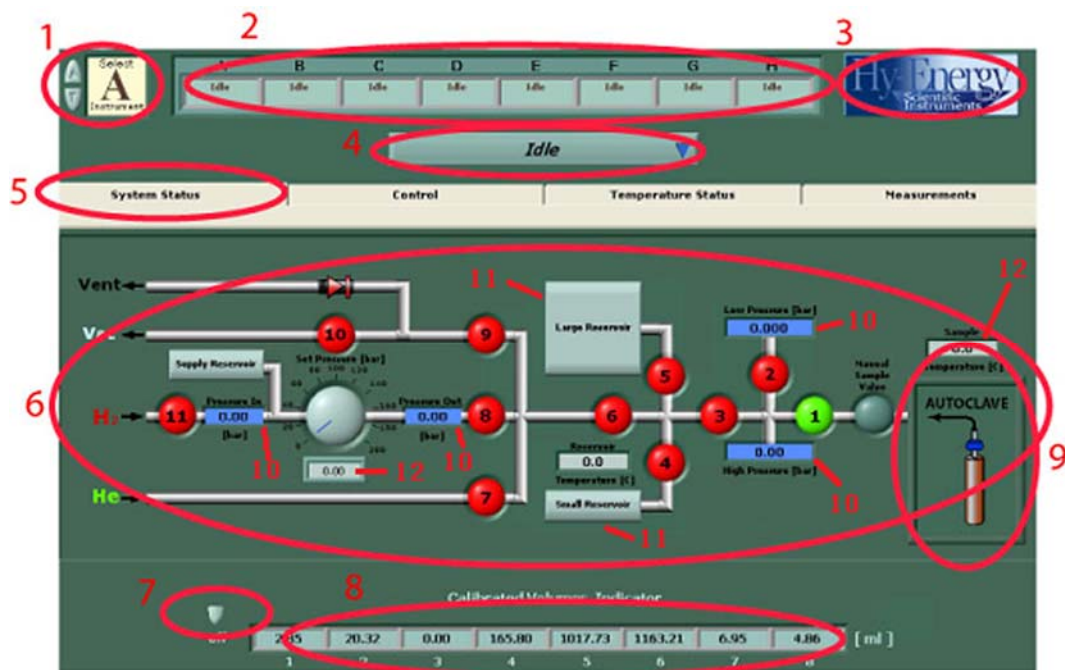


Figure 3.2 Master control panel of PCT-Pro 2000 ¹¹⁴

(Indicators: 1-allows selection of any one of a number of instruments; 2-shows the status of up to 8 different instruments labeled A to H; 3-corporation logo; 4-allows the user to select a process to be performed; 5-control tab used to select; 6-operational status; 7-allows the user to see which physical volumes in the instrument correspond to the calibrated volumes used for making measurements; 8-instrument's volume calibrations; 9-sample holder; 10-barometers; 11-reservoirs; 12-thermometers. reprinted with permission from American Chemical Society, see Appendix F)

Prior to the test, the samples were dried in an oven at 105 °C for 12 h and then moved into the sample holder and evacuated at 100 °C for 2 h to ensure the removal of any contaminations on the sample surface. Around 300 mg sample was used in each run. Ultrapure (99.99999%) hydrogen and helium gases were used for all calibrations and measurements. All the adsorption measurements were conducted under room temperature (22±0.8 °C). A blank test was also performed to exclude possible adsorption of hydrogen on the inner wall of the sample holder.

Two methods were used to provide an electric field to the testing sample. One was

putting a charge generating material inside the adsorbent and the other was applying an external electric potential to the sample holder. The specific illustrations are given as follows.

3.3.1 Measurements with electric field generated by piezoelectric element

Piezoelectric elements are energy transformation devices that are capable of transforming mechanical energy into electricity and vice versa. They are often found in wide applications of sound production and detection, high voltages generation, electronic frequency generation, etc. Piezoelectric elements are typically based on lead oxide compounds. At present, PMN-PT ((1-x)Pb(Mg_{1/3}Nb_{2/3})O₃-xPbTiO₃) based piezoelectric materials are very popular due to the large dielectric constant, outstanding piezoelectric properties and high electrostriction¹¹⁵.

In this study, a piezoelectric element was designed to be surrounded by the adsorbent. Under hydrogen pressure, charges will be generated and accumulated at the surface of the element in response to the applied mechanical stress. The electrical charge generated at the surface of PMN-PT under static hydrogen pressure can be calculated by¹¹⁶

$$Q = d_{33}PS \quad (3.1)$$

where Q stands for the electrical charge, d_{33} is the piezoelectric charge constant, P represents the hydrogen pressure, and S is the surface area upon which hydrogen pressure is exerted.

The experimental setup is depicted in Figure 3.3. Adsorbent and a PMN-PT slab were placed inside a glass container, which was capped by a paper filter and put inside the

stainless sample holder to stop the charges produced from spreading out. The PMT-PT was purchased from Morgan Electroceramics with a dimension of $5 \times 5 \times 1$ mm and a weight of ~ 0.2 g, as shown in Figure 3.4. One side of the slab was covered by an Al_2O_3 thin film (prepared from Al_2O_3 aerosol) to ensure the generation of only negative or positive charges. The d_{33} value of the material is in the range of $1200 - 2000$ pC/N⁹².

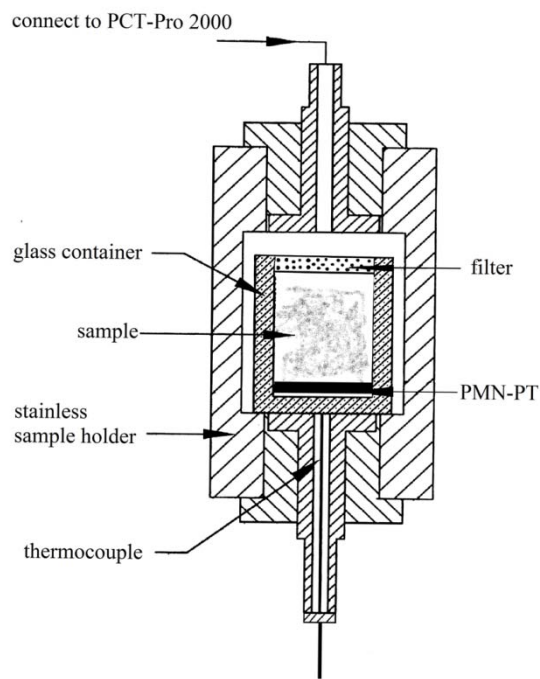


Figure 3.3 Experimental setup for hydrogen adsorption measurement in the presence of PMN-PT

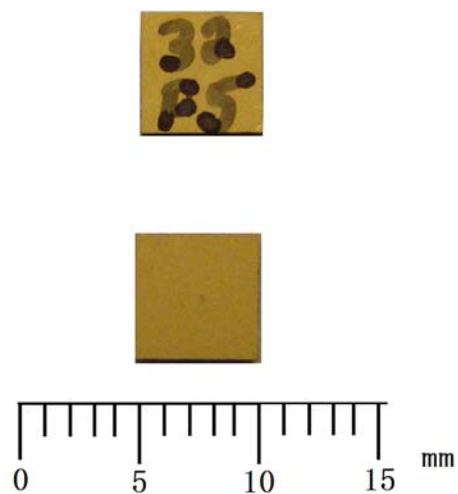


Figure 3.4 Configuration of PMN-PT

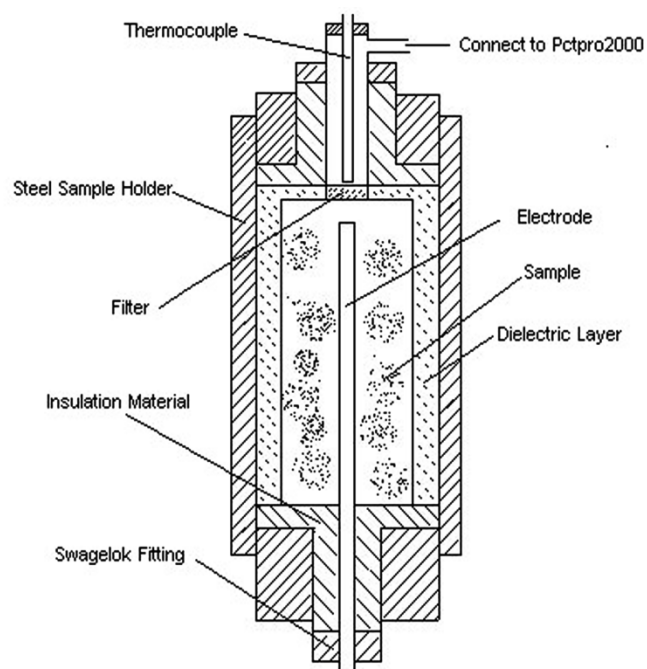


Figure 3.5 Cross-section view of modified sample holder⁹⁰ (reprinted with permission from American Carbon Committee, see Appendix H)

3.3.2 Measurements with electric field generated by applied electric potential

Electric potentials of opposite directions were introduced by two different sets of equipment. A high voltage DC power supply device from Del High Voltage Corporation (model RLPS 100-100 P), which was capable of providing voltage from 200 to 20,000 V, was used to provide positive electric potential. A high voltage switch and an electro-circuit were connected between the power supply and the sample holder. An incorporated ammeter is sensitive to current greater than 0.001 mA. Negative potential was provided by a laboratory DC power supply (72-2085, Tenma) associated with a high voltage DC/DC converter (P10-250, American Power Design). The devices are able to provide voltage from -833 to -2500 V.

The electrode in the center of the cylindrical sample holder was connect to the power supply, while the upper end of the sample holder was electrically grounded. The sample holder has been modified for introducing an electric potential to the testing material, as shown in Figure 3.5. The Inner wall was coated with 2 mm dielectric layer to hold charges. The filter was used for preventing carbon particles from entering the PCT-Pro 2000 instrument. The thermocouple was used for measuring the temperature.

3.4 Characterization methods

X-ray diffraction (XRD) was carried out using a Scintag XDS2000 powder diffractometer at a scan rate of 0.08 °/s with Cu radiation at 45 kV, 35 mA.

A Hitachi S-4700 field emission-scanning electron microscope (FE-SEM) was used to examine the microstructure of the samples.

The surface area and pore volume synthesized samples was measured with a

Micromeritics ASAP2000 instrument using nitrogen adsorption at liquid nitrogen temperature (77 K). Total surface area was calculated by BET equation¹¹⁷. Micropore volume was obtained from t-plot analysis using the Jura-Harkins equation¹¹⁸.

Thermogravimetric analysis (TGA) was performed under 50ml/min oxygen flow at a heating rate of 10 °C/min from 30 °C to 1200 °C by using TGA/DSC 1 (Mettler Toledo).

The electrical resistivity was tested by a digital multimeter (Agilent 34405 A) with around 500 mg of sample powder loosely placed inside a specially designed sample holder, as shown in Figure 3.6.

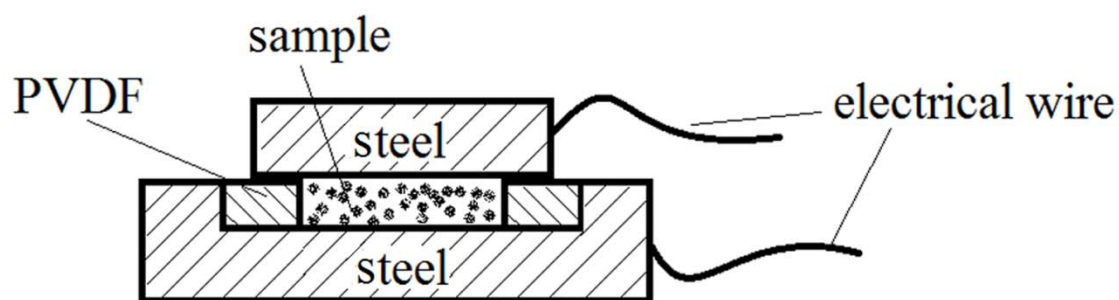


Figure 3.6 Cross-section view of sample holder used for resistivity test

CHAPTER 4 CHARACTERIZATIONS

4.1 Characterizations of TiO₂/Carbon species

4.1.1 Mechanically mixed TiO₂/Carbon mixture

The BET surface area and micropore volume of TCM sample are 613.19 m²/g and 0.12 cm³/g. Compared to NAC, the surface area and micropore volume of the mixture were largely decreased due to the addition of TiO₂ particles. On the other hand, the electric resistivity of TCM is greater than 100 MΩ. The introduction of dielectric TiO₂ converted conductive carbon into a dielectric material.

4.1.2 TiO₂/Carbon synthetics prepared from premix of TiO₂ powder

The studies are focused on synthesized samples P1H1, P2H1, P3H1 and P4H1. P1, P2, P3 and P4 have been previously studied by Wen ¹¹⁹ and some results are also provided here for comparison.

The X-ray diffraction patterns of synthetics P1H1, P2H1, P3H1 and P4H1 are given in Figure 4.1. The XRD analyses clearly show the existence of rutile phase. According to composition of the TiO₂ premix, the TiO₂ contents in P1H1, P2H1, P3H1 and P4H1 were calculated as 1.0, 4.8, 9.1 and 13.0 wt.%, respectively. It is obvious that the peaks of TiO₂ become sharper as the TiO₂ content increases.

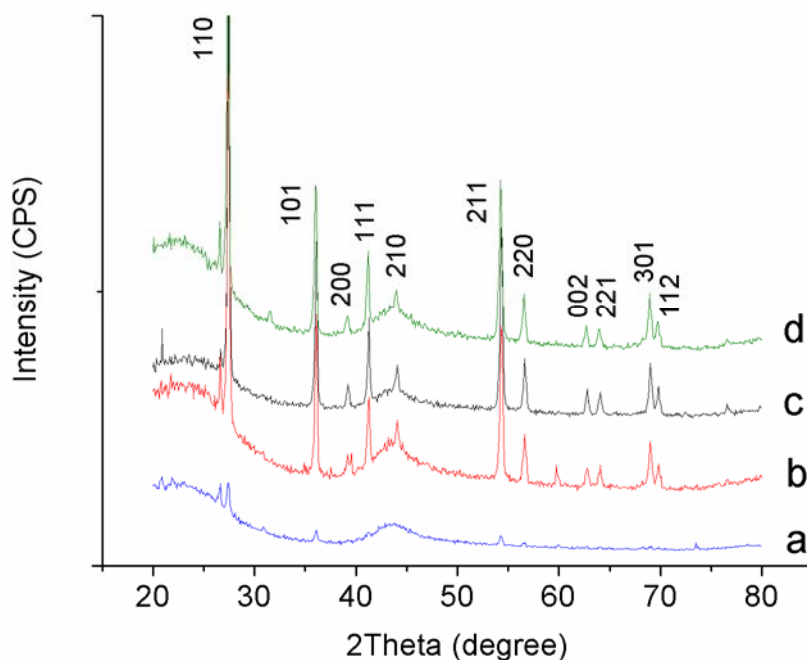


Figure 4.1 XRD patterns of TiO_2 /Carbon synthetics P1H1, P2H1, P3H1 and P4H1

Figure 4-2 shows FE-SEM images of the P4 and P4H1 species. It can be clearly seen that the TiO_2 particles coated on the carbon surface are in tetragonal prism or tetragonal pyramid form with uniform size around 200 nm. Residual organics are obviously observed in P4, as circled in Figure 4.2b. After heating, the organics are thoroughly removed, as shown in Figure 4.2d.

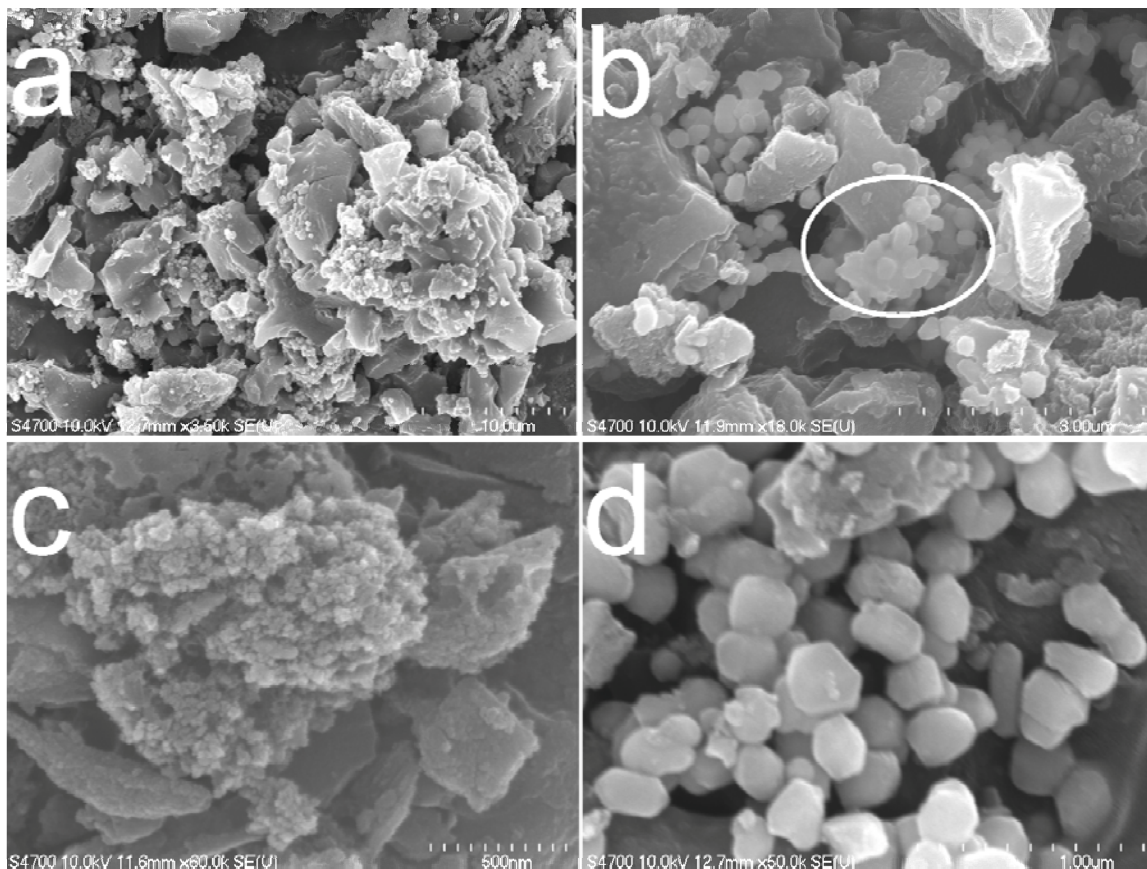


Figure 4.2 FE-SEM images of P4 (a and b) and P4H1 (c and d)

BET surface areas and micropore volumes of the prepared synthetics are listed in Table 4.1. As shown in the table, for the two sets of samples, BET surface area and micropore volume decrease with the increasing TiO_2 content. BET analysis of PTPD showed surface area of only $1.9 \text{ m}^2/\text{g}$. The small surface area could explain the increase in surface area after the removal of the organics for P2, P3 and P4. Surface area of P1 was reduced due to small amount of organic residues and pore collapse caused by heating. Figure 4.3 shows the relationship between BET surface area and micropore volume of the eight samples, which indicates micropore almost linearly increases with the increasing of surface area.

Table 4.1
BET analyses of TiO₂/Carbon synthetics prepared from premix of TiO₂ powder

Sample ID	P1	P2	P3	P4
BET surface area (m ² /g)	1787.2	1167.0	896.2	719.8
Micropore V (cm ³ /g)	0.21	0.13	0.09	0.05
Sample ID	P1H1	P2H1	P3H1	P4H1
BET surface are (m ² /g)	1615.5	1361.0	1086.2	846.1
Micropore V (cm ³ /g)	0.19	0.14	0.11	0.07

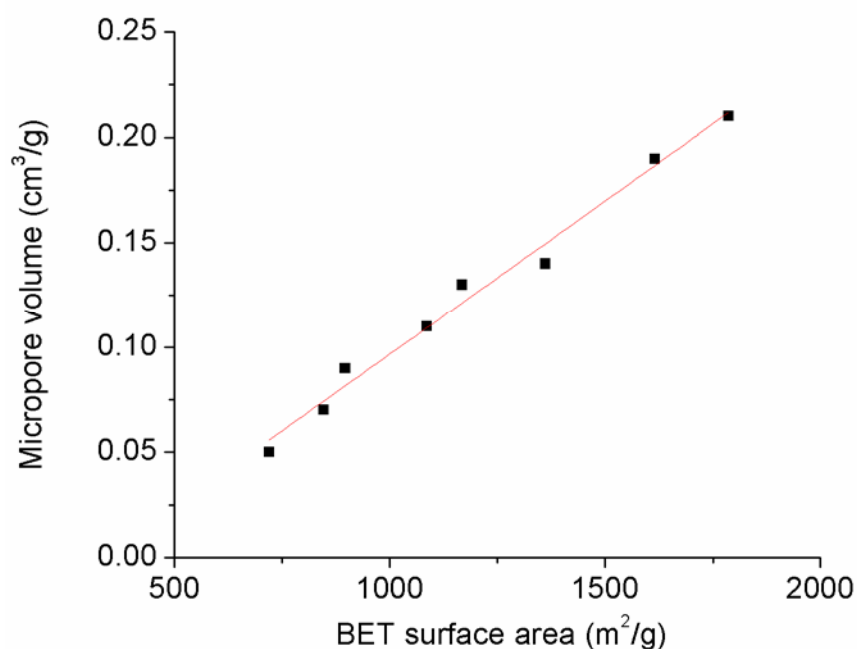


Figure 4.3 Relationship between BET surface area and micropore volume of TiO₂/Carbon synthetics

Electric resistivity data of the prepared synthetics is given in Table 4.2. It is indicated that resistivity increases with the rising TiO₂ content for both series. It is known that the addition of insulating material into a conductive matrix would raise the resistivity of the matrix. However, the addition of dielectric materials would largely decrease the surface

area of the composite and adversely affect a relative high storage capacity. What we expect is a conductor-insulator transition point which can not only offer the ideal charged zone but also enough available sites for hydrogen adsorption. It is also noted that heating treatment reduced resistivity of the synthetics due to the absence of the organics.

Table 4.2
Electrical resistivity of TiO₂/Carbon synthetics prepared from premix of TiO₂ powder

Sample ID	P1	P2	P3	P4
Resistivity (MΩ)	0.035	2	20	> 50
Sample ID	P1H1	P2H1	P3H1	P4H1
Resistivity (MΩ)	0.01	0.9	2.0	20.0

4.1.3 TiO₂/Carbon synthetics prepared through chemical deposition

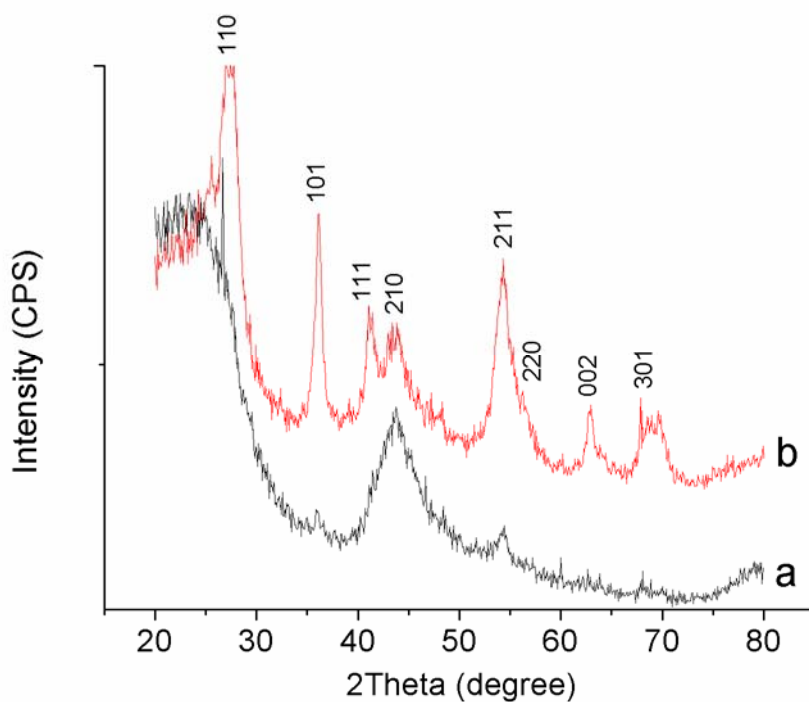


Figure 4.4 XRD patterns of chemical deposited TiO₂/Carbon synthetics TC1 (a) and TC2 (b)

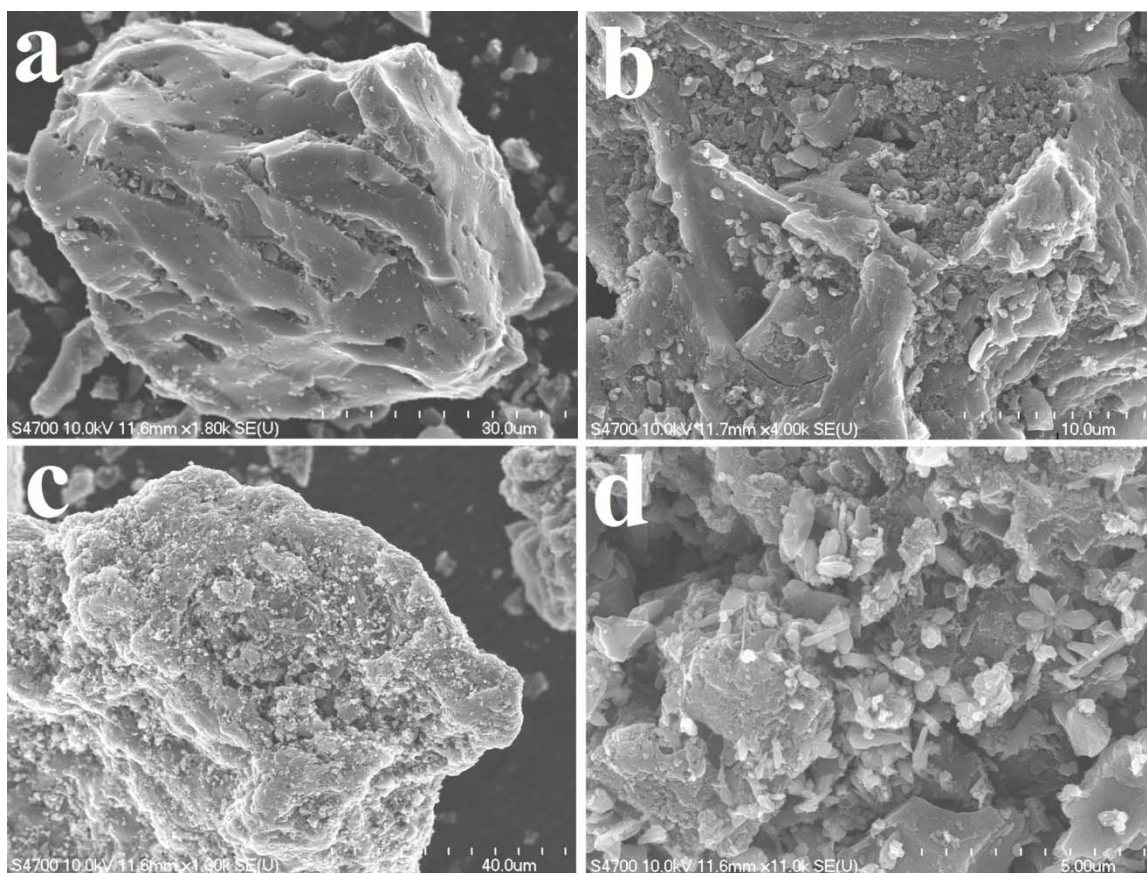


Figure 4.5 FE-SEM images of chemically deposited TiO_2 /Carbon synthetics TC1 (a and b) and TC2 (c and d)

X-ray diffraction spectra of prepared TC1 and TC2 are shown in Figure 4.4. It is seen that the XRD analyses show Rutile peaks. The peaks of TC2 are much sharper than TC1. The broadening of the peaks indicates crystal size of the synthesized TiO_2 particles is very small ⁶⁴.

FE-SEM images of TC1 and TC2 are shown in Figure 4.5. For both species, TiO_2 particles have been uniformly deposited on the carbon surface. It is also noticed that for TC2 particles on the carbon are much denser than TC1, indicating a higher TiO_2 content.

TGA analysis results of TC1 and TC2 are given in Figure 4.6. Two weight-loss steps

were observed for each test. The first occurred in the range of 30-300 °C, corresponding to around 2.5% weight loss for both samples, which is related to the elimination of water and residual HCl. The second started at 400 °C, which is due to the combustion of activated carbon. The final residue was considered to be TiO₂, which takes up 5.8 and 18.8 wt.% of TC1 and TC2, respectively.

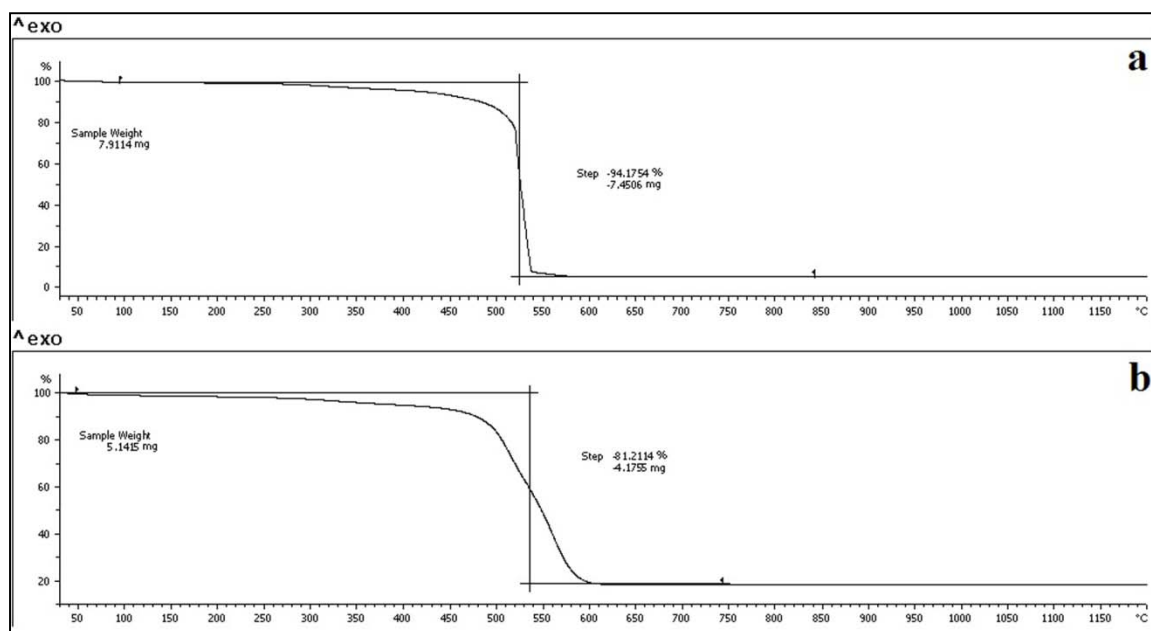


Figure 4.6 TGA analyses of TiO₂/Carbon synthetics TC1 (a) and TC2 (b)

BET analyses of TC1 and TC2 are given in Table 4.3. The BET surface area and micropore volume of TC1 are relatively larger than those of TC2. No heating process was involved in the preparation, resulting in synthetics with relative high surface area, which is favorable for hydrogen storage.

Electric resistivity data of TC1 and TC2 is given in Table 4.4. It is seen that the sample with a higher TiO₂ content has a larger resistivity because of the better isolation of carbon particles.

Table 4.3**BET analyses of chemically deposited TiO₂/Carbon synthetics TC1 and TC2**

Sample ID	BET surface area (m²/g)	Micropore V (cm³/g)
TC1	1563.2	0.15
TC2	1248.3	0.07

Table 4.4**Electrical resistivity of chemically deposited TiO₂/Carbon synthetics TC1 and TC2**

Sample ID	TC1	TC2
Resistivity (MΩ)	2.0	>50

4.2 Characterizations of MgO/Carbon species

X-ray diffraction spectrum of synthesized MgO/Carbon sample is shown in Figure 4.7. Only MgO peaks were observed. SEM images of the species are displayed in Figure 4.8, which indicate cubic crystals with uniform size. BET analysis for MC showed that surface area is 538.3 m²/g and micropore volume is 0.04 cm³/g. Electrical resistivity of MC is greater than 100 MΩ.

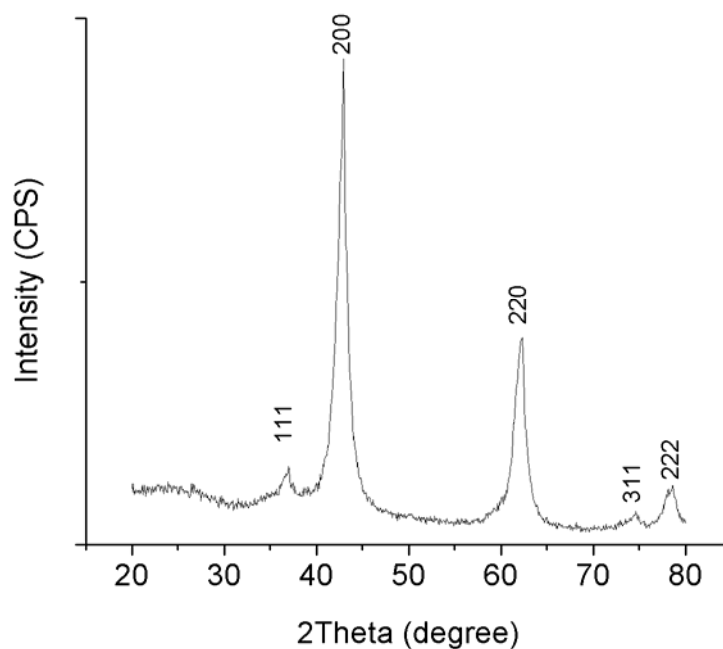


Figure 4.7 XRD pattern of MgO/Carbon synthetic MC

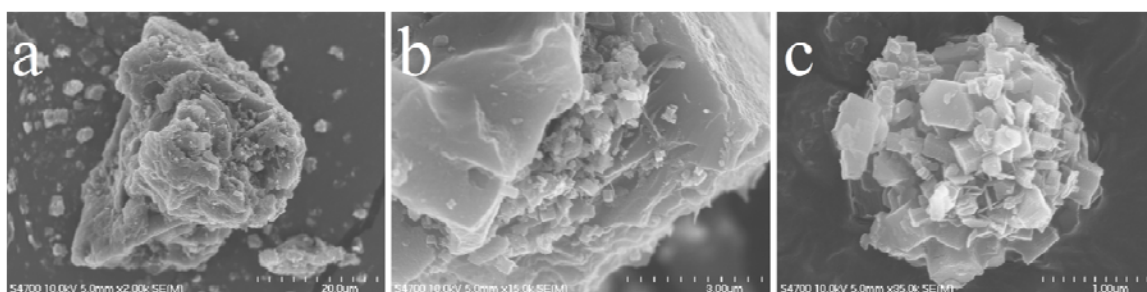


Figure 4.8 FE-SEM images of MgO/Carbon synthetic MC

For ZC and BC, only resistivity measurement was carried out. The results showed that the resistivity is greater than 100 MΩ for both samples.

CHAPTER 5 EXAMINATION OF HYDROGEN ADSORPTION ON ACTIVATED CARBON UNDER ELECTRIC FIELD

The study started with verifying the effect of electric field on carbon materials. Direction of electric potential as well as intensity was varied in the examination. The adsorption enhancement is defined as follows

$$ads. enhancement (\%) = \frac{ads. with E_{potential} - ads. w/o E_{potential}}{ads. w/o E_{potential}} \times 100\%$$

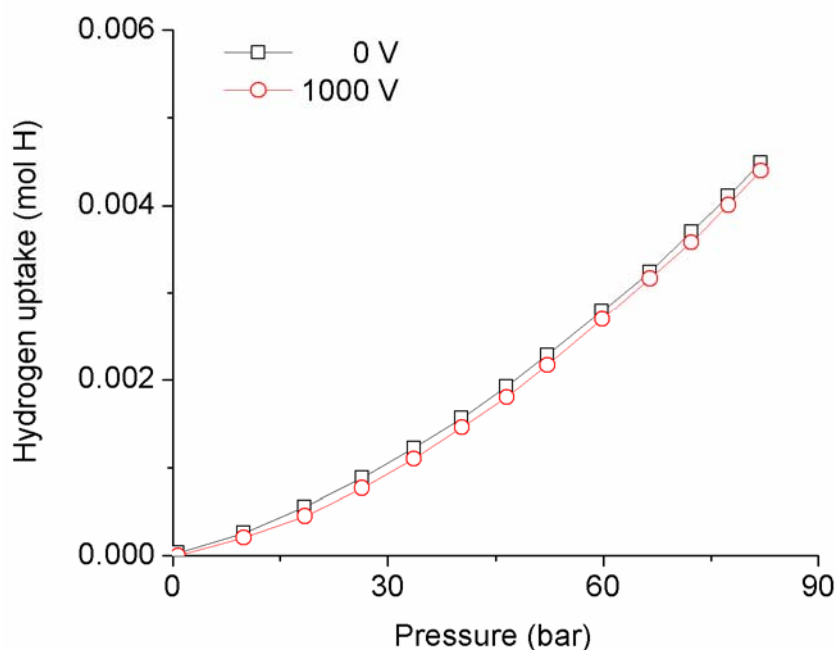


Figure 5.1 Hydrogen adsorption on blank sample holder with and without 1000 V electric potentials

Blank experiment was first addressed by applying 0 V and 1000 V electric potential to the blank sample holder, as shown in Figure 5.1. The adsorption curves indicate negligible difference between the two tests. It was therefore concluded that the electric potential does not affect the adsorption performance of the background. All the variations are due

to the electric field effect on adsorption over the adsorbent.

5.1 Hydrogen adsorption on pristine activated carbon

5.1.1 Positive electric potential

Hydrogen adsorption measurements of pristine NAC with 0, 1000, 2000 and 3000 V electric potentials can be seen in Figure 5.2. The hydrogen uptake shown here was the net weight percentage of uptake after elimination of the adsorption on the blank sample holder. The error bars represent stand errors, which are 4-6% and < 3% for the measurements with and without voltage based on three repeated experiments. As shown in the picture, all the adsorption isotherms at room temperature have a linear trend and locate close to each other. Unlike previous findings^{90,93}, applying an electric potential to the activated carbon led to no adsorption improvement but some decrease in this study. The hydrogen storage capacity of NAC reached 0.43 wt.% at 80 bar. With electric potentials of 1000, 2000 and 3000 V, the uptakes were 0.33, 0.41 and 0.36 wt.% at 80 bar, which meant 23%, 5% and 16% decreases, respectively. No specific correlation has been found between the potential intensity and the hydrogen adsorption in this case.

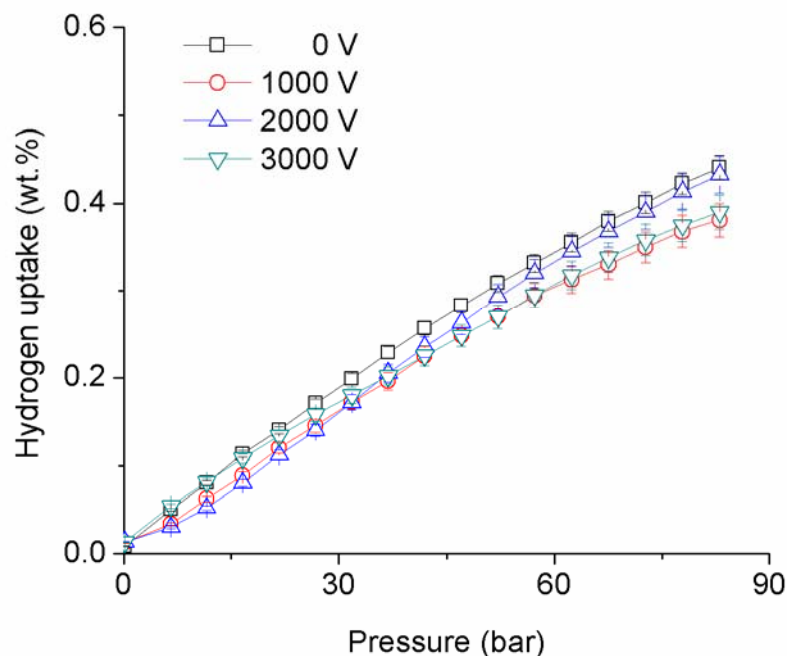


Figure 5.2 Hydrogen adsorption on NAC under various electric potentials

The interaction between activated carbon and hydrogen molecules is weak van der Waals force, leading to very low storage capacity at ambient temperature. Under a positive electric field, positive charges can be introduced to the carbon adsorbent and reside at the surface of carbon body when the system reaches equilibrium. Only hydrogen molecules located near to the charged area are possible to form stronger electrostatic interaction. Compared to the large surface area of activated carbon, the charged area takes up a very small proportion and thus the ratio of strongly bonded hydrogen is negligible. Moreover, the stronger bond between hydrogen and adsorbent can create longer H-H bond length, which indicates less stable state of hydrogen molecules. Under a sufficiently high electric field, dissociation and ionization of hydrogen molecules probably exist^{120,121}. Movement of hydrogen ions in the electric field causes less adsorbed hydrogen. As no electricity was detected by the ammeter, ionized hydrogen molecules are not abundant. Besides, either increases of reported findings and decreases of our experimental results are not

significant. Experimental errors caused by differences in experiment conditions may be another reason for the deviation of results.

5.1.2 Negative electric potential

Previous studies only examined adsorption behaviors with positive electric potential. To discover the effect of the direction of electric potential on adsorption, electric potential with opposite direction was applied to the sample. Hydrogen adsorption isotherm with negative electric potential of 1000 V is shown in Figure 5.3. The error for the measurement is around 10%, much bigger than that with positive potential. A sharp decrease was observed in the presence of a negative potential. Hydrogen adsorption at 80 bar with -1000 V voltage was 0.26 wt.%, corresponding to 40% decrease. Current leak of around 0.1 A was detected by the incorporated ammeter of the power supply, indicating the transportation of electrons from the negative electrode to the ground. Moreover, the current continuously grew up as the voltage gradually increased. Measurement was not conducted at higher voltage due to the distinct current flow.

In the environment of a negative potential, some of hydrogen molecules will probably gain electrons from the electrode to form negative hydrogen ions (H^-) or hydrogen ion clusters (H_n^- , $n=3,5,7,9\dots$). However, the negative hydrogen ions or ion clusters are very unstable and impossible to form steady interaction with adsorbent surface¹⁰⁶. The obtained electrons are about to be released in no time and run to the grounded electrode, resulting in a detected current. Additionally, the current flow would increase the temperature of the adsorbent, further reducing the adsorption capacity.

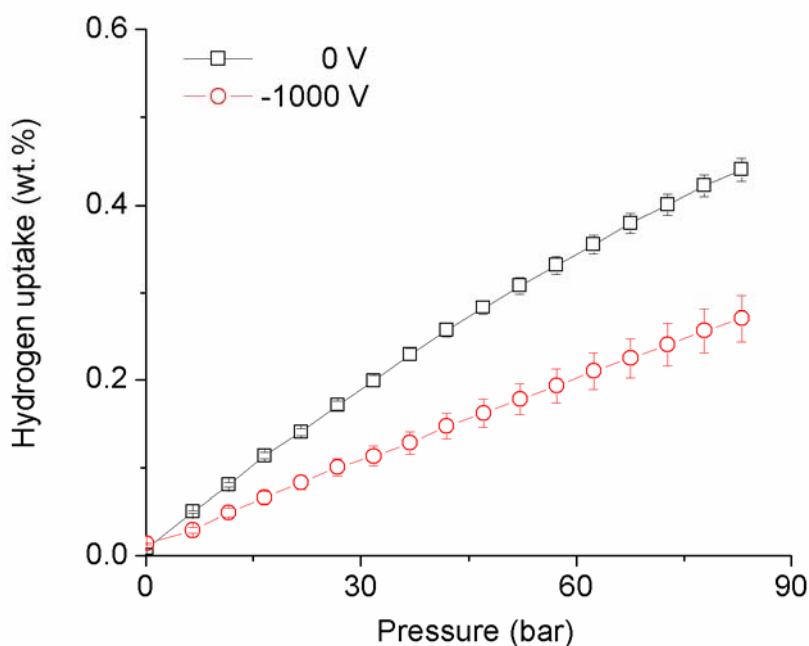


Figure 5.3 Hydrogen adsorption on NAC with and without -1000 V electric potential

In the light of above observations, introducing an electric field to pristine carbon materials did not achieve any enhancement in hydrogen adsorption. Adsorbents with some specific characteristics may be required to form an effective system with the applied electric field.

5.2 Hydrogen adsorption on Pt-doped activated carbon

It has been demonstrated that Pt-doped activated carbon is able to dissociate hydrogen molecules and obtain improved adsorption through spillover. Experiment was carried out to determine the effect of an electric potential on the mixture of activated carbon and Pt-doped carbon (PAC). Hydrogen adsorption isotherms with and without a 2000 V electric potential are shown in Figure 5.4. Obvious enhancement was observed, even at low hydrogen pressure. At 80 bar, hydrogen adsorption capacities for 0 V and 2000 V applied potential were 0.42 and 0.51 wt.%, resulting in a 21% increase.

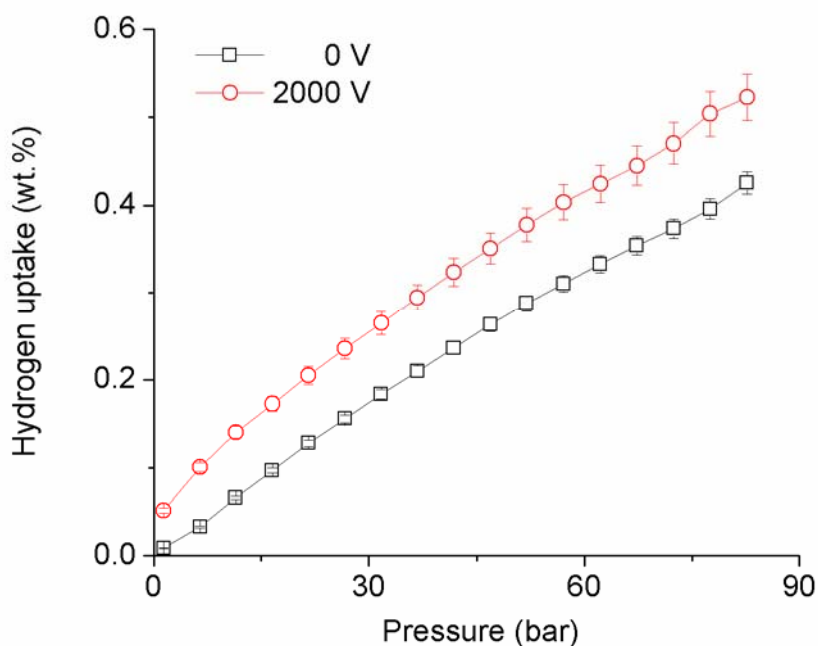


Figure 5.4 Hydrogen adsorption on PAC with and without 2000 V electric potential

In previous experiments, introduction of electric field did not lead to any adsorption enhancement over the activated carbon. The enhancement obtained on PAC could be ascribed to the existence of Pt particles. The mechanism may be illustrated by the following reasons. First, hydrogen molecules can be polarized by the electric field and the charges at adsorbent surface, facilitating the dissociation of hydrogen molecule on Pt particles. Also, the charges may accelerate the diffusion of H atoms into the bulk material. Therefore, more hydrogen can be adsorbed, indicating the application of electric field is capable of promoting the spillover effect.

CHAPTER 6 EXAMINATION OF HYDROGEN ADSORPTION ON

ACTIVATED CARBON SEPARATED BY TITANIUM DIOXIDE

UNDER ELECTRIC FIELD

6.1 Hydrogen adsorption on mechanically mixed TiO₂/Carbon mixture

Hydrogen uptakes of prepared TCM sample under 0 V and 2000 V are shown in Figure 6.1. The error for measurements is between 2% and 5%. Using mixture of NAC and TiO₂ nanopowder as adsorbent is a convenient way to check if introduction of electric field could affect hydrogen adsorption over activated carbon separated with dielectric material. It is told from the figure that introducing electric field could efficiently increase hydrogen storage over the mixture. For cases with and without electric field, 0.19 wt.% and 0.15 wt.% uptakes were obtained at 80 bar and room temperature respectively, resulting in 26.7% improvement. However, compared to hydrogen adsorption on NAC, the adsorption without an electric field decreased remarkably. The platform of the adsorption curve at high hydrogen pressure indicated saturation of available adsorption sites.

The significant uptake reduction at 0 V was mainly caused by the addition of TiO₂ powder, which is demonstrated as a very poor hydrogen storage material ¹²². The enhancement with 2000 V applied electric potential is then considered primarily causing by enlarged charged zone. In this case, TiO₂ particles would uniformly lie around carbon particles through mixing and could hold a large number of electrical charges generated at the interface of carbon and dielectric material. Then hydrogen molecules were possible to be polarized and form a stronger interaction with adsorbent, which was reflected as higher hydrogen uptake. Here we used a qualitative way to verify our hypothesis and agreeable results were obtained. However, the mechanism may be more complicated and

further studies are needed.

6.2 Hydrogen adsorption on TiO₂/Carbon synthetics prepared from TiO₂ premix

6.2.1 Hydrogen adsorption with applied electric field

TiO₂-coated activated carbon samples with different content of TiO₂ were prepared from the premix of TiO₂ powder for investigating the effect of electric field on adsorption. The hydrogen adsorption isotherms of the prepared synthetics in the absence of an electric field are shown in Figure 6.2. For comparison, the measurement of pristine NAC is also included. It is found from the data that hydrogen uptake almost increases linearly with the growing pressure, while drops remarkably with increasing TiO₂ content. The adsorption difference between P3H1 and P4H1 is very small. At 80 bar, the hydrogen storage capacity of NAC was 0.43 wt.%, while uptakes of P1H1, P2H1, P3H1 and P4H1 were 0.35 wt.%, 0.28 wt.%, 0.23 wt.% and 0.23 wt.%, respectively.

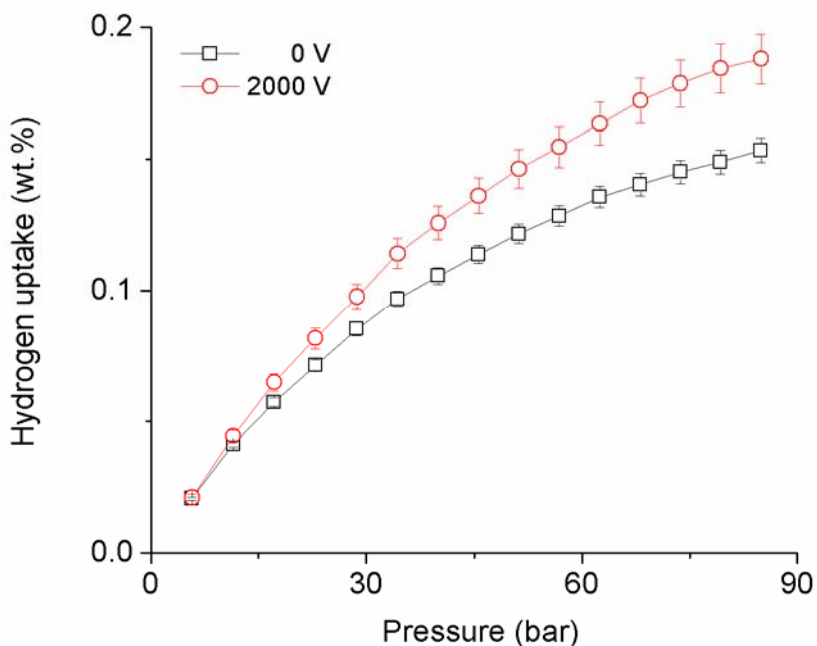


Figure 6.1 Hydrogen adsorption on sample MM with and without 2000 V electric potential

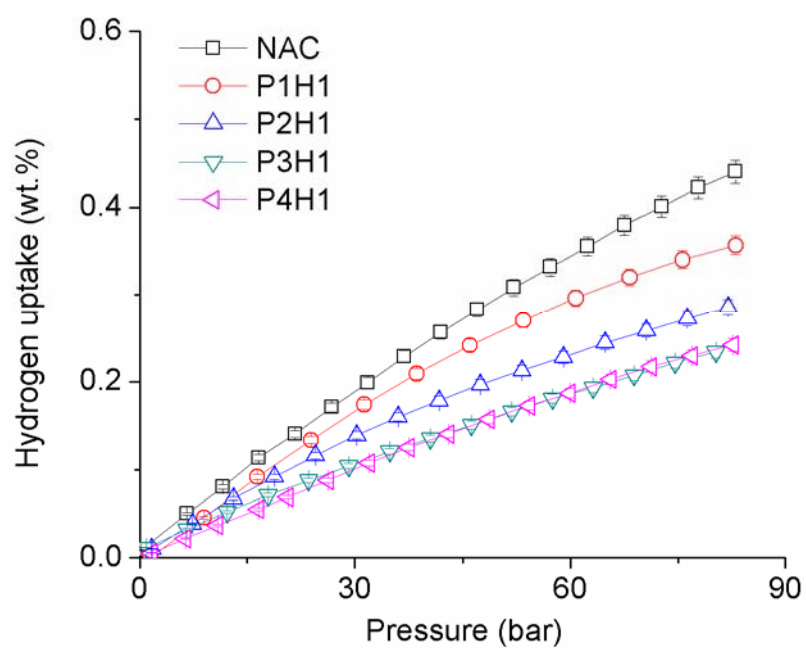


Figure 6.2 Hydrogen adsorption on $\text{TiO}_2/\text{Carbon}$ synthetics P1H1, P2H1, P3H1, P4H1 and NAC

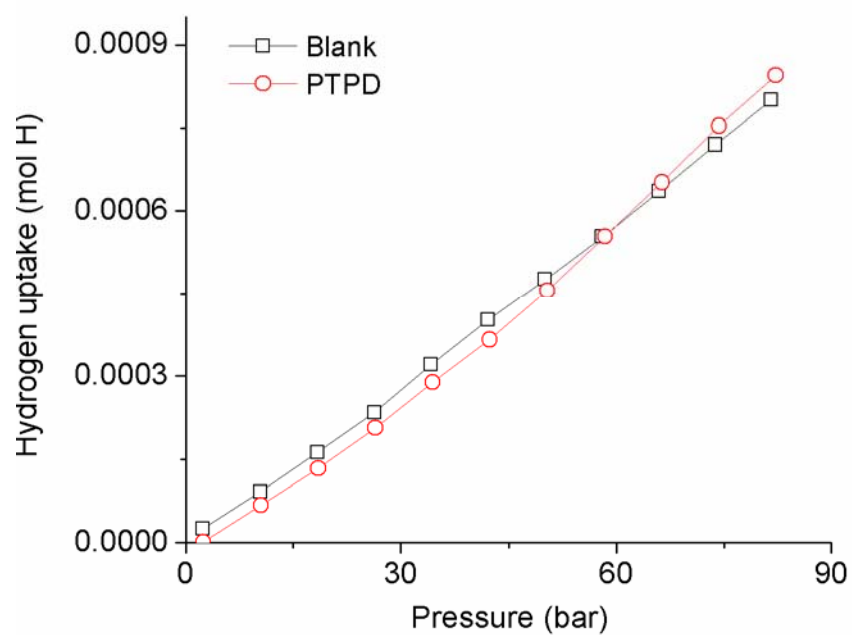


Figure 6.3 Hydrogen adsorption isotherms of PTPD and blank test

Figure 6.3 shows the adsorption isotherms of PTPD and blank test. A negligible difference between the two experiments reveals that the PTPD itself adsorb little hydrogen.

An electric potential of 1000 V was then introduced to the testing samples and the results are shown in Figure 6.4. The error for this set of tests is around 5%. Measurements for samples without voltage are also included for comparison. As shown in Figure 6.4a, for sample P1H1, suspected adsorption increase was observed under low pressure but was replaced by a slight decrease with pressure over 30 bar. Figure 6.4b shows an enhancement for P2H1, a sample with higher TiO_2 content, which was very obvious even at very low hydrogen pressure. As for P3H1 in Figure 6.4c, the gap between the two data curves become larger, indicating even higher adsorption improvement. P4H1 showed a nice adsorption jump under electric field in Figure 6.4d, which meant a remarkable increase in adsorption capacity. At 80 bar of hydrogen pressure, the adsorption capacities of P2H1, P3H1 and P4H1 under electric field were 0.36, 0.33 and 0.38 wt.% and corresponding increases were 29%, 43% and 65%, respectively. The results revealed that adsorption enhancement increases with the increasing of TiO_2 content. It should be noted that the dehydrated PTP alone has little adsorption. Such adsorption increases are considered to occur on the activated carbon substrate.

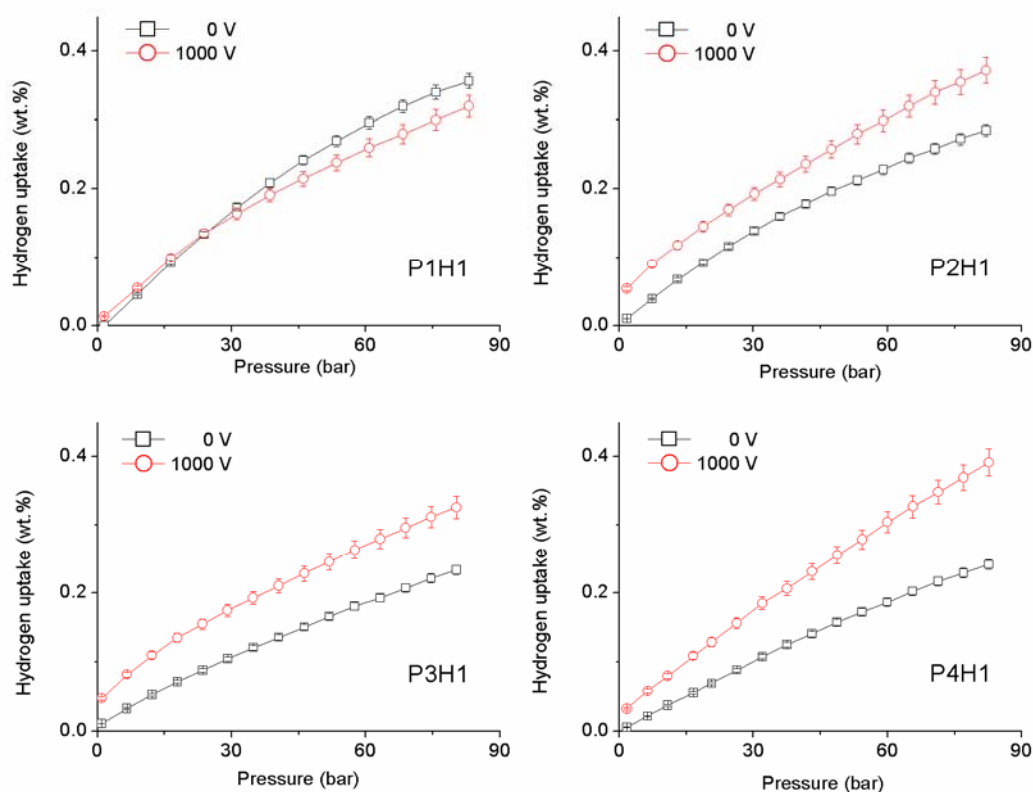


Figure 6.4 Hydrogen adsorption on TiO₂/Carbon synthetics P1H1, P2H1, P3H1 and P4H1 with and without 1000 V electric potential

As the surface area of the synthetics varies greatly, it is insufficient to simply compare hydrogen uptakes on different samples. We normalized the adsorption capacity with the BET surface area, as shown in Figure 6.5. It is indicated that application of an electric field enabled more hydrogen to be adsorbed on unit area for P2H1, P3H1 and P4H1. Among all the results, P4H1 under 1000 V voltage had the highest normalized uptake. Additionally, under an electric field the amount of hydrogen adsorbed on equivalent area increased with the increasing TiO₂ content in the species.

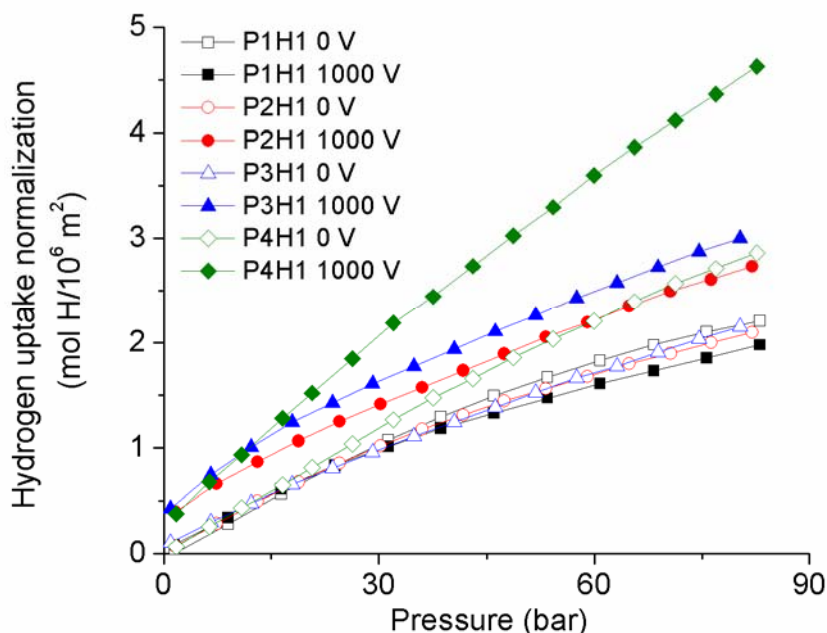


Figure 6.5 Hydrogen adsorption normalized by BET surface area

A higher storage capacity is in fact due to larger adsorption energy. The adsorption process between carbon and hydrogen is primarily weak van der Waals attraction between the π bonds of aromatic rings and the σ bonds of hydrogen molecules. After decorating activated carbon with TiO_2 particles, hydrogen molecules may dissociate and migrate onto carbon host, which is known as spillover. However, Mishra and co-workers⁶⁸ found reversible hydrogen storage (more than 90%) over $\text{TiO}_2/\text{Carbon}$ composite at room temperature, which indicated the adsorption mainly depended on physisorption. In addition, according to the report of Lim et al.⁷⁰, around 25% of the H_2 was chemisorbed to the self-prepared TiO_2 nanotubes due to spillover, in which half was weakly chemisorbed and reversible. Moreover, the supported TiO_2 particles are relatively large and poorly distributed on carbon surface, and thus largely limit spillover. It is therefore considered that the spillover effect could be ignored in this case and the changes in adsorption were primarily attributed to the presence of electric field. According to the

experimental observations, no obvious loss in adsorption capacity was found after several repeated experiments, indicating approximately complete desorption of hydrogen.

When an electric potential is applied, dielectric TiO₂ coated on carbon surface will be polarized and induced charges can be generated in carbon. The coating allows charges induced to stay at the interface of carbon particles and dielectric materials, resulting in an enlarged charged zone. Hydrogen molecules and charged carbon surface can then build electrostatic interactions, which are stronger than van der Waals forces. Shi et al. also mentioned that orbital defects may be produced in adsorbent with an applied electric field, resulting in intensified orbital interactions⁹².

As TiO₂ content varied in samples, carbon particles were isolated at different levels, or in other words, charged zones were different in size. Resistivity is a reflection of isolation. Higher resistivity corresponds to better isolation. P1H1 has a low resistivity due to the small amount of TiO₂, exhibiting similar phenomenon as pristine carbon adsorbent under electric field. On the other hand, the sample holder can be treated as a capacitor with applied electric potential. The relationship of related parameters in a capacitor can be expressed using the following equations

$$C = \varepsilon_r \varepsilon_o \frac{S}{d} \quad (6.1)$$

$$Q = C V \quad (6.2)$$

where C is the capacitance, ε_r is dielectric constant of the material between the two electrodes of the capacitor, ε_o is the electric constant ($\varepsilon_o \approx 8.854 \times 10^{-12}$ F/m), S is the area of overlap of the two electrodes, d is the separation of the electrodes, Q is the amount of induced charges and V is the electric potential applied. The dielectric constant of

synthetics rises with a growing ratio of dielectric materials until conductor-insulator transition is approached ¹²³. With other conditions unchanged, more charges would be generated as TiO₂ content goes up. Therefore, both the enlarged charged zone and increased charge amounts are responsible for more intensified hydrogen polarization, leading to improved hydrogen adsorption increase on P2H1, P3H1 and P4H1 samples.

In previous experiment, adsorption increase has been observed on mixture of activated carbon and anatase powder under electric field. Also, electric field enhanced adsorption was demonstrated when rutile particles was introduced to the carbon. The results indicate that the phase of TiO₂ does not play a very important role in the adsorption enhancement with an applied electric potential.

6.2.2 Hydrogen adsorption with the presence of piezoelectric element

Hydrogen adsorption isotherms with one side insulated PMN-PTs are shown in Figure 6.6. Since a small difference in free volume would result in a big effect on hydrogen uptake via volumetric measurement, experiments have been carefully carried out with < 0.1% volume differences. Standard error for the measurements with the presence of PMN-PT is around 5%. The obtained results indicated that the addition of positive side insulated PMN-PT (denoted as PMN-PT(-)) could lead to significant hydrogen adsorption enhancement while the presence of PMN-PT with the negative side insulated (denoted as PMN-PT(+)) caused reduction in storage capacity. In other words, introduction of negative charges was able to strengthen the interaction between hydrogen and adsorbent, but positive charges would weaken the interaction.

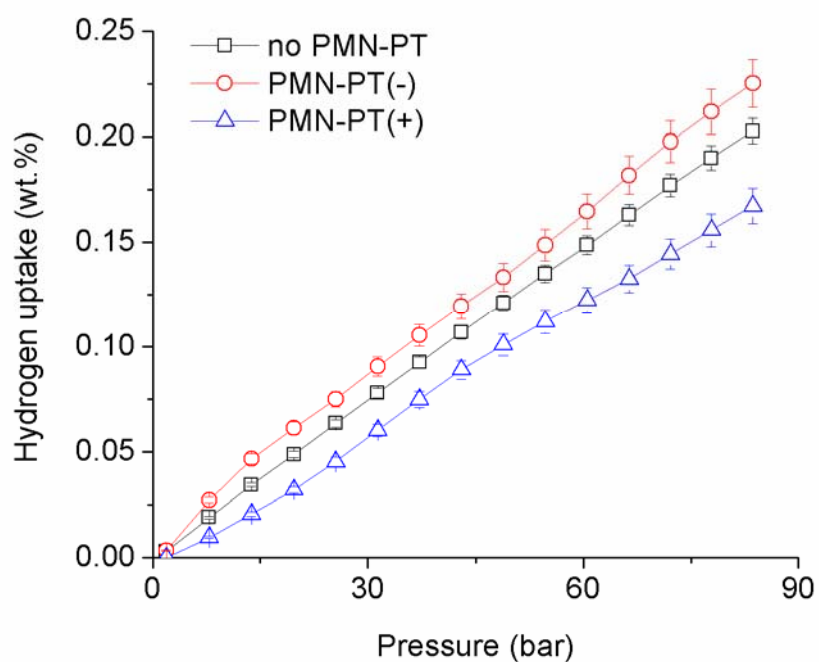


Figure 6.6 Hydrogen adsorption on P4 with the presence of a PMN-PT

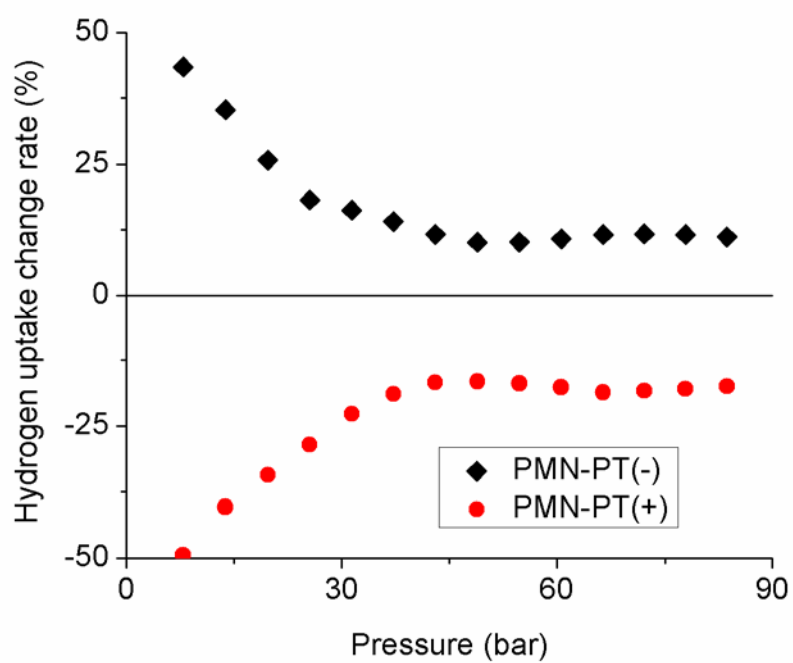


Figure 6.7 Change rate of hydrogen adsorption with the presence of a PMN-PT

Change rates of hydrogen adsorption with two kinds of PMN-PT are shown in Figure 6.7. Hydrogen adsorption with PMN-PT(-) and PMN-PT(+) at 80 bar were 0.22 and 0.16 wt.%, corresponding to 10% increase and 20% decrease. In hydrogen atmosphere, charges will be generated and stay around the piezoelectric element due to the high electric resistivity of the adsorbent. Unlike an applied electric field, the charges generated by PMN-PT would not be capable of dissociating or ionizing hydrogen molecules. The adsorption takes place in the form of hydrogen molecule. The accumulated charges can be considered as a big point charge. As the field intensity of point charge falls off as the square of the distance from the charge, only the TiO_2 particles locating near to the PMN-PT can be efficiently polarized. Charge distribution with the presence of PMN-PT(+) is described in Figure 6.8. Given the low surface area of the TiO_2 , it contributes few adsorption sites for hydrogen. Hydrogen is stored directly in activated carbon at the carbon- TiO_2 interface or by initial binding on TiO_2 and subsequent spillover in activated carbon^{69,75}. The experimental results reflected that hydrogen molecules have stronger interaction with negatively charged TiO_2 than positively charged TiO_2 . The principle of the phenomenon is attributed to the difference in binding energy. Computational calculations in the following chapter will provide more detailed explanation.

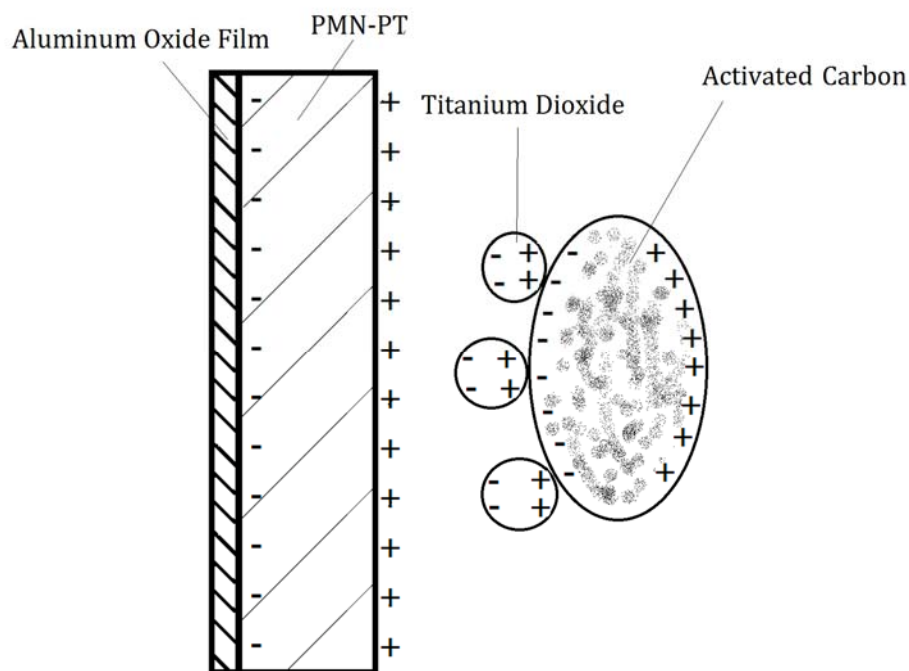


Figure 6.8 Schematic of charge distribution with the presence of PMN-PT(+)

It is also noted that for both measurements the rate of change went down as the pressure went up at low pressure (< 30 bar), and then became stable as the pressure further increased. According to Equation 3-1, relation between charges generated from PMN-PT and hydrogen pressure can be described in Figure 6.9 ($d_{33} = 1800$ pC/N), which indicates the amount of charges linearly increases with the pressure. At low pressure, the amount of hydrogen molecules is small and thus the adsorption related to the generated charges would take up a considerable portion of total hydrogen adsorbed. As the pressure goes higher, the portion of influenced molecules falls down, leading to a reduction in either increase or decrease.

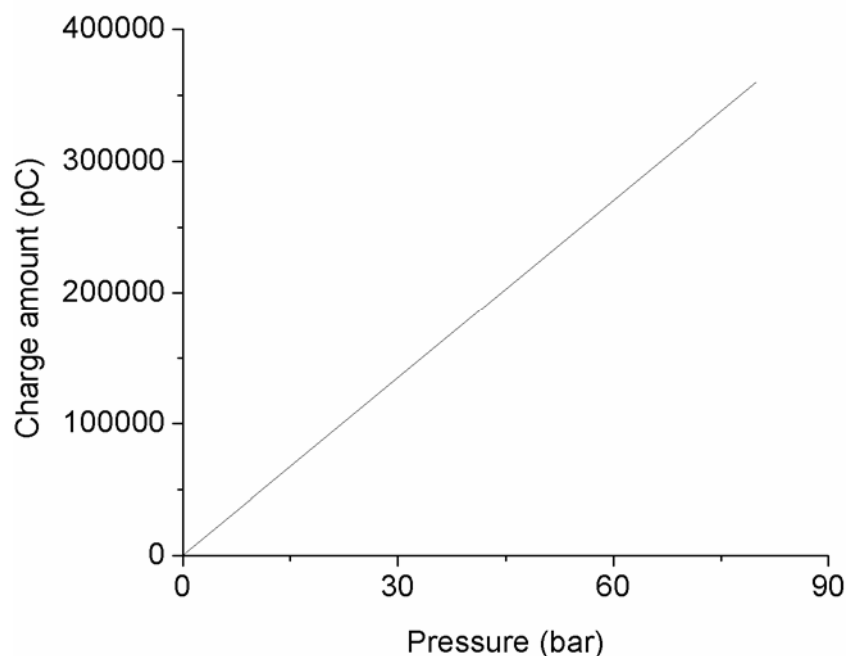


Figure 6.9 Relationship between hydrogen pressure and charges generated

The introduction of PMN-PT is a very convenient way to obtain storage enhancement based on current material processing techniques. However, the method merely affects the adsorption occurring around PMN-PT and the effect is not obvious. Bigger size or increased number of piezoelectric element is needed for large scale applications.

6.3 Hydrogen adsorption on chemically deposited TiO_2 /Carbon synthetics

The hydrogen adsorption isotherms of prepared TiO_2 /Carbon species in the absence of an electric field are shown in Figure 6.10. The measurement of pristine NAC is also included for comparison. At 80 bar, the hydrogen adsorption capacity of NAC was 0.43 wt.%, while uptakes of TC1 and TC2 were 0.40 wt.% and 0.37 wt.%, respectively.

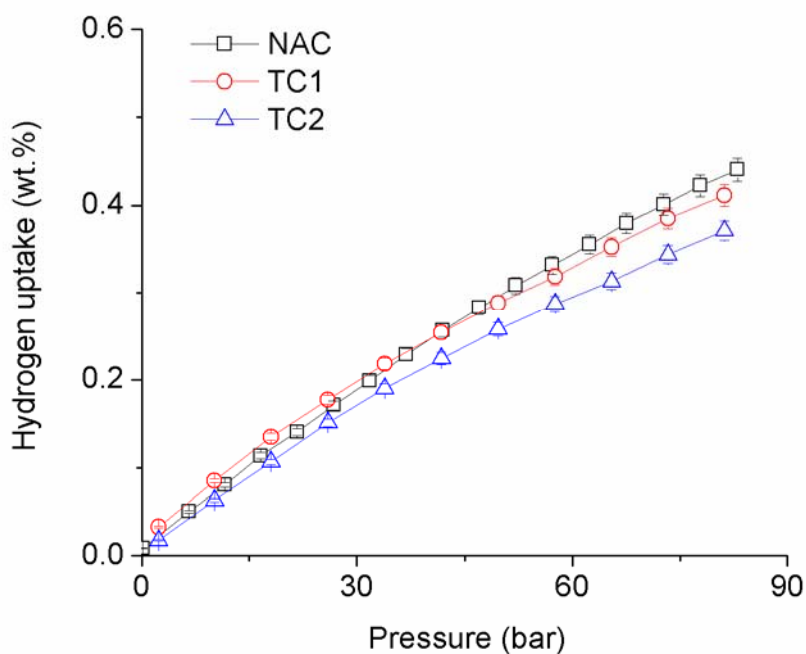


Figure 6.10 Hydrogen adsorption on TC1, TC2 and NAC

An electric potential of 1000 V was then introduced to TC1 and TC2 and the results are shown in Figure 6.11. For comparison, measurements for samples without voltage are also included. It is clear that both adsorbents have obtained adsorption enhancements with a 1000 V voltage. Adsorption capacities of TC1 and TC2 at 80 bar were 0.45 and 0.56 wt.%, corresponding to 13% and 51% increase, respectively. A greater enhancement has been expectedly achieved by TC2, the sample with higher TiO_2 content, which is consistent with our proposed theory. It is also noted that at 80 bar adsorption capacities of both TC1 and TC2 under electric field exceed that of NAC (0.43 wt.%).

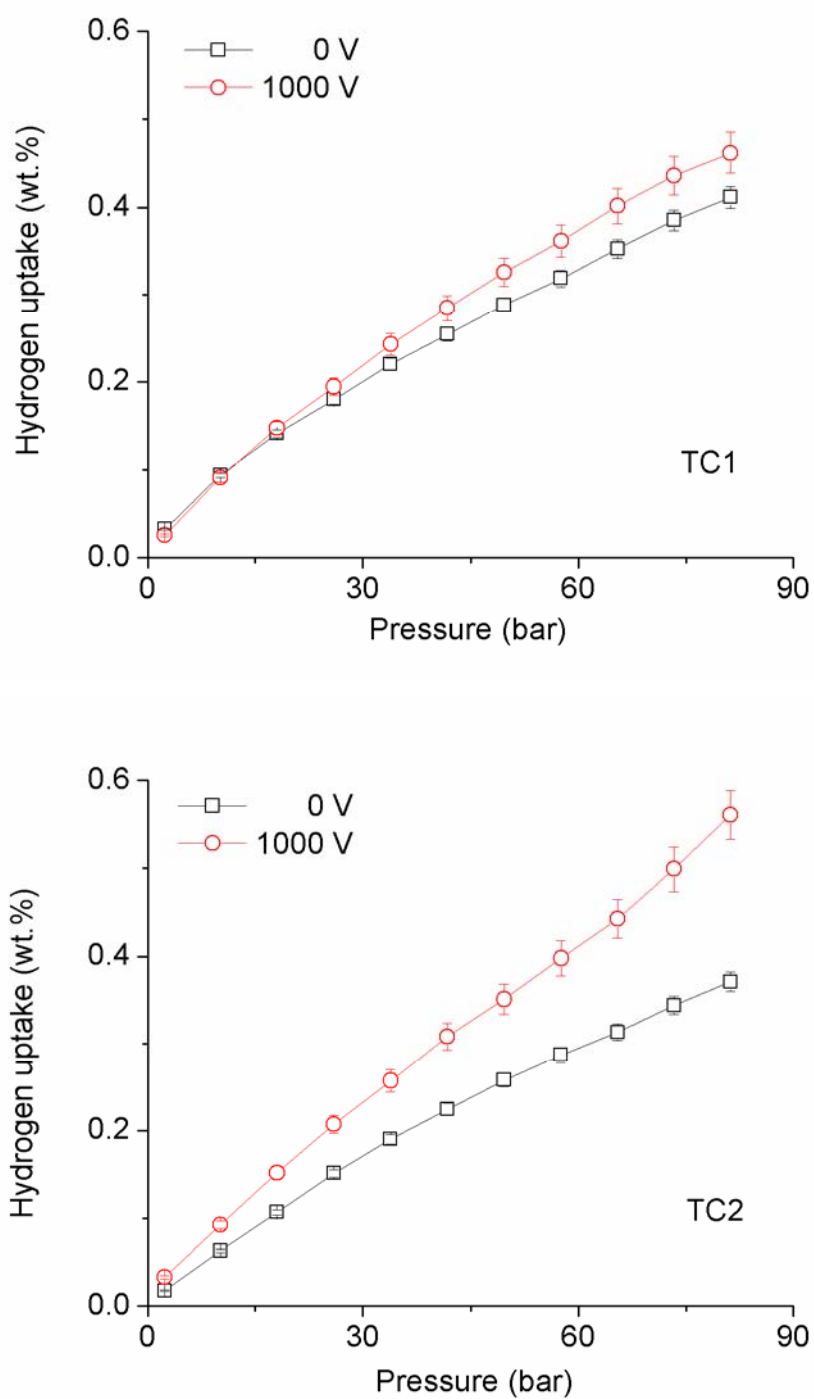


Figure 6.11 Hydrogen adsorption on TC1 and TC2 with and without 1000 V electric potential

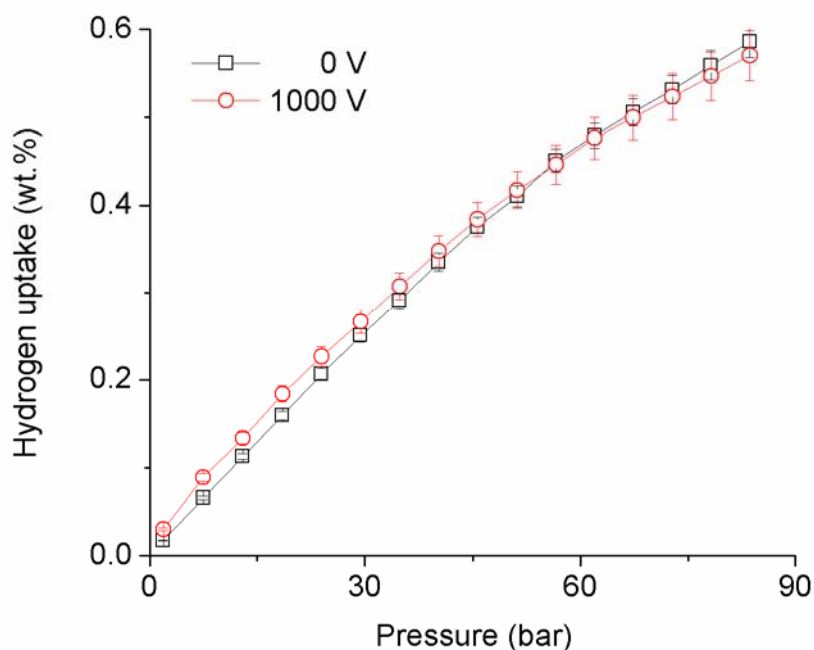


Figure 6.12 Hydrogen adsorption on HCl/NAC with and without 1000 V electric potential

To exclude the possible effect of Cl^- ions, adsorption experiments with or without 1000 V electric potential were carried out on HCl/NAC, as shown in Figure 6.12. The data curves showed a negligible difference between the two experiments. It could be concluded that the presence of Cl^- ions did not affect hydrogen uptake during the measurement. Adsorption enhancement was attributed to the introduction of TiO_2 particles.

As TC2 possesses uniform TiO_2 coating and has achieved significant adsorption enhancement with applied electric field, it was chosen as the object to study the effect of field intensity on adsorption performance over TiO_2 /Carbon synthesis. Hydrogen adsorption measurements with different electric potentials were conducted on TC2 and the results are shown in Figure 6.13. Within the range of applied potential from 0 to 3000 V, the highest storage capacity was obtained at 1000 V, while the lowest was gotten at

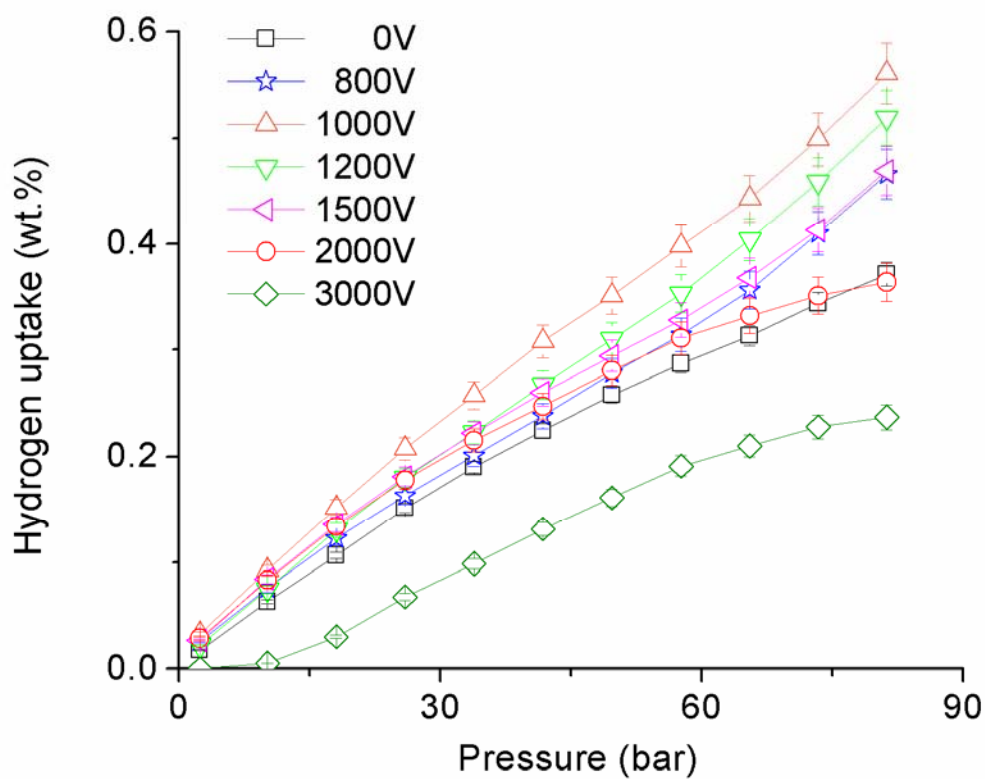


Figure 6.13 Hydrogen adsorption on TiO₂/Carbon synthetics TC2 under various electric potentials

3000 V. Additionally, as shown in Figure 6.14, the incorporated ammeter showed an electricity of around 0.1mA at 3000 V, while no electricity was detected at other voltages.

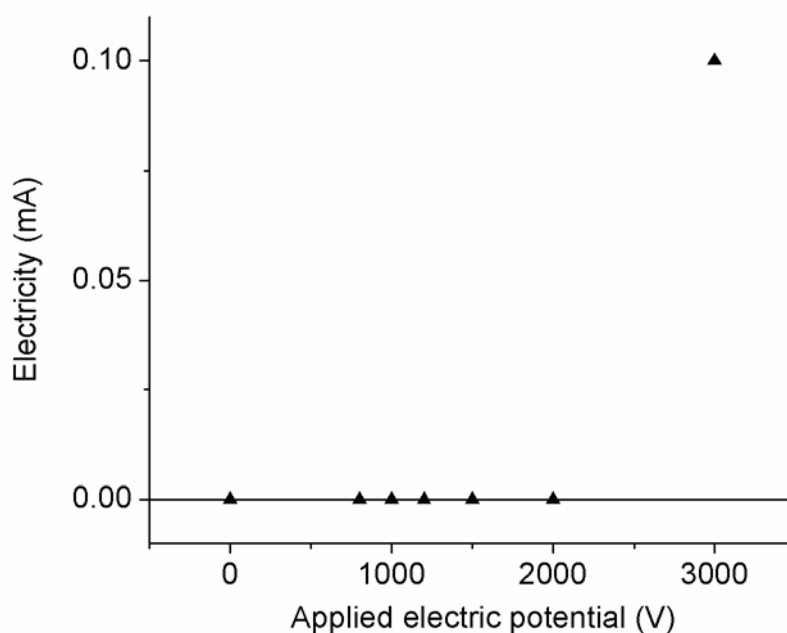


Figure 6.14 Electricity detected by ammeter under various electric potentials

To provide a more obvious comparison, variance ratios of hydrogen uptake at 20, 50 and 80 bar under different electric potential were given in Figure 6.15. Hydrogen adsorption at 20, 50 and 80 bar in the absence of an electric field were 0.12, 0.26 and 0.37 wt.%. As the potential increased, the storage capacity at each selected pressure first increased and then decreased. Enhanced hydrogen adsorptions were observed when applied potentials were less than 2000 V. The most significant adsorption enhancements were achieved at 1000 V, which were 42%, 35%, and 51% for 20, 50 and 80 bar. At 2000 V, improvements become less obvious, and even a little decrease (3%) was found at 80 bar. When the potential was raised to 3000 V, a sharp decrease occurred. Hydrogen uptakes at 20, 50 and 80 bar with a 3000 V voltage were 0.04, 0.16 and 0.24 wt.% respectively, corresponding to decreases of 66%, 38% and 35%.

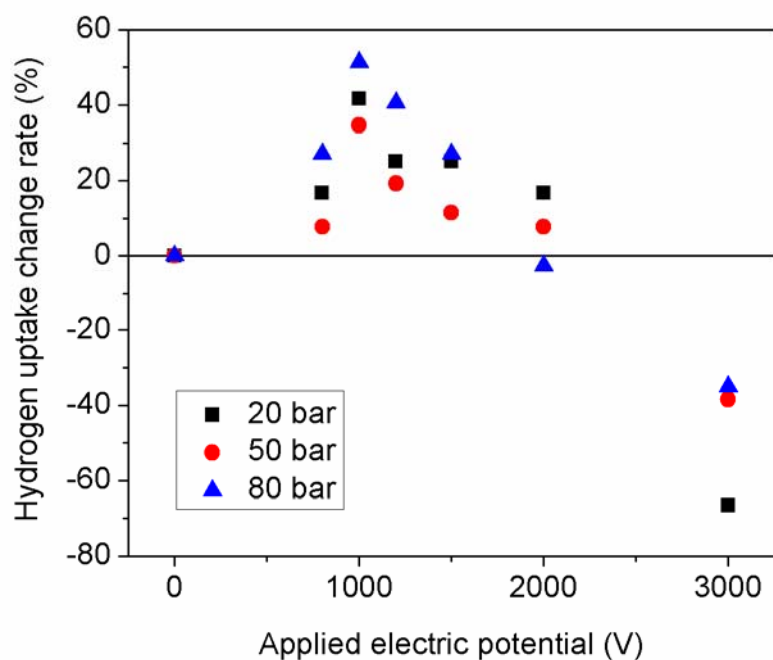


Figure 6.15 Adsorption change rate of TC2 at 20, 50 and 80 bar under various electric potentials

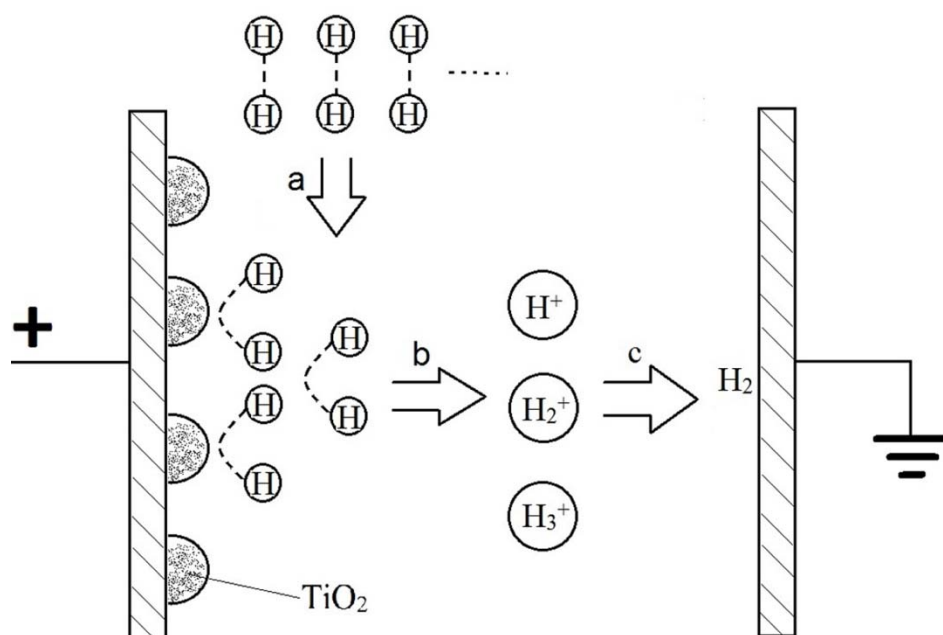
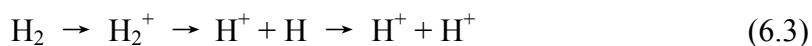


Figure 6.16 Illustration of hydrogen adsorption mechanism under electric field

As discussed before, the application of an external electric field can polarize the dielectric TiO₂ coating and induce charges on carbon. The coating also ensures the charges stay on carbon, leading to stronger electrostatic interactions between hydrogen and adsorbent. Increasing the field strength is expected to intensify the polarization and facilitate the attraction, resulting in a higher storage capacity. However, the results showed that further increase of electric potential adversely decreased the hydrogen uptake. There must be a reason for the phenomenon.

Hydrogen ions (H⁺ and H₂⁺) were reported to be formed under a strong electric field due to field ionization and field induced dissociation of H₂¹²¹, which can be described by the following reactions¹²⁴



Another kind of hydrogen ion, H₃⁺, was also detected by mass spectrum. Its formation is generally accepted as¹²⁵



According to Clements and Müller¹²⁴, H₂⁺ is predominant at low fields, but with increasing field the contributions of protons to the total ions increases. Field condition of H₃⁺ is difficult to determine. As a result, the positive charged hydrogen ions will move towards the grounded electrode and release their charges there. The observed electricity at 3000 V was an indication of the activity. Moreover, it is noticed that no current flow and remarkable decrease in adsorption were detected when a 3000 V electric potential was applied to activated carbon sample. The reason should be that TiO₂ is a kind of

material with intrinsic dipole moment. The external electric field could further enhance the dipole moment, so that the nearby hydrogen molecules would be strongly polarized and easily ionized.

Therefore, the measured hydrogen uptakes were the reflection of strengthened binding between hydrogen and adsorbent, accompanied by the influence of hydrogen ions transportation, as illustrated in Figure 6.16. Enhanced hydrogen storage obtained under a low electric potential (< 2000 V) indicated electrostatic interaction plays the leading role. A high applied potential (> 2000 V) created more hydrogen ions and an even larger electric force exerted on the ions made the ions transportation very violent, resulting in a reduced storage capacity and current flow. Moreover, the current flow would create heat in the adsorbent, which is not favorable for adsorption. To obtain an ideal storage capacity, an electric field with optimized strength is needed. For different samples, the strength may be different.

6.4 Hydrogen adsorption on TiO₂-coated Pt/AC

As the effects of electric field on TiO₂-coated activated carbon and Pt-doped carbon have been demonstrated, experiments were conducted to examine the hydrogen adsorption on TiO₂-coated Pt/AC under electric field. Figure 6.16 shows the hydrogen uptakes on TiO₂-coated Pt/AC with and without a 2000 V electric potential. Error for the measurement with voltage is about 8%. It is seen in the picture that exceptionally high enhancement in adsorption has been achieved during the entire measurement process. The adsorption capacity at 80 bar of hydrogen pressure increased from 0.13 wt.% to 0.37 wt.% with the presence of electric field, corresponding to a 185% enhancement.

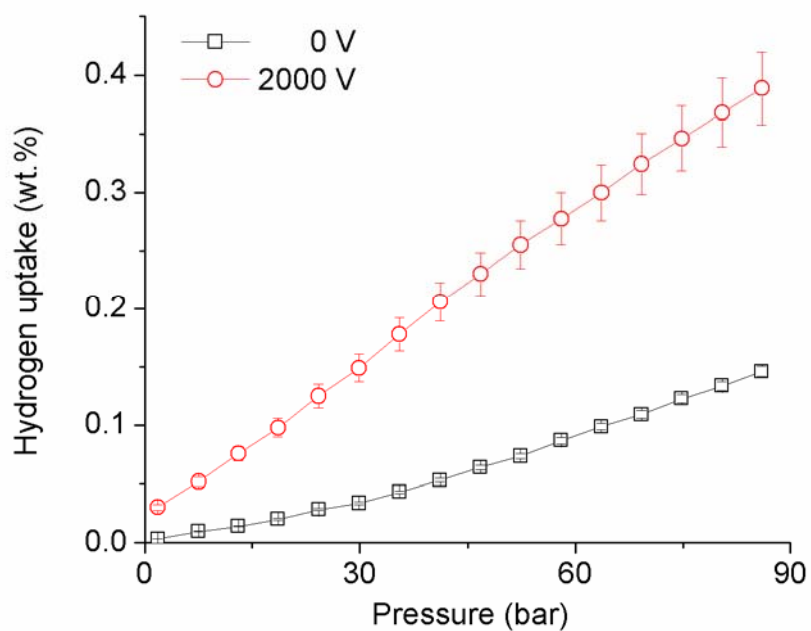


Figure 6.17 Hydrogen adsorption on TiO₂-coated Pt/AC synthetic TPC under electric potential

The adsorption enhancement over PAC demonstrated that spillover can be facilitated by applied electric field. Introduction of TiO₂ particles to the Pt/AC would result in more charges, further promoting the dissociation of hydrogen molecules. In addition, the Pt particles interacted with both carbon and TiO₂ particles. Hydrogen adsorption on TiO₂ particles might also be increased due to the spillover mechanism.

CHAPTER 7 EXAMINATION OF HYDROGEN ADSORPTION ON

ACTIVATED CARBON SEPARATED BY OTHER DIELECTRIC

MATERIALS UNDER ELECTRIC FIELD

Hydrogen adsorption enhancement over TiO_2 -coated activated carbon under proper electric field has been demonstrated by previous experimental work. The increased adsorption is considered primarily due to the enhanced dipole moment of dielectric TiO_2 . TiO_2 is a material with good dielectric properties and its dielectric constant is ~ 100 ^{126,127}. In this chapter, hydrogen adsorption performances over activated carbon separated by three other dielectric materials (MgO , ZnO and BaTiO_3) are investigated. Compared to TiO_2 , MgO and ZnO have much smaller dielectric constants, which are ~ 10 and $8-10$, respectively¹²⁸⁻¹³⁰. BaTiO_3 was selected because of the unusually high dielectric constant up to several thousand¹³¹. The study was initiated to reveal the effect of dielectric degree on hydrogen adsorption.

7.1 Hydrogen adsorption on MgO /Carbon species

Hydrogen adsorption isotherms of MC with and without an electric potential are shown in Figure 7.1. Electric fields with two different strengths were applied to the testing sample. Unlike the species coated with TiO_2 , negligible difference was shown among the tests, indicating no influence of electric field on hydrogen adsorption over activated carbon separated by MgO . Given the relative small dielectric constant of MgO , the applied electric field may not be sufficient to polarize MgO , or the degree of polarization is not enough to form stronger electrostatic interaction between hydrogen and adsorbent. Ionization of hydrogen molecule certainly becomes less probable. Therefore, no obvious enhancement or decline was found in adsorption capacity.

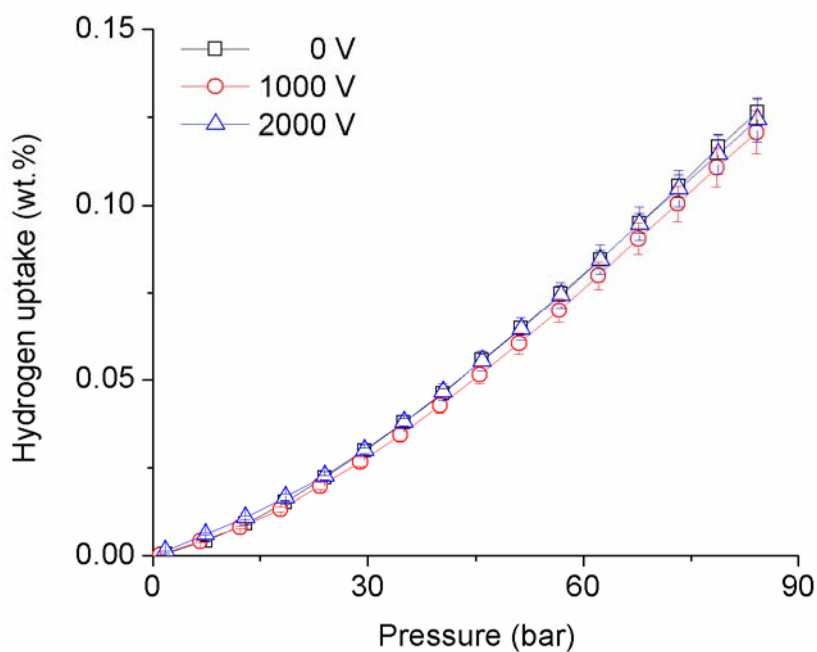


Figure 7.1 Hydrogen adsorption on MgO/Carbon synthesis MC with and without electric potential

7.2 Hydrogen adsorption on ZnO/Carbon species

Hydrogen adsorption on ZC with and without a 2000 V electric potential is given in Figure 7.2. Overlap of the error bars of the two data sets indicates no distinctive increase or decrease with an applied electric field. A slight decrease under electric field may be caused by ionization of a small amount of hydrogen. ZnO has a dielectric constant quite close to MgO, resulting in a similar adsorption phenomenon as that of MC.

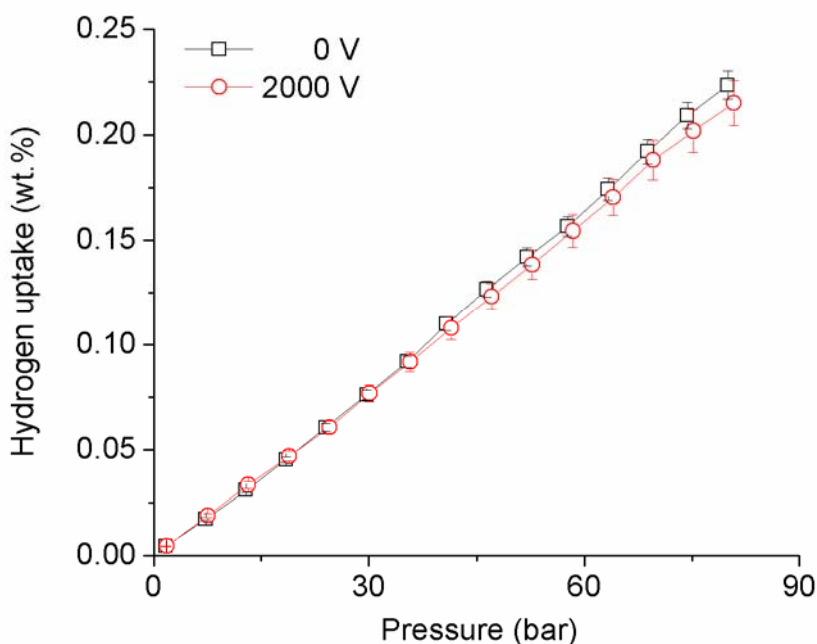


Figure 7.2 Hydrogen adsorption on ZnO/Carbon mixture ZC with and without electric potential

7.3 Hydrogen adsorption on BaTiO₃/Carbon species

Figure 7.3 shows the hydrogen adsorption on BC in the presence of absence of a 2000 V electric potential, respectively. It can be seen that adsorption enhancement showed up under very low hydrogen pressure, and the gap between the curves increase with the increase of the pressure. At 80 bar of hydrogen pressure, adsorption capacities with and without an electric field were 0.19 and 0.21 wt.%, indicating 10% increase. Although the adsorption enhancement is not impressive, it confirms that the adsorption enhancement under electric field is related to separation of activated carbon with material involving high dielectric constant. However, TiO₂ and BaTiO₃ are materials with relatively large molecular weight, which is not favorable for hydrogen storage with high weight percentage. Many light polymer-based composites with high dielectric constant, such as polyvinylidene fluoride (PVDF) with conductive additive¹³², have been well investigated and can be considered as alternatives in further study.

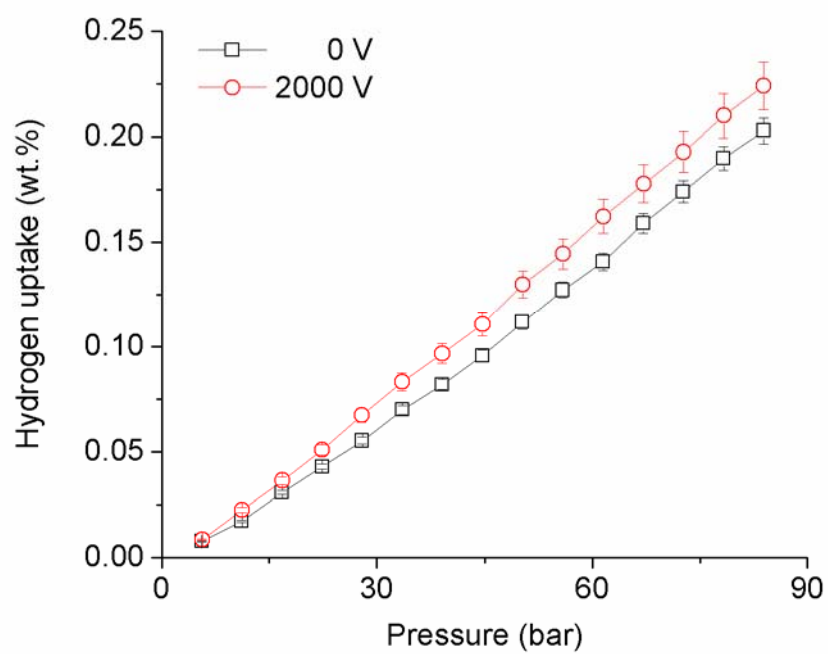
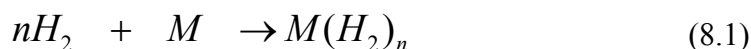


Figure 7.3 Hydrogen adsorption on BaTiO₃/Carbon mixture BC with and without electric potential

CHAPTER 8 COMPUTATIONAL CALCULATIONS

8.1 Introduction

Compared to huge amount lab work, computer modeling is an easier approach to find and evaluate suitable substances for hydrogen storage. For a generic Hydrogen adsorption process, it can be presented using a schematic equation like the one below



where M is the substrate for Hydrogen adsorption. Commonly used models with the function of adsorbing H₂ molecules include graphitic carbon-based materials^{133,134}, metal⁸², metal oxides^{64,82} and combined structures^{82,135}.

For theoretical study for the adsorption process outlined in Equation 8.1 under constant temperature and pressure, we will need to evaluate the association (or binding) Gibbs free energy, which can be expressed by

$$\Delta_r G = G[M(H_2)_n] - [nG(H_2) + G(M)] \quad (8.2)$$

In this equation, all Gs on the right hand side are the Gibbs free energy of all species relative the zero point of the state, in which all nuclei and electrons are apart to infinite distance and at rest. So these quantities are different from those normally used in thermal chemistry, in which we usually use quantities like Gibbs free energy of formation. The free energies listed on the right side of equation can be computed theoretically using ab initio methods.

In order to obtain the association Gibbs free energy $\Delta_r G$ accurately, it is ideal that the reaction represented by Equation 8.2 would be the one so called “isodesmic”, which means that the number of various bonds and lone pairs on both sides of the equation are exactly identical. The reason is that with identical chemical bonds and lone pairs on both sides, the error arising from calculating electronic correlation will mainly be cancelled out by making use of Equation 8.2. And all processes in this project are close to be isodesmic since we expect no intensive chemical bond overlap interaction taking place during the process of hydrogen adsorption, although there are some reports claiming the covalent force involvement.

By definition, association Gibbs free energy G is calculated according to equations below

$$G = H - TS \quad (8.3)$$

$$H = U + PV \quad (8.4)$$

Here, P and V are temperature and volume. H , U and S are enthalpy, internal energy and entropy with the same relative point as G defined above. U and S can be directly computed based on Statistic Mechanics principles, given that energy levels for all energy components are known. The relevant energy components are electronic, vibrational, rotational and translational parts. The latter three are often referred as thermal contribution and have been ignored in many computational works. Electronic energy is necessary to compute total internal energy and entropy and thus enthalpy and Gibbs free energy. Quantum mechanics computations are needed to obtain the electronic energy.

For quantum mechanics computations (ab initio computations), we need to solve the Schrödinger equation for the system with a Hamiltonian given below¹³⁶

$$\begin{aligned}
H = & - \sum_{\mu}^m \frac{\hbar^2}{2m_e} \nabla_{\mu}^2 - \sum_K^N \frac{\hbar^2}{2M_K} \nabla_K^2 - \sum_{\mu}^m \sum_K^N \frac{e^2 Z_K}{R_{\mu K}} \\
& + \sum_{\mu < \nu} \frac{e^2}{R_{\mu\nu}} + \sum_{K < L} \frac{e^2 Z_K Z_L}{R_{KL}}
\end{aligned} \tag{8.5}$$

On the right hand side of the equation, we have the terms in the order given for the kinetic energy for the m electrons, kinetic energy for N nuclei, nuclear-electron attraction, electron-electron repulsion and nuclear-nuclear repulsion. M_K is the mass of K th nucleus, m_e is the electronic mass, $R_{\mu K}$ is the distance between the μ th electron and K th nucleus, $R_{\mu\nu}$ is the distance between the μ th and ν th electrons, and R_{KL} is the distance between the K th and L th nuclei. And e is the electronic charge and Z_K and Z_L are the atomic numbers for K th and L th nuclei.

Usually the solution to Schrödinger equation is started with separating electrons from nuclei by invoking so called “Born-Oppenheimer Approximation”, which is based on the fact that that protons and neutrons are about 1800 times heavier than electrons¹³⁶. Because of the enormous mass difference, we can assume at any moment, the electrons move in an environment where all nuclear positions are fixed. This makes it possible to separate the motion of the electrons from that of the nuclei. At each specific nuclear configuration, all nuclear coordinates are treated as constants and the electronic wave-function is solved according to the nuclear configuration, so all electronic wave-functions have nuclear coordinates in it as parameters. Then we change the nuclear configuration according to certain algorithm and compute the electronic wave-function again. And this is repeated until the lowest possible electronic energy is reached. The nuclear configuration (nuclei position relative to one another) corresponding to the electronic wave-function with lowest energy is called equilibrium structure. The whole

process illustrated here is called “geometry optimization” since it is a process seeking for the structure with lowest electronic energy.

There are many methods for solving for the electronic wave functions and vibrational analysis, such as RHF (Restricted Hartree-Fock), DFT (Density Functional Theory), MPn (n= 1, 2, 3...) (Møller-Plesset perturbation calculation), CI (Configuration Interaction) and CC (Coupled-/Cluster theory) etc. Usually we expand the wave-function as a series of certain set of known mathematic functions with unknown coefficients. Then the problem is converted to solve for the coefficients, which is normally completed using variation theorem. Those known mathematic functions are often referred as basis sets. For more information please refer to relevant literatures¹³⁶.

In this section, Density Functional Theory investigations corresponding to the experiments have been carried out for more detailed explanations on adsorption mechanisms. Simulations were first performed on interaction of H₂ with charged TiO₂ molecule. Then, effects of electric field on H₂ adsorption over TiO₂ molecule, graphene and TiO₂-doped graphene were studied.

8.2 Computational methods

DFT calculations in this section were all performed with the program Gaussian 09¹³⁷, using the B3LYP functional and the LANL2DZ basis sets for all atom types. LANL2DZ has been widely used in quantum chemistry, particularly in the calculations of transition metal compounds^{138,139}. The coronene molecule (C₂₄H₁₂) was chosen as the model for graphite surface, as shown in Figure 8.1. Previous studies have shown that coronene is a reliable model for the graphite (0001) surface^{140,141}. A TiO₂ molecule was used to represent the metal oxide phase.

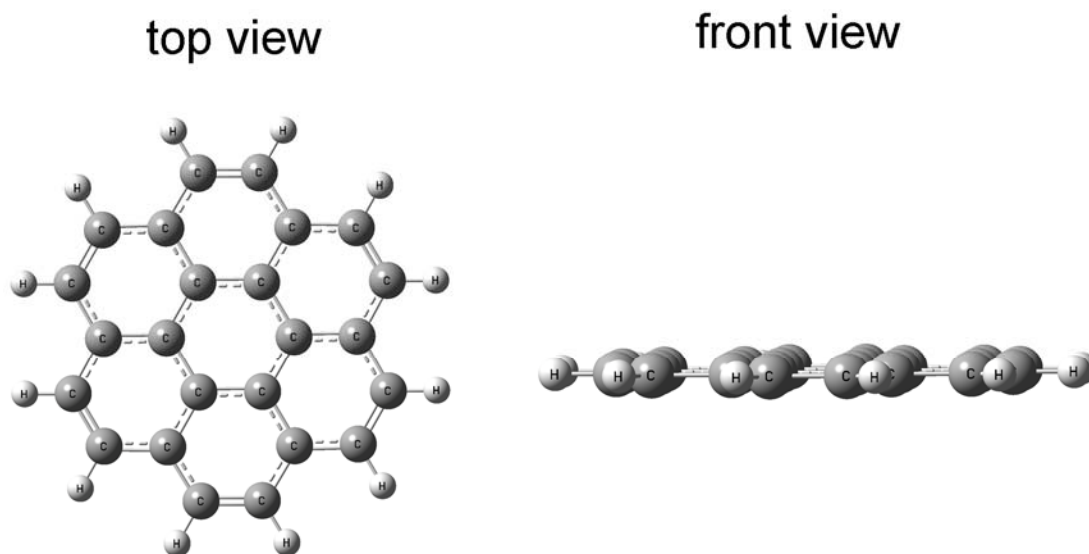


Figure 8.1 Structure of coronene

The total adsorption energy under an electric field (f) was calculated by the difference between the total energy of the whole adsorption system and the total energy of the separate objects before combination, as presented in the following equation:

$$E_{\text{ad}} = E_f(\text{H}_2 + \text{S}) - E_f(\text{S}) - E_f(\text{H}_2) \quad (8.6)$$

where E_{ad} is the adsorption energy, $E_f(\text{S} + \text{H}_2)$ is the total energy of the whole adsorption system in the presence of an electric field (f), $E_f(\text{S})$ and $E_f(\text{H}_2)$ stand for the energy of the substrate H_2 and the H_2 molecule under the intensity field f . The negative value of E_{ad} indicates that the adsorption is exothermic, while the positive means endothermic.

8.3 Results and discussion

8.3.1 Hydrogen adsorption on charged TiO_2 molecule

The simulations on H_2 adsorption with charged TiO_2 molecule were first addressed, starting with the structure shown in Figure 8.2. The optimized geometries and adsorption energies are readily seen in Table 8.1. The free hydrogen molecule optimized by B3LYP/LANL2DZ possesses an H-H bond length of 0.7435 Å. The interaction of H_2 and neutral TiO_2 molecule shows a slightly elongated H-H bond, indicating a small perturbation from the TiO_2 molecule. When H_2 interacts with negatively charged TiO_2 molecule, the shorter bond distance of 4H-2Ti and 5H-2Ti illustrate that the H_2 has been attracted closer to the TiO_2 . As a result, the binding energy increases dramatically to -7.8838 kJ/mol, which is almost three times that of H_2 and neutral TiO_2 . For the case of positively charged TiO_2 molecule as the adsorption substrate, the hydrogen molecule is less perturbed due to a shorter H-H bond and thus weakly tied to the TiO_2 . These phenomena are consistent with the experimental observations.

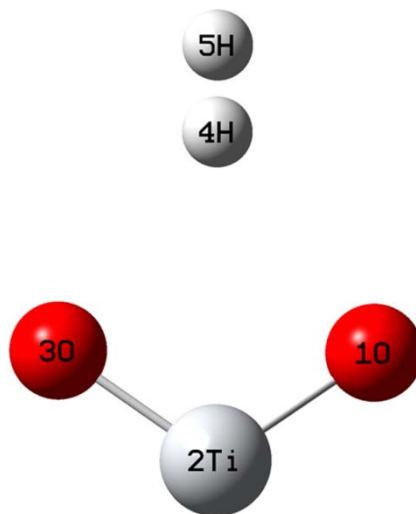


Figure 8.2 Initial state of H_2 - TiO_2 system

Table 8.1
Geometric parameters and binding energies of H₂ and charged TiO₂

Charge	Bond length (Å)			Binding energy (kJ/mol)
	4H-5H	4H-2Ti	5H-2Ti	
0	0.7451	3.6233	4.3685	-2.8597
-1	0.7483	3.3640	4.1123	-7.8838
1	0.7441	4.0795	4.8236	-1.1762

8.3.2 Hydrogen adsorption on TiO₂ molecule under electric field

Initial state H₂ and TiO₂ molecule is the same as the structure shown in Figure 8.2. Electric field is parallel to the plane that all the atoms locate. The positive direction of electric field is defined as upward and the negative is downward. The optimized geometries and binding results of H₂ and TiO₂ in the presence of an electric field are listed in Table 8.2. As shown in the table, in the field range of $f = 0$ to $+0.06$ au, H-H bond length increases with the increasing electric field strength, and meanwhile the distance between H atoms and Ti decreases with the increasing field. With applied electric fields of $+0.05$ and $+0.06$ au, the binding affinities lie between 20-40 kJ/mol, indicating reversible hydrogen storage. The calculations confirm that a positive field can evidently improve the interaction between H₂ and TiO₂. In contrast, opposite binding trends are observed when direction of the field is reversed although the decreases are not significant.

Simulations with stronger electric field have not been conducted. However, it is reasonable to predict that H-H bond would be further elongated under stronger field. As a result, hydrogen molecule becomes unstable and is prone to get ionized or broken when electric field is strong enough. This deduction can be confirmed in the light of findings from Zhou et al.⁹⁵, which illustrated molecular hydrogen adsorption is achieved only

below a certain critical electric field. Hydrogen atoms or ions can be more easily captured than molecules, leading to a promising storage capacity.

Table 8.2
Geometric parameters and binding energies of H₂ and TiO₂ under electric field

E field f (au)	Bond length (Å)			Binding energy (kJ/mol)
	4H-5H	4H-2Ti	5H-2Ti	
0	0.7451	3.6233	4.3685	-2.8597
+0.01	0.7469	3.5002	4.2471	-4.6790
+0.02	0.7504	3.4082	4.1586	-7.4171
+0.03	0.7564	3.3060	4.0623	-11.3564
+0.04	0.7655	3.2207	3.9861	-16.9582
+0.05	0.7793	3.1499	3.9292	-24.9291
+0.06	0.8014	3.0915	3.8929	-36.5103
-0.01	0.7449	3.7413	4.4862	-1.8387
-0.02	0.7461	3.9400	4.6862	-1.6179

8.3.3 Hydrogen adsorption on coronene under electric field

The initial state of H₂-coronene system is shown in Figure 8.3. Electric fields were applied perpendicular to the coronene plane, in the upward (+) or downward (-). The optimized geometries and adsorption energies of H₂ and coronene are given in Table 8.3. Little bonding energy is obtained between hydrogen molecule and coronene plane without the presence of electric field, which can be taken as the reason of the negligible adsorption capacity over carbon materials at ambient temperature. Compared to H-H bond of free hydrogen molecule (0.7435 Å), only a tiny perturbation occurs to hydrogen molecule. When a positive electric field is applied, an improvement in adsorption energy and an increase in H-H bond length are observed, which indicate a stronger interaction.

An electric field with a higher intensity further strengthens the binding between H_2 and coronene. Additionally, the application of negative field also leads to some increase in binding energy. However, it is noted that the improvements are very small and corresponding influences in hydrogen adsorption capacity should be negligible. As discussed in previous chapter, our experimental observations did not show any increase in storage capacity. Furthermore, Shi et al.⁹³ reported a slight adsorption enhancement over activated carbon with a 2000 V applied voltage. Therefore, introduction of electric field to pristine carbon materials is unlikely to efficiently improve the hydrogen adsorption capacities.

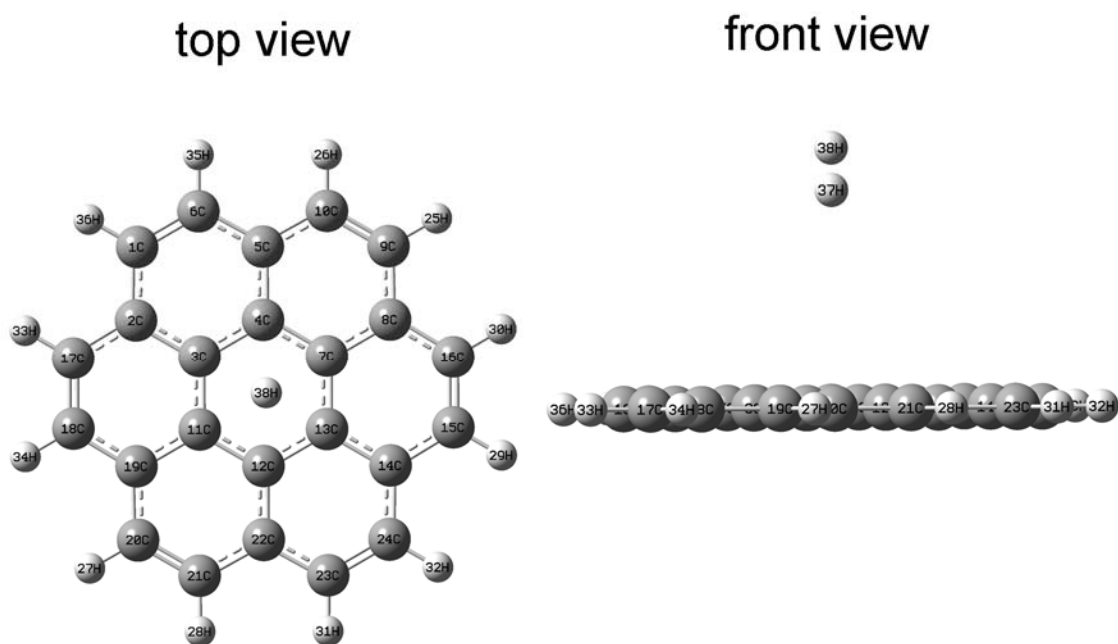


Figure 8.3 Initial state of H_2 -coronene system

Table 8.3
Geometric parameters and binding energies of H₂ and coronene under electric field

E field f (au)	Bond length (Å)			Binding energy (kJ/mol)
	37H-38H	37H-3C	38H-3C	
0	0.7436	4.1462	4.8503	0.0667
+0.01	0.7443	4.0530	4.7559	-0.4895
+0.02	0.7465	3.5700	3.5729	-1.7870
-0.01	0.7439	11.1292	11.8672	0.0005
-0.02	0.7455	3.7363	4.4333	-0.1639

8.3.4 Hydrogen adsorption on TiO₂-doped coronene under electric field

The initial state of H₂-TiO₂-coronene system is shown in Figure 8.4. Electric fields were also applied perpendicular to the coronene plane, in the upward (+) or downward (-). Considering different doping sites, our simulations showed that the most stable position for TiO₂ is perpendicularly lying above the center of the middle ring. Optimized geometries and adsorption energies of H₂ and TiO₂-doped coronene are given in Table 8.4. Calculations with TiO₂ doping showed a much higher binding energy in the absence of a field than that of pristine coronene. Given the weak adsorption energy for hydrogen on pristine coronene, the hydrogen storage capacity can be significantly increased via TiO₂ doping. However, TiO₂ itself has a large molecular weight, which is not beneficial to a high storage capacity. When a 0.005 au electric field is introduced, binding energy increases by 2.44 kJ/mol, corresponding to a 38% binding enhancement. Moreover, an approximate 100% enhancement of binding energy is achieved with the presence of a 0.01 au field. It is also found in the table that the H-H bond increases with the increasing strength of electric field, which is identical to the energy data.

The simulations show that a stronger electric field can lead to more intensive interactions

between H_2 and TiO_2 -doped graphene. The phenomenon seems very different from the experimental results, which indicated a decreased storage capacity with 3000 V electric potential. As discussed before, the strong interaction between H_2 and TiO_2 under electric field makes H_2 ionized. The formation and transportation of hydrogen ions is responsible for a reduced adsorption under relatively strong electric field. Although the calculations here failed to show the formation and transportation of hydrogen ions, they provided the reason of a stronger interaction between adsorbate and adsorbent under field, which is consistent with our experimental observations.

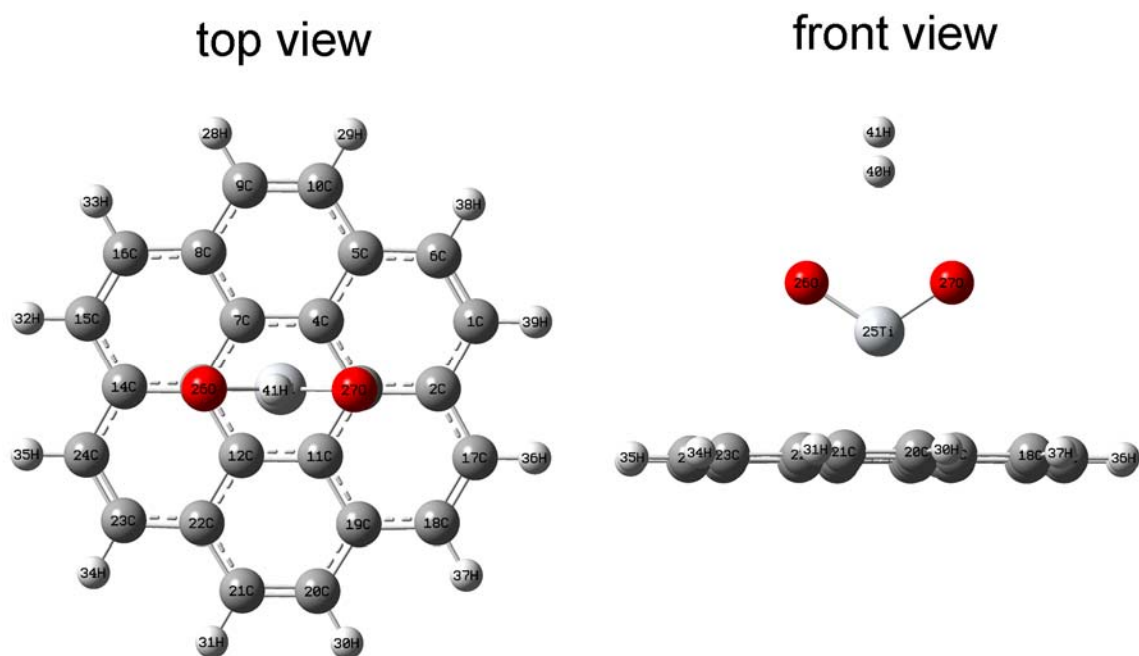


Figure 8.4 Initial state of H_2 - TiO_2 -coronene system

Table 8.4
Geometric parameters and binding energies of hydrogen and TiO₂-doped coronene under electric field

E field f (au)	Bond length (Å)				Binding energy (kJ/mol)
	40H-41H	40H-25Ti	41H-25Ti	40H-3C	
0	0.7485	4.0083	4.7545	5.5529	-6.4592
0.005	0.7511	3.8474	4.5857	5.6476	-8.9008
0.01	0.7552	3.7337	4.4699	6.9294	-12.6368

CHAPTER 9 SUMMARY AND CONCLUSIONS

In this project, a hydrogen storage system has been developed and used to investigate the effect of an applied electric field on hydrogen adsorption over activated carbon separated by different dielectric materials. The experimental results indicated that introducing an electric field to the activated carbon materials partitioned with high dielectric materials, such as TiO_2 and BaTiO_3 , could efficiently improve the hydrogen adsorption at ambient temperature.

Intensive experimental studies have been performed on TiO_2 -coated activated carbon. A 1000 V electric potential was applied to synthetics with different TiO_2 contents. Increasing enhancements of 29%, 43% and 65% were obtained at 80 bar for the samples containing 4.8, 9.1 and 13.0 wt.% TiO_2 , respectively. No improvement was observed for the sample with 1.0 wt.% due to the poor isolation of carbon particles. Normalized adsorption by the BET surface area further revealed that, under an electric field, the amount of hydrogen adsorbed on a specific area increased with the increasing TiO_2 content. Electric fields with various strengths were subsequently introduced to a carbon sample coated with 18.8 wt.% TiO_2 nanoparticles. The results showed the hydrogen uptake first increased and then decreased with the increasing strength of electric field. Enhanced storage capacities were observed when the applied electric potentials were no greater than 2000 V. The most significant adsorption enhancement was obtained at 1000 V, which showed a 51% increase at 80 bar. Experiment was also carried out on TiO_2 coated Pt/AC. Exceptionally high enhancement of 185% was achieved at 80 bar with a 2000 V applied electric potential.

The addition of dielectric TiO_2 to carbon isolates carbon particles, resulting in an

enlarged charged zone and increased charges with applied electric field. The charges are responsible for the stronger electrostatic interaction between hydrogen and the solid surface. A large amount of hydrogen molecules may be ionized under a sufficiently high electric field, resulting in a reduced hydrogen uptake.

Density Functional Theory calculations related to the experiments were also conducted and consistent with the observations. It was found that, under an external electric field, adsorption energy between hydrogen and TiO_2 -doped coronene is much higher than that in the absence of a field, leading to the enhancement in adsorption capacity.

The findings from this work indicated a potential for developing high-capacity hydrogen storage system. Further studies can be focused on the search of a light weight dielectric phase, which is an ideal hydrogen adsorbent. Limitation of current devices for hydrogen adsorption testing is also a big issue needing attentions.

REFERENCES

1. Davis SC, Diegel SW, Boundy RG. U.S. Transportation Energy Data Book. 29th Ed. Washington, D.C.: Department of Energy Press; 2010.
2. Environment News Service. New York: Environment News Service. Bush Hydrogen Initiative Faces Many Obstacles; 2003 [updated 2003 Feb 6, cited 2012 Mar 22].

Available from:
<http://www.ens-newswire.com/ens/feb2003/2003-02-06-10.html>
3. National Research Council (U.S.), National Academy of Engineering (U.S.). 2004. The Hydrogen Economy: Opportunities, Costs, Barriers, and R&D Needs. Washington D.C.: National Academies Press.
4. Hu YH. 2010. Materials for Energy Applications (Courseware). Houghton, MI: Michigan Technological University.
5. Haryanto A, Fernando S, Murali N, Adhikari S. Current status of hydrogen production techniques by steam reforming of ethanol: a review. Energy Fuels. 2005;19:2098-2106.
6. U.S. Department of Energy. A national vision of America's transition to a hydrogen economy to 2030 and beyond. Washington, DC: U.S. Department of Energy Press; 2002.
7. Ohi J. Hydrogen energy cycle: an overview. Journal of Materials Research. 2005;20:3180-3187.
8. EERE Information Center – U.S. Department of Energy. Washington, DC: U.S. Department of Energy. Comparison of fuel cell technologies; 2011[updated 2011 Feb, cited 2012 Mar 22].

Available from:

http://www1.eere.energy.gov/hydrogenandfuelcells/fuelcells/pdfs/fc_comparison_chart.pdf

9. EERE Information Center – U.S. Department of Energy. Washington, DC: U.S. Department of Energy. Types of fuel cells; 2011[updated 2011 Mar 8, cited 2012 Mar 22].

Available from:

http://www1.eere.energy.gov/hydrogenandfuelcells/fuelcells/fc_types.html#pem

10. Zhou L. Progress and problems in hydrogen storage methods. *Renewable & Sustainable Energy Reviews*. 2005;9:395-408.
11. Fichtner M. Nanotechnological aspects in materials for hydrogen storage. *Advanced Engineering Materials*. 2005;7(6):443-455.
12. Züttel A. Materials for hydrogen storage. *Materialstoday*. 2003;6(9):23-33.
13. EERE Information Center – U.S. Department of Energy. Washington, DC: U.S. Department of Energy. 2011interim update: Technical plan – storage; 2011[updated 2011, cited 2012 Mar 22].

Available from:

<http://www1.eere.energy.gov/hydrogenandfuelcells/mypp/pdfs/storage.pdf>

14. Züttel A. Hydrogen storage methods. *Naturwissenschaften*. 2004;91:157-172.
15. Eberle U, Felderhoff M, Schüth. Chemical and Physical solutions for hydrogen storage. *Angewandte Chemie International Edition*. 2009;48:6608-6630.
16. Selvam P, Visvanathan B, Swamy CS, Srinivasan V. Magnesium and magnesium alloy hydrides. *International Journal of Hydrogen Energy*. 1986;11(3):169-192.
17. Libowitz GG, Hayes HF, Gibb TRP Jr. The system zirconium-nickel and hydrogen. *Journal of Physical Chemistry*. 1958;62(1):76-79.
18. Reilly JJ Jr, Wiswall RH Jr. Reaction of hydrogen with alloys of magnesium and

- nickel and the formation of Mg_2NiH_4 . *Inorganic Chemistry*. 1968;7(11):2254-2256.
19. Reilly JJ Jr, Wiswall RH Jr. Formation and properties of iron titanium hydride. *Inorganic Chemistry*. 1974;13(1):218-222.
 20. Sakintuna B, Lamari-Darkim F, Hirscher M. Metal hydride materials for solid hydrogen storage: a review. *International Journal of Hydrogen Energy*. 2007;32(9):1121-1140.
 21. Bogdanovic B, Schwickardi M. Ti-doped alkali metal aluminium hydrides as potential novel reversible hydrogen storage materials. *Journal of Alloys and Compounds*. 1997;253–254:1-9.
 22. Orimo S, Nakamori Y, Eliseo JR, Züttle A, Jensen CM. Complex hydrides for hydrogen storage. *Chemical Reviews*. 2007;107(10):4111-4132.
 23. Dafert FW, Miklaur R. Über einige neue Verbindungen von Stickstoff und Wasserstoff mit Lithium. *Monatshefte für Chemie*. 1910;31:981-996.
 24. Graetz J. New approach to hydrogen storage. *Chemical Society Reviews*. 2009;38:73-82.
 25. Yurum Y, Taralp A, Veziroglu TN. Storage of hydrogen in nanostructured carbon materials. *International Journal of Hydrogen Energy*. 2009;34:3784-3798.
 26. Gupta BK, Tiwari RS, Srivastava ON. Studies on synthesis and hydrogenation behaviour of graphitic nanofibres prepared through palladium catalyst assisted thermal cracking of acetylene. *Journal of Alloys and Compounds*. 2004;381(1-2):301-308.
 27. de la Casa-Lillo MA, Lamari-Darkrim F, Cazorla-Amorós D, Linares-Solano A. Hydrogen storage in activated carbons and activated carbon fibers. *Journal of Physical Chemistry B*. 2002;106(42):10930-10934.
 28. Bauhman RH, Zakhidov AA, de Heer WA. Carbon nanotubes – the route toward

- applications. *Science*. 2002;297(5582):787-792.
29. Ansón A, Callejas MA, Benito AM, Maser WK, Lzquierdo MT, Rubio B, Jagiello J, Thommes M, Parra JB, Martínez MT. Hydrogen adsorption studies on single wall carbon nanotubes. *Carbon*. 2004;42(7):1243-1248.
 30. Cao D, Feng P, Wu J. Molecular simulation of novel carbonaceous materials for hydrogen storage. *Nano Letters*. 2004;4(8):1489-1492.
 31. Dillon AC, Heben MJ. Hydrogen storage using carbon adsorbents: past, present and future. *Applied Physics A: Materials Science & Processing*. 2001;72(2):133-142.
 32. Yang Z, Xia Y, Mokaya R. Enhanced hydrogen storage capacity of high surface area zeolite-like carbon materials. *Journal of the American Chemical Society*. 2007;129(6):1673-1679.
 33. Kayiran SB, Lamari FD, Levesque D. Adsorption properties and structural characterization of activated carbons and nanocarbons. *Journal of Physical Chemistry B*. 2004;108(39):15211-15215.
 34. Wang LF, Yang RT. New sorbent for hydrogen storage by hydrogen spillover -- a review. *Energy & Environmental Science*. 2008;1(2):268-279.
 35. Dillon AC, Jones KM, Bekkedahl TA, Kiang CH, Bethune DS, Heben MJ. Storage of hydrogen in single-walled carbon nanotubes. *Nature*. 1997;386:377-379.
 36. Pandey SK, Singh RK, Srivastava ON. Investigations on hydrogenation behavior of CNT admixed Mg_2Ni . *International Journal of Hydrogen Energy*. 2009;34:9378-9384.
 37. Heine T, Zhechkov L, Seifert G. Hydrogen storage by physisorption on nanostructured graphite platelets. *Physical Chemistry Chemical Physics*. 2004;6:980-984.

38. Chen P, Wu X, Lin J, Tan KL. High H₂ uptake by alkali-doped carbon nanotubes under ambient pressure and moderate temperatures. *Science*. 1999;285:91-93.
39. Tibbetts GG, Meisner GP, Olk CH. Hydrogen storage capacity of carbon nanotubes, filaments, and vapor grown fibers. *Carbon*. 2001;39(15):2291-2301.
40. Yang RT. Hydrogen storage by alkali-doped carbon nanotubes – revisited. *Carbon*. 2000;38:623-641.
41. Shiraishi M, Takenobu T, Kataura H, Ata M. Hydrogen adsorption and desorption in carbon nanotube systems and its mechanisms. *Applied Physics A*. 2004;78:947-954.
42. Kayiran SB, Lamari FD, Levesque D. Adsorption properties and structural characterization of activated carbons and nanocarbons. *Journal of Physical Chemistry B*. 2004;108(39):15211-15215.
43. Jin H, Lee YS, Hong I. Hydrogen adsorption characteristics of activated carbon. *Catalysis Today*. 2007;120(3-4):399-406.
44. Züttel A, Nützenadel Ch, Sudan P, Mauron Ph, Emmenegger Ch, Rentsch S, Schlapbach L, Weidenkaff A, Kiyobayashi T. Hydrogen sorption by carbon nanotubes and other carbon nanostructures. *Journal of Alloys and Compounds*. 2002;330-332:676-682.
45. Zheng Q, Gu A, Lu X, Lin W. Temperature-dependent state of hydrogen molecules within the nanopore of multi-walled carbon nanotubes. *International Journal of Hydrogen Energy*. 2004;29(5):481-489.
46. Thomas KM. Hydrogen adsorption and storage on porous materials. *Catalysis Today*. 2007;120(3-4):389-398.
47. Ye Y, Ahn CC, Witham C, Fultz B, Liu J, Rinzler AG. Hydrogen adsorption and cohesive energy of single-walled carbon nanotubes. *Applied Physics Letters*. 1999;74:2307-2309.

48. Rosi NL, Eckert J, Eddaoudi M, Vodak DT, Kim J, O'Keeffe M, Yaghi OM. Hydrogen storage in microporous metal-organic frameworks. *Science*. 2003;300(5622):1127-1129.
49. Yildirim T, Hartman MR. Direct observation of hydrogen adsorption sites and nanocage formation in metal-organic frameworks. *Physical Review Letters*. 2005;95(21):215504 1-4.
50. Li H, Eddaoudi M, O'Keeffe M, Yaghi OM. Design and synthesis of an exceptionally stable and highly porous metal –organic framework. *Nature*. 1999;402:276-279.
51. Hirscher M, Panella B, Schmitz B. Metal-organic frameworks for hydrogen storage. *Microporous and Mesoporous Materials*. 2010;129:335-339.
52. Hu YH, Zhang L. Hydrogen storage in metal-organic frameworks. *Advanced Energy Materials*. 2010;22:E117-E130.
53. Yang Q, Zhong C. Molecular simulation of adsorption and diffusion of hydrogen in metal-organic frameworks. *Journal of Physical Chemistry B*. 2005;109(24):11862-11864.
54. Rowsell JLC, Eckert J, Yaghi OM. Characterization of H₂ binding sites in prototypical metal-organic frameworks by inelastic neutron scattering. *Journal of the American Chemical Society*. 2005;127(42):14904-14910.
55. Rowsell JLC, Millward AR, Park KS, Yaghi OM. Hydrogen sorption in functionalized metal-organic frameworks. *Journal of the American Chemical Society*. 2004;126:5666-5667.
56. Rowsell JLC, Yaghi OM. Effects of functionalization, catenation, and variation of the metal oxide and organic linking units on the low-pressure hydrogen adsorption properties of metal-organic frameworks. *Journal of the American Chemical Society*. 2006;128:1304-1315.

57. Chae H, Siberio-Perez DY, Kim J, Go Y, Eddaoudi M, Matzger AJ, O’Keeffe M, Yaghi OM. A route to high surface area, porosity and inclusion of large molecules in crystals. *Nature*. 2004, 427, 523-527.
58. Furukawa H, Miller M, Yaghi OM. Independent verification of the saturation hydrogen uptake in MOF-177 and establishment of a benchmark for hydrogen adsorption in metal–organic frameworks. *Journal of Materials Chemistry*. 2007;17:3197-3204.
59. Berman A, Karn RK, Epstein M. Steam reforming of methane on a Ru/Al₂O₃ catalyst promoted with Mn oxides for solar hydrogen production. *Green Chemistry*. 2007;9(6):626-631.
60. Hu YH, Ruckenstein E. Catalytic conversion of methane to synthesis gas by partial oxidation and CO₂ reforming. *Advances in Catalysis*. 2004;48:297-345.
61. Li Y, Li X, Li J, Yin J. Photocatalytic degradation of methyl orange by TiO₂-coated activated carbon and kinetic study. *Water Research*. 2006;40:1119-1126.
62. Wang J, Wang L, Ma Li, Zhao J, Wang B, Wang G. Structures, electronic properties, and hydrogen-storage capacity of single-wall TiO₂ nanotubes. *Physica E*. 2009;41:838-842.
63. Dai XP, Li RJ, Yu CC, Hao ZP. Unsteady-state direct partial oxidation of methane to synthesis gas in a fixed-bed reactor using AFeO₃ (A = La, Nd, Eu) perovskite-type oxides as oxygen storage. *Journal of Physical Chemistry B*. 2006;110(45):22525-22531.
64. Sun X, Hwang JY, Shi SZ. Hydrogen storage in mesoporous metal oxide with catalyst and external electric field. *Journal of Physical Chemistry C*. 2010;114(15):7178-7184.
65. Korotcenkov G. Metal oxides for solid-state gas sensors: What determines our

- choice? *Materials Science and Engineering B*. 2007;139(1):1-23.
66. Bushnell JE, Kemper PR, Maitre P, Bowers MT. Insertion of Sc^+ into H_2 : The first example of cluster-mediated σ -bond activation by a transition metal center. *Journal of the American Chemical Society*. 1994;116(21):9710-9718.
 67. Manard MJ, Bushnell JE, Bernstein SL, Bowers MT. Origin of bonding interactions in $\text{Cu}_2^+(\text{H}_2)_n$ clusters: An experimental and theoretical investigation. *Journal of Physical Chemistry A*. 2002;106(42):10027-10032.
 68. Mishra A, Banerjee S, Mohapatra SK, Graeve OA, Misra M. Synthesis of carbon nanotube- TiO_2 nanotubular material for reversible hydrogen storage. *Nanotechnology*. 2008;19(44):445607-445613.
 69. Rather S, Mehraj-ud-din N, Zacharia R, Hwang SW, Kim AR, Nahm KS. Hydrogen storage of nanostructured TiO_2 -impregnated carbon nanotubes. *International Journal of Hydrogen Energy*. 2009;34(2):961-966.
 70. Lim SH, Luo J, Zhong Z, Ji W, Lin J. Room-temperature hydrogen uptake by TiO_2 nanotubes. *Inorganic Chemistry*. 2005;44(12):4124-4126.
 71. Bavykin DV, Lapkin AA, Plucinski PK, Friedrich JM, Walsh FC. Reversible storage of molecular hydrogen by sorption into multilayered TiO_2 nanotubes. *Journal of Physical Chemistry B*. 2005;109(41):19422-19427.
 72. Pan H, Luo J, Sun H, Feng Y, Poh C, Lin J. Hydrogen storage of ZnO and Mg doped ZnO nanowires. *Nanotechnology*. 2006;17:2963-2967.
 73. Ahmad M, Rafi-ud-Din, Pan C, Zhu J. Investigation of hydrogen storage capacities of ZnO-based nanostructures. *Physical Chemistry C*. 2010;114(6):2560-2565.
 74. Dag S, Ozturk Y, Ciraci S, Yildirim T. Adsorption and dissociation of hydrogen molecules on bare and functionalized carbon nanotubes. *Physical Review B*. 2005;72 (15):155404-155411.

75. Lueking AD, Yang RT. Hydrogen spillover from a metal oxide catalyst onto carbon nanotubes -- implications for hydrogen storage. *Journal of Catalysis*. 2002;206(1):165-168.
76. Lueking AD, Yang RT. Hydrogen spillover to enhance hydrogen storage – study of the effect of carbon physicochemical properties. *Applied Catalysis A*. 2004;265:259-268.
77. Yang FH, Lachawiec AJ, Yang RT. Adsorption of spillover hydrogen atoms on single-wall carbon nanotubes. *Journal of Physical Chemistry B*. 2006;110(12):6236-6244.
78. Lachawiec AJ, Qi G, Yang RT. Hydrogen storage in nanostructured carbons by spillover: bridge-building enhancement. *Langmuir*. 2005;21(24):11418-11424.
79. Li Y, Yang RT. Hydrogen storage on platinum nanoparticles doped on superactivated carbon. *Journal of Physical Chemistry C*. 2007;111(29):11086-11094.
80. Li Y, Yang RT. Significantly enhanced hydrogen storage in metal-organic frameworks via spillover. *Journal of the American Chemical Society*. 2006;128(3):726-727.
81. Li Y, Yang RT. Hydrogen storage in metal-organic frameworks by bridged hydrogen spillover. *Journal of the American Chemical Society*. 2006;128(25):8136-8137.
82. Cheng H, Chen L, Cooper CA, Sha X, Pez GP. Hydrogen spillover in the context of hydrogen storage using solid-state materials. *Energy & Environmental Science*. 2008;1(3):338-354.
83. Adelhelm P, de Jongh PE. The impact of carbon materials on the hydrogen storage properties of light metal hydrides. *Journal of Materials Chemistry*. 2010;21:2417-2427.

84. Bouaricha S, Dodelet JP, Guay D, Huot J, Schulz R. Study of the activation process of Mg-based hydrogenstorage materials modified by graphite and other carbonaceous compounds. *Journal of Materials Research*. 2001;16(10):2893-2905.
85. Bouaricha S, Dodelet JP, Guay D, Huot J, Schulz R. Activation characteristics of graphite modified hydrogen absorbing materials. *Journal of Alloys and Compounds*. 2001;325(1):245-251.
86. Amirkhiz BS, Danaie M, Barnes M, Simard B, Mitlin D. Hydrogen sorption cycling kinetic stability and microstructure of single-walled carbon nanotube (SWCNT) magnesium hydride (MgH_2) nanocomposites. *Journal of Physical Chemistry C*. 2010;114(7):3265-3275.
87. Imamura H, Usui Y, Takashima M. Preparation and hydriding properties of magnesium-containing hydrogen storage materials chemically deposited from a homogeneous phase. *Journal of the Less Common Metals*. 1991;175(1):171-176.
88. Liang JJ, Kung WCP. Confinement of Mg- MgH_2 systems into carbon nanotubes changes hydrogen sorption energetics. *Journal of Physical Chemistry C*. 2005;109(38):17837-17841.
89. Baldé CP, Hereijgers BPC, Bitter JH, de Jong KP. Sodium alanate nanoparticles – linking size to hydrogen storage properties. *Journal of the American Chemical Society*. 2008;130 (21):6761–6765.
90. Li X, Hwang JY, Shi S, Sun X, Zhang Z. Effect of electric potential on hydrogen adsorption. *Carbon*. 2010;48(3):876-880.
91. Li X, Hwang JY, Shi S, Sun X, Zhang Z. Effect of piezoelectric material on hydrogen adsorption. *Fuel Processing Technology*. 2010;91(9):1087-1089.

92. Shi S, Hwang JY, Li X, Sun X. Enhanced hydrogen sorption on carbon and NiO in the presence of a piezoelectric element. *Energy & Fuels*. 2009;23(12):6085-6088.
93. Shi S, Hwang JY, Li X, Sun X, Lee BI. Enhanced hydrogen sorption on carbonaceous sorbents under electric field. *International Journal of Hydrogen Energy*. 2010;35(2):629-631.
94. Liu W, Zhao YH, Nguyen J, Li Y, Jiang Q, Lavernia EJ. Electric field induced reversible switch in hydrogen storage based on single-layer and bilayer graphenes. *Carbon* 2009;47(15):3452-3460.
95. Zhou J, Wang Q, Sun Q, Jena P, Chen XS. Electric field enhanced hydrogen storage on polarizable materials substrates. *Proceedings of the National Academy of Science of the United States of America*. 2010;107(7):2801-2806.
96. Kubas GJ. 2001. *Metal Dihydrogen and σ -bond Complexes: Structure, Theory, and Reactivity*. New York: Kluwer Academic/Plenum Publishers.
97. Lochan RC, Head-Gordon M. Computational studies of molecular hydrogen binding affinities: The role of dispersion forces, electrostatics, and orbital interactions. *Physical Chemistry Chemical Physics*. 2006;8(12):1357-1370.
98. Froudakis GE. Why alkali-metal-doped carbon nanotubes possess high hydrogen uptake. *Nano Letters*. 2001;1(10):531-533.
99. Zhao YL, Zhang RQ, Wang RS. The role of lithium in hydrogen storage in aromatic carbon materials. *Chemical Physics Letters*. 2004;398(1-3):62-67.
100. Paul W, Lucke B, Schlemmer S, Gerlich D. *International Journal of Mass Spectrometry and Ion Processes*. On the dynamics of the reaction of positive hydrogen cluster ions (H_5^+ to H_{23}^+) with para and normal hydrogen at 10 K. 1995;149-150:373-387.
101. Thomson JJ. Further experiments on positive rays. *Philosophical Magazine Series*

6. 1912;24(140):209-253.
102. Kurosaki Y, Takayanagi T. An *ab initio* molecular orbital study of even-membered hydrogen cluster cations: H_6^+ , H_8^+ , H_{10}^+ , H_{12}^+ , and H_{14}^+ . Journal of Chemical Physics. 1998;109(11):4327-4334.
103. Dykstra CE, Gaylord AS, Gwinn WD, Swope WC, Schaefer HF III. The uncoupled symmetric stretching frequency of H_3^+ . Journal of Chemical Physics. 1978;68(8):3951-3952.
104. Hiraoka K, Kebarle P. A determination of the stabilities of H_5^+ , H_7^+ , H_9^+ , and H_{11}^+ from measurement of the gas phase ion equilibria $H_n^+ + H_2 = H_{n+2}^+$ ($n = 3, 5, 7, 9$). Journal of Chemical Physics. 1975;62(6):2267-2270.
105. Mills RL. Novel hydrogen compounds from a potassium carbonate electrolytic cell. Fusion Science and Technology. 2000;37(2):157-182.
106. Hirao K, Yamabe S. Theoretical study on the structure and stability of hydrogen-ion clusters H_n^+ and H_n^- ($n = 3, 5, 7, 9, 11, 13$). Chemical Physics. 1983;80(3):237-243.
107. Kubas GJ, Ryan RR, Swanson BI, Vergamini PJ, Wasserman HJ. Characterization of the first examples of isolable molecular hydrogen complexes, $M(CO)_3(PR_3)_2(H_2)$ ($M =$ molybdenum or tungsten; $R =$ Cy or isopropyl). Evidence for a side-on bonded dihydrogen ligand. Journal of the American Chemical Society. 1984;106(2):451-452.
108. Long JR, Dincă M. Hydrogen storage in microporous metal-organic frameworks with exposed metal sites. Angewandte Chemie International Edition (English). 2008;47(36):6766-6779.
109. Bushnell JE, Maitre P, Kemper PR, Bowers MT. Binding energies of $Ti^+(H_2)_{1-6}$ clusters: theory and experiment. Journal of Chemical Physics. 1997;106:10153-10167.

110. Weis P, Kemper PR, Bowers MT. $Mn^+(H_2)_n$ and $Zn^+(H_2)_n$ clusters: Influence of 3d and 4s orbitals on metal–ligand bonding. *Journal of Physical Chemistry A*. 1997;101(15):2809-2816.
111. Zhao XB, Xiao B, Fletcher AJ, Thomas KM. Hydrogen adsorption on functionalized nanoporous activated carbons. *Journal of Physical Chemistry B*. 2005;109(18):8880-8888.
112. Lin CJ, Tu WK, Kuo CK, Chien SH. Single-step fabrication of phase-controllable nanocrystalline TiO_2 films for enhanced photoelectrochemical water splitting and dye-sensitized solar cells. *Journal of Power Sources*. 2011;196:4865-4869.
113. Yacob AR, Mustajab MKAA, Samadi NS. Calcination temperature of nano MgO effect on base transesterification of palm oil. *World Academy Science, Engineering and Technology*. 2009;56:408-412.
114. Hy-Energy LLC. 2007. PCT-Pro 2000 User Guide. Newark, CA: Hy-Energy LLC.
115. Uršič H, Zarnik MS, Kosec M. $Pb(Mg_{1/3}Nb_{2/3})O_3$ – $PbTiO_3$ (PMN-PT) material for actuator applications. *Smart Material Research*. 2011;2011:452901 1-6.
116. van Randeraat J, Setterington RE. 1974. *Piezoelectric Ceramics*. London, UK: Mullard Ltd.
117. Brunauer S, Emmett PH, Teller EE. Adsorption of gases in multimolecular layers. *Journal of the American Chemical Society*. 1938;60(2):309-319.
118. Harkins WD, Jura G. Surfaces of solids. XIII. A vapor and adsorption method for the determination of the area of a solid without the assumption of a molecular area, and the areas occupied by nitrogen and other molecules on the surface of a solid. *Journal of the American Chemical Society*. 1944;66:1366-1373.
119. Wen C. 2010. Enhancement of Hydrogen Adsorption with Titanium Dioxide Coated Carbon. Houghton, MI: Michigan Technological University.

120. Glab WL, Hessler JP. Ionization and dissociation of H_2 in a static electric field: Levels near the ionization threshold. *Physical Review A*. 1990(9);42:5486-5498.
121. Ernst N, Block JH. Electron-stimulated field desorption of diatomic and triatomic hydrogen. *Physical Review B*. 1984;29(12):7092-7095.
122. Hu X, Skadtchenko BO, Trudeau M, Antonelli DM. Hydrogen storage in chemically reducible mesoporous and microporous Ti oxides. *Journal of the American Chemical Society*. 2006;128(36):11740.
123. Ahmad K, Pan W, Shi SL. Electrical conductivity and dielectric properties of multiwalled carbon nanotube and alumina composites. *Applied Physics Letters*. 2006;89(13):133122-133124.
124. Clements TC, Müller EW. Occurrence of H_3^+ in the field ionization of hydrogen. *Journal of Chemical Physics*. 1962;37(11):2684-2687.
125. Eyring H, Hirschfelder JO, Taylor HS. The theoretical treatment of chemical reactions produced by ionization processes Part I. The ortho-para hydrogen conversion by alpha-particles. *Journal of Chemical Physics*. 1936;4:479-91.
126. Breckenridge RG, Hosler WR. Electrical properties of titanium dioxide semiconductors. *Physical Review*. 1953;91(4):793-802.
127. Lundstrom JM, Rinehart LF, Pate RC, Smith TL. Measurement of the dielectric strength of titanium dioxide ceramics. *IEEE*. 1999. 1489-1491.
128. Subramanian MA, Shannon RD, Chai BHT, Abraham MM, Wintersgill MC. Dielectric constants of BeO, MgO, and CaO using the two-terminal method. *Physics and Chemistry of Minerals*. 1989;16(8):741-746.
129. Yang Y, Guo W, Wang X, Wang Z, Qi J, Zhang Y. Size dependence of dielectric constant in a single pencil-like ZnO nanowire. *Nano Letters. Proceeding*.
130. Langton NH, Matthews D. The dielectric constant of zinc oxide over a range of frequencies. *British Journal of Applied Physics*. 1958;9:453-456.

131. Hoshina T, Takizawa K, Li J, Kasama T, Kakemoto H, Tsurumi T. Domain size effect on dielectric properties of barium titanate ceramics. *Japanese Journal of Applied Physics*. 2008;47(9):7607-7611.
132. Chen Q, Du P, Jin L, Weng W, Han G. Percolative conductor/polymer composite film with significant dielectric properties. *Applied Physics Letters*. 2007;91:0022912 1-3.
133. Park N, Hong S, Kim G, Jhi SH. Computational study of hydrogen storage characteristics of covalent-bonded graphenes. *Journal of the American Chemical Society*. 2007;129:8999-9003.
134. Han SS, Lee HM. Adsorption properties of hydrogen on (10,0) single-walled carbon nanotube through density functional theory. *Carbon*. 2004;42:2169-2177.
135. Psfogiannakis GM, Froudakis GE. DFT study of the hydrogen spillover mechanism on Pt-Doped graphite. *Journal of Physical Chemistry C*. 2009;113:14908-14915.
136. Cramer CJ. 2004. *Essentials of Computational Chemistry: Theories and Models*. Second Edition. Chichester, England: John Wiley & Sons Ltd.
137. Frisch, M. J.; Trucks, G. W.; Schlegel, H. B.; Scuseria, G. E.; Robb, M. A.; Cheeseman, J. R.; Scalmani, G.; Barone, V.; Mennucci, B.; Petersson, G. A.; Nakatsuji, H.; Caricato, M.; Li, X.; Hratchian, H. P.; Izmaylov, A. F.; Bloino, J.; Zheng, G.; Sonnenberg, J. L.; Hada, M.; Ehara, M.; Toyota, K.; Fukuda, R.; Hasegawa, J.; Ishida, M.; Nakajima, T.; Honda, Y.; Kitao, O.; Nakai, H.; Vreven, T.; Montgomery, Jr., J. A.; Peralta, J. E.; Ogliaro, F.; Bearpark, M.; Heyd, J. J.; Brothers, E.; Kudin, K. N.; Staroverov, V. N.; Kobayashi, R.; Normand, J.; Raghavachari, K.; Rendell, A.; Burant, J. C.; Iyengar, S. S.; Tomasi, J.; Cossi, M.; Rega, N.; Millam, N. J.; Klene, M.; Knox, J. E.; Cross, J. B.; Bakken, V.; Adamo, C.; Jaramillo, J.; Gomperts, R.; Stratmann, R. E.; Yazyev, O.; Austin, A. J.;

- Cammi, R.; Pomelli, C.; Ochterski, J. W.; Martin, R. L.; Morokuma, K.; Zakrzewski, V. G.; Voth, G. A.; Salvador, P.; Dannenberg, J. J.; Dapprich, S.; Daniels, A. D.; Farkas, Ö.; Foresman, J. B.; Ortiz, J. V.; Cioslowski, J.; Fox, D. J. Gaussian 09, Revision B.01. Gaussian, Inc., Wallingford CT, 2009.
138. Chiodo S, Russo N, Sicilia E. LANL2DZ basis sets recontracted in the framework of density functional theory. *Journal of Chemical Physics*. 2006;125(104107):1-8.
139. Cao Y, Zhao X, Xin B, Xiong S, Tang Z. Reactions of M^+ and MO^+ ($M = V, Nb, Ta$) with methanol. *Journal of Molecular Structure*. 2004;683(1-3):141-146.
140. Jelaica L, Sidis V. DFT investigation of the adsorption of atomic hydrogen on a cluster-model graphite surface. *Chemical Physics Letters*. 1999;300(1-2):157-162.
141. Bonfanti M, Martinazzo R, Tantardini GF, Ponti A. Physisorption and diffusion of hydrogen atoms on graphite from correlated calculations on the H-Coronene model system. *Journal of Physical Chemistry C*. 2007;111(16):5825-5829.

APPENDIX A

Figure 1.1 used in this dissertation was originally published in Transportation Energy Data Book (29th Edition) by DOE. The work was sponsored by the U.S. Government. The U.S. Government retains a nonexclusive, royalty-free license to publish or reproduce these documents, or to allow others to do so. These documents may be freely distributed and used for non-commercial, scientific and education purpose.

APPENDIX B

Figure 1.2 used in this dissertation was originally published on EERE web site. Materials on the EERE Web site are in the public domain. EERE requests that it be acknowledged as the source in any subsequent use of its information.

APPENDIX C

Table 1.3 used in this dissertation was originally published on EERE web site. Materials on the EERE Web site are in the public domain. EERE requests that it be acknowledged as the source in any subsequent use of its information.

APPENDIX D

Figure 1.3 used in this dissertation was originally published on EERE web site. Materials on the EERE Web site are in the public domain. EERE requests that it be acknowledged as the source in any subsequent use of its information.

APPENDIX E

Figure 2.1 used in this dissertation was originally published in the Catalysis Today, Elsevier, "Hydrogen adsorption and storage on porous materials", Volume 120, 2007, 389-398. Permission to reuse material from the published work was obtained with kind permission from Elsevier. A copy of the granting permission for reproduction is shown below.

This is a License Agreement between Zheng Zhang ("You") and Elsevier ("Elsevier") provided by Copyright Clearance Center ("CCC"). The license consists of your order details, the terms and conditions provided by Elsevier, and the payment terms and conditions.

Customer name: Zheng Zhang

Customer organization: Michigan Technological University

License number: 2926140534926

License date: JUN 11, 2012

Publication: Catalysis Today

Article title: Hydrogen adsorption and storage on porous materials

Author: Thomas KM

DOI: 10.1016/J.CATTOD.2006.09.015

Date: Feb 28, 2007

ISSN: 0920-5861

Publication type: Journal

Volume: 120

Issue: 3-4

Start Page: 389

Publisher: ELSEVIER BV

Permission status: Granted

Permission type: Republish or display content

Type of use: reuse in a thesis/dissertation

Number of page: 10

Portion: figures/tables/illustrations

Number of figures/tables/illustrations: 2

Format: both print and electronic

Are you the author of this Elsevier article? No

Will you be translating? No

Order reference number:

Title of your thesis/dissertation: Effect of External Electric Field on Hydrogen Adsorption over Activated Carbon Separated by Dielectric Materials

Expected completion date: JUN 2012

Estimated size (number of pages): 120

Elsevier VAT number: GB 494 6272 12

Permissions price: 0.00 USD

VAT/Local Sales Tax: 0.0 USD / 0.0 GBP

Total: 0.00 USD

APPENDIX F

Figure 2.2 used in this dissertation was originally published in the Journal of Physical Chemistry B, "Hydrogen adsorption on functionalized nanoporous activated carbons", Volume 109, 2005, 8880-8888. Permission to reuse material from the published work was obtained with kind permission from American Chemical Society. A copy of the granting permission for reproduction is shown below.

This is a License Agreement between Zheng Zhang ("You") and American Chemical Society ("American Chemical Society") provided by Copyright Clearance Center ("CCC"). The license consists of your order details, the terms and conditions provided by American Chemical Society, and the payment terms and conditions.

Permission is granted for your request in both print and electronic formats, and translations. If figures and/or tables were requested, they may be adapted or used in part. Please print this page for your records and send a copy of it to your publisher/graduate school. Appropriate credit for the requested material should be given as follows: "Reprinted (adapted) with permission from (COMPLETE REFERENCE CITATION). Copyright (YEAR) American Chemical Society." Insert appropriate information in place of the capitalized words. One-time permission is granted only for the use specified in your request. No additional uses are granted (such as derivative works or other editions). For any other uses, please submit a new request.

Customer name: Zheng Zhang

Customer organization: Michigan Technological University

License date: JUN 11, 2012

Publication: Journal of Physical Chemistry B

Licensed content ISSN: 1520-6106

Publication year(s): 1997 - present

Author/Editor: American Chemical Society

Publication type: Journal

Publisher: AMERICAN CHEMICAL SOCIETY

Language: English

Country of publication: United States of America

Rightsholder: AMERICAN CHEMICAL SOCIETY

Permission type selected: Republish or display content

Type of use selected: reuse in a Thesis/Dissertation

Article title: Hydrogen Adsorption on Functionalized Nanoporous Activated Carbons

Author(s): Zhao XB; et al

DOI: 10.1021/JP050080Z

Date: May 1, 2005

Volume: 109

Issue: 18

APPENDIX G

Figure 3.2 used in this dissertation was originally published in the Installation and Operations Manual for PCT-Pro 2000. Permission to reuse material from the published work was obtained with kind permission from Hy-Energy LLC.

APPENDIX H

Figure 3.5 used in this dissertation was originally published in the Journal of Carbon, “Effect of electric potential on hydrogen adsorption”, Volume 48, 2010, 876-880. Permission to reuse material from the published work was obtained with kind permission from American Carbon Committee. A copy of the granting permission for reproduction is shown below.

This is a License Agreement between Zheng Zhang ("You") and American Carbon Committee ("American Carbon Committee") provided by Copyright Clearance Center ("CCC"). The license consists of your order details, the terms and conditions provided by American Carbon Committee, and the payment terms and conditions.

Customer name: Zheng Zhang

Customer organization: Michigan Technological University

License number: 2926170557059

License date: JUN 11, 2012

Publication: Carbon

Article title: Hydrogen adsorption and storage on porous materials

Author: Li X; et al

DOI: 10.1016/J.CARBON.2009.10.042

Date: Mar 01, 2010

ISSN: 0008-6223

Publication type: Journal

Volume: 48

Issue: 3

Start Page: 876

Publisher: PERGAMON

Author/Editor: AMERICAN CARBON COMMITTEE

Permission status: Granted

Permission type: Republish or display content

Type of use: reuse in a thesis/dissertation

Number of page: 5

Portion: figures/tables/illustrations

Number of figures/tables/illustrations: 1

Format: both print and electronic

Are you the author of this Elsevier article? Yes

Will you be translating? No

Order reference number:

Title of your thesis/dissertation: Effect of External Electric Field on Hydrogen Adsorption over Activated Carbon Separated by Dielectric Materials

Expected completion date: JUN 2012

Estimated size (number of pages): 120

Elsevier VAT number: GB 494 6272 12

Permissions price: 0.00 USD

VAT/Local Sales Tax: 0.0 USD / 0.0 GBP

Total: 0.00 USD